

Air Force Institute of Technology AFIT Scholar

Theses and Dissertations

Student Graduate Works

3-11-2011

Osculating Relative Orbit Elements Resulting from Chief Eccentricity and J2 Perturbing Forces

Joshuah A. Hess

Follow this and additional works at: <https://scholar.afit.edu/etd>

Part of the [Aerospace Engineering Commons](#)

Recommended Citation

Hess, Joshuah A., "Osculating Relative Orbit Elements Resulting from Chief Eccentricity and J2 Perturbing Forces" (2011). *Theses and Dissertations*. 1328.

<https://scholar.afit.edu/etd/1328>

This Thesis is brought to you for free and open access by the Student Graduate Works at AFIT Scholar. It has been accepted for inclusion in Theses and Dissertations by an authorized administrator of AFIT Scholar. For more information, please contact richard.mansfield@afit.edu.



OSCULATING RELATIVE ORBIT ELEMENTS
RESULTING FROM CHIEF ECCENTRICITY AND J_2
PERTURBING FORCES

THESIS

Joshuah A. Hess, Second Lieutenant, USAF

AFIT/GA/ENY/11-M07

DEPARTMENT OF THE AIR FORCE
AIR UNIVERSITY

AIR FORCE INSTITUTE OF TECHNOLOGY

Wright-Patterson Air Force Base, Ohio

APPROVED FOR PUBLIC RELEASE; DISTRIBUTION UNLIMITED

The views expressed in this thesis are those of the author and do not reflect the official policy or position of the United States Air Force, Department of Defense, or the United States Government. This material is declared a work of the U.S. Government and is not subject to copyright protection in the United States.

AFIT/GA/ENY/11-M07

OSCULATING RELATIVE ORBIT ELEMENTS RESULTING FROM
CHIEF ECCENTRICITY AND J_2 PERTURBING FORCES

THESIS

Presented to the Faculty

Department of Aeronautics and Astronautics

Graduate School of Engineering and Management

Air Force Institute of Technology

Air University

Air Education and Training Command

In Partial Fulfillment of the Requirements for the
Degree of Master of Science in Astronautical Engineering

Joshuah A. Hess, B.S. Aerospace Engineering

Second Lieutenant, USAF

March 2011


APPROVED FOR PUBLIC RELEASE; DISTRIBUTION UNLIMITED

AFIT/GA/ENY/11-M07

OSCULATING RELATIVE ORBIT ELEMENTS RESULTING FROM CHIEF
ECCENTRICITY AND J_2 PERTURBING FORCES

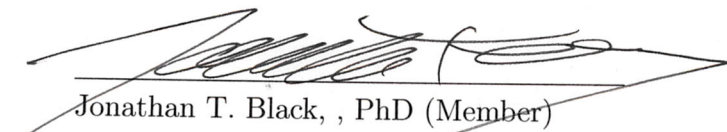
Joshuah A. Hess, B.S. Aerospace Engineering
Second Lieutenant, USAF

Approved:




Douglas D. Decker, PhD (Chairman)

4 MAR 2011
Date



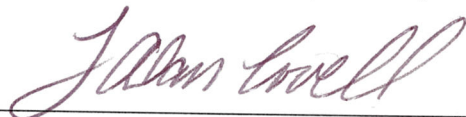
Jonathan T. Black, , PhD (Member)

04 MAR 2011
Date



Richard G. Cobb, PhD (Member)

4 MAR 2011
Date



Thomas A. Lovell, PhD (Member)

15 Mar 2011
Date

Abstract

Relative orbit elements (ROEs) based on a circular chief satellite orbit are erroneous when applied to a perturbed, non-circular reference orbit. In those situations, the ROEs will encounter geometric instability and drift. To counter this, a set of time-variant ROEs have been derived to describe the relative orbit for both the unperturbed, elliptical chief and the perturbed, circular chief. A highly coupled relationship is found that describes the relative trajectory to higher accuracy when compared to numeric integration. To show the applicability of the ROEs to formation design, methods to initialize a stationary relative orbit are detailed and an algorithm for ROE-based guidance and navigation is proposed. The results provide a method to predict the relative motion, while examining time-varying parameters of the motion. Eccentricity effects are shown to induce severe time-variance to the system and introduce a level of mathematical abstraction. Perturbing J_2 effects are shown to introduce periodic effects and compound the secular variations to the circular ROEs.

Acknowledgements

I would foremost like to thank Dr. Douglas Decker for taking me on as a student the day before his retirement; the appreciation of his support, insight, dedication, and attention to detail can hardly be expressed. Similarly, I also express sincere gratitude to Dr. Thomas Lovell for his constant motivation, wisdom, and inspiration, despite a significant separation of half the country between us. I want to thank Dr. Jonathan Black for serving on my committee, and for his passing hallway salutations that, in reality, mean more than one would think. I also would like to thank Dr. Richard Cobb for also serving on my committee and for his intuitive insights and commentary during his lectures.

I am indebted to Luke Hagen as a mentor, Ryan Meritt as a friend, and Lauren Morgan forever, with their uncanny ability to listen to my complaints and provide professional feedback, lifetime advice, and dedication. In addition, to Michelle Rife, my high school calculus teacher, you paved the path I have walked on for so many years, and I can only hope to emulate your impact in the future. Lastly, the support of my family proved an undeniable resource during my time here and I will most likely never be able to express my gratitude for them as well as I should.

Joshuah A. Hess

Table of Contents

	Page
Abstract	iv
Acknowledgements	v
List of Figures	ix
I. Introduction	1
1.1 Problem Statement	3
1.1.1 Phase One: Osculating ROEs Perturbed by Chief Eccentricity	4
1.1.2 Phase Two: Osculating ROEs Perturbed by the J_2 Harmonic .	4
1.1.3 Applications of Osculating ROEs	4
II. Background	6
2.1 Relative Satellite Motion Throughout History	6
2.1.1 Historical Examples	6
2.1.2 Model Development	7
2.2 Coordinate Frames	12
2.2.1 Inertial Reference Frame	12
2.2.2 Local Vertical-Local Horizontal	12
2.2.3 Curvilinear Reference Frame	14
2.3 The Clohessy-Wiltshire Model	15
2.3.1 Derivation	15
2.3.2 Solving the HCW Differential Equations	20
2.3.3 System Behavior	22
2.4 The Relative Orbit Element Realization	23
2.4.1 Derivation	23
2.4.2 System Behavior	28
2.4.3 Summary	29
2.5 Theoretical Impacts of Eccentricity and J_2 on the Relative Trajectory	30
2.5.1 The Impact of a Non-Circular Chief Orbit on Relative Motion .	32
2.5.2 The Impact of the J_2 Perturbation	33
III. Description of Applied Models and Methodology	38
3.1 Applied Models	38
3.1.1 Gim-Alfriend	38
3.1.2 Yamanaka-Ankersen	40
3.1.3 Schweighart-Sedwick	42
3.1.4 Numerically Integrated Truth Model	43
3.2 Methodology	45

	Page
3.2.1 Analytical Expressions for the Relative Orbit Elements	46
3.2.2 Applications of Osculating Relative Orbit Elements	47
IV. Osculating Relative Orbit Elements	49
4.1 The Non-Circular Chief	49
4.1.1 State Propagation	49
4.1.2 Analytical Derivation of Relative Orbit Elements for the Un- perturbed Noncircular Chief	53
4.1.3 Perigee Epoch Simplification	58
4.1.4 Numerical Examples	59
4.1.5 Physical Interpretation of the Osculating Relative Orbit Ele- ments for the Unperturbed Non-Circular Chief	64
4.2 The Perturbed, Circular Chief	69
4.2.1 Relative Orbit Elements for the Perturbed, Circular Chief Using Geometrical Insight and Linearized Mapping	69
4.2.2 Relative Orbit Elements for the Perturbed, Circular Chief De- veloped by the Schwieghart-Sedwick Differential Equations with Arbitrary Initial Conditions	78
4.2.3 Numerical Examples and Deviations from the Clohessy-Wiltshire Assumptions	85
4.3 Applications of Osculating Relative Orbit Elements	88
4.3.1 Guidance and Navigation	88
V. Conclusions and Future Work	92
5.1 A Dialogue on the Realism of Osculating Relative Orbit Elements . .	92
5.2 Recommendations for Future Work	93
5.2.1 Velocity Independence	93
5.2.2 Mathematical Inspection of the Yamanaka-Ankersen Topology	93
5.2.3 Higher-Order Terms in the Virtual Chief Model	94
5.2.4 Drag Effects on the Relative Orbit Elements	94
5.2.5 Perturbation Methods	94
Appendix A. State Transition Matrix Properties	95
Appendix B. Derivation of the Eccentric Osculating Relative Orbit Elements	96
B.1 Relative Semi-major Axis, a_e	96
B.2 Radial Displacement, x_d	97
B.3 In-Track Displacement, y_d	98
B.4 In-Plane Phasing, β	98
B.5 Out-of-Plane ROEs	99

	Page
Appendix C. Time-Varying Parameters of the Yamanaka-Ankersen Derived Relative Orbit Elements	100
C.1 Matrices	100
C.1.1 Members of the A Matrix	100
C.1.2 Members of the B Matrix	102
C.1.3 Members of the C Matrix	102
C.1.4 Members of the D Matrix	102
C.2 Time Varying Coefficients	103
C.2.1 α Coefficients	103
C.2.2 σ Coefficients	103
C.2.3 Σ Coefficients	103
Appendix D. Translational Osculation for the J_2 Perturbed Circular Chief	104
Appendix E. Circularizing the Virtual Chief Parameters	108
E.1 Simplifying A_1	110
E.2 Simplifying ϕ_1	110
E.3 Simplifying A_2	112
E.4 Simplifying ϕ_2	112
E.5 Simplifying z_{max}	113
E.6 Simplifying Ψ	114
E.7 Boundedness	114
E.8 Summary	115
Appendix F. Stationary Orbit Initialization	117
Bibliography	123
Index	125

List of Figures

Figure		Page
2.1	Earth Centered Inertial Reference Frame	13
2.2	Local Vertical Local Horizontal Reference Frame	14
2.3	Relative Position Vector in the LVLH Frame	15
2.4	Visualization of the In-Plane Relative Orbit Using ROEs	31
2.5	Visualization of the Out-of-Plane Relative Orbit Using ROEs	31
4.1	Three-Dimensional Relative Trajectory using Osculating ROEs Compared to Numerical Integration with Chief Eccentricity of 0.01	60
4.2	In-Plane Osculating Relative Orbit Elements with Chief Eccentricity of 0.01	61
4.3	Out-of-Plane Osculating Relative Orbit Elements with Chief Eccentricity of 0.01	61
4.4	Three-Dimensional Relative Trajectory using Osculating ROEs Compared to Numerical Integration with Chief Eccentricity of 0.3	62
4.5	In-Plane Osculating Relative Orbit Elements with Chief Eccentricity of 0.3	63
4.6	Out-of-Plane Osculating Relative Orbit Elements with Chief Eccentricity of 0.3	64
4.7	In-Plane Relative Orbit Element Characterization for the Eccentric Chief	65
4.8	Osculational Translation	66
4.9	Cross-Track Attenuation	67
4.10	In-Plane Osculating Relative Orbit Elements for J_2 Perturbed, Low Altitude Circular Chief	86
4.11	Out-of-Plane Osculating Relative Orbit Elements for J_2 Perturbed, Low Altitude Circular Chief	87
4.12	Coupling Among the Spatial ROEs with Respect to Three-Dimensional Impulsive Velocity Burns	91
E.1	ϕ_2 Visualization	113

Figure		Page
F.1	Boundedness Parameters as Functions of Chief Eccentricity with a Chief Semi-major Axis of 8000 km	120
F.2	Radial Ratio at Perigee as a Function of Chief Eccentricity with Varying Semi-major Axis	121

OSCULATING RELATIVE ORBIT ELEMENTS RESULTING FROM CHIEF ECCENTRICITY AND J_2 PERTURBING FORCES

I. Introduction

Relative satellite motion has seen vast usage and progress in recent years. Numerous well-defined solution sets mapping the motion of a reference satellite, the chief, with a target satellite, the deputy, have been developed. Dynamic models of satellite motion strongly influence close proximity operations including rendezvous and docking. A past example of proximity operations exists in the Apollo era, during which dynamic algorithms were utilized for modular rendezvous [1]. However, these operations were conducted under the assistance of astronauts in the loop, not allowing for full autonomy. The idea of autonomous close proximity operations correlates with and motivates the attempt to further generalize the dynamics of relative satellite motion.

As a vital role in the Apollo program, these special operations were studied primarily for docking procedures. Current operations still maintain focus on the same docking and rendezvous problem. In order to actively control this maneuver, the relative separation between the two bodies is gradually forced to zero. For example, the resupply, modification, and construction of the International Space Station is effected by the use of autonomous unmanned orbit transfer vehicles, relying heavily on control of the rendezvous problem [2].

Formation flight is another defining example of the application of dynamic models for relative motion between two or more satellites. By utilizing several simple and smaller satellites, the size and complexity of single large spacecraft missions can be reduced. For example, a reconnaissance satellite scaled to support a large aperture could be reduced to a formation of multiple smaller bodies to support the same mission [3]. Failsafe options are also inherent in formation flight, in that a catastrophic

failure in one subsystem does not necessarily imply mission failure; this is known as "gradual degradation." Dynamic models of relative motion can be applied to formations by selecting a reference satellite and propagating the relative equations of motion simultaneously for each deputy, setting a design point via initial conditions.

Any model used in real-time application will tend towards a trade between complexity and accuracy. The representation of every possible force on a body is impossible, and also unnecessary in practice. The model can be looked at in terms of kinematic and kinetic terms. The kinematic terms will include the differential equations mapping the motion, while the kinetic terms can be thought of as forcing terms to the motion. From a deterministic standpoint, the kinematic part of the model can be found, while the forcing terms are set and assumed for the application. More than likely, the forcing terms will be analytically expressed through kinematic variables, implying that the inclusion of various forces will directly impact the coupling and complexity of the differential equations of motion for the model. The assumptions made in each model will have a substantial mission impact. Software constructed in accordance with analytical Newtonian dynamics can often be implemented in an autonomous loop. In this regard, there is trade off between model simplicity and dynamical error in the software. In addition, the simplicity of the model drives the computing power needed to numerically solve the differential equations. This would not be a problem if a generalized analytical solution of relative satellite motion could be derived; however, the stochastic perturbations of spaceflight allow only for approximations and numerical solutions based on *a priori* operations.

Inherent in these models are assumptions constraining the orbit of the chief, and, in addition, the proximity between the two satellites. The most common assumptions are those required for the linearization of the model derived by Clohessy and Wiltshire [4] (HCW): a circular chief, unperturbed two-body Keplerian dynamics, and close proximity. The HCW model often manifests itself with respect to rendezvous, docking maneuvers, and the dynamics of satellite clusters [5], but the linearization carries with it limitations in real world applications.

Of high importance to the present study is one particular realization of the HCW solution, which is the parameterization of the resulting trajectory by six relative orbit elements (ROEs). The HCW model will be discussed in great detail later in this study, along with the derivation of the ROEs and their utility.

The linear time-invariant ordinary differential equations of the HCW formulation allow for an elegant closed form solution. A fallout of the HCW model shows that the relative orbit between the deputy and the chief will be an ellipse with a semi-major axis that is twice the semi-minor axis (a 2x1 ellipse) when projected into the orbital plane of the chief. The previously mentioned ROEs provide an instantaneous snapshot of the relative orbit that describes the size, shape, and orientation of the projected relative ellipse. The derivation of the ROEs is performed under the identical assumptions as the HCW model. The inclusion of orbital perturbations to the HCW model represents an insertion of non-linearity and time-variance to the ROEs. In that the ROEs are linear and non-linear combinations of the relative state vector and a stand-alone parameterization, the question stands as to what impacts are made on the ROEs when operating with a perturbed or non-circular chief. These resulting relative orbit elements are, in the context of this study, defined as osculating relative orbit elements. To increase the utility and applicability of the relative orbit element parameterization, the osculating relative orbit response to both the relaxation of the unperturbed motion assumption and the dynamics of the non-circular chief is the aim of the current study. The following section provides detail on the individual aspects of the study.

1.1 Problem Statement

The purpose of this study is to develop numerical and analytical results for perturbations in the relative orbit elements initiated by chief eccentricity and the J_2 zonal harmonic. The study will be divided into two primary phases, investigating the eccentricity and J_2 effects separately, followed by proposed applications.

1.1.1 Phase One: Osculating ROEs Perturbed by Chief Eccentricity. The first phase will be a look at how the relative orbit elements vary as a result of a non-circular chief. Numerically integrated two-body Keplerian motion (2BP) will be assumed as truth, with the 2BP state vector numerically substituted as the arguments for the ROE analytic functions. Stationary orbits will be primarily investigated. Using the Yamanaka-Ankersen (YA [6]) state transition matrix for relative motion, full expressions for the ROEs will be derived as a function of initial conditions. The objective of this exercise is to determine the validity and applicability of ROEs for geometric visualization of the unperturbed relative orbit.

1.1.2 Phase Two: Osculating ROEs Perturbed by the J_2 Harmonic. Ignoring atmospheric drag, the spherical central body assumption in the Clohessy-Wiltshire equations serves as a primary error source. The second phase, following in a similar fashion as Phase One, will examine the behavior of the ROEs for a circular chief perturbed by the J_2 harmonic. Having been well documented in the literature as a well-behaved model for the J_2 perturbed chief, the Schweighart-Sedwick [7] model is fully utilized to derive analytical expressions for the ROEs as a function of initial conditions. The Gim-Alfriend [8] model will be used as a purely analytical study to understand the physical effects. Being that the ROEs are a HCW realization, baseline comparisons are made to the unperturbed HCW model.

1.1.3 Applications of Osculating ROEs.

1.1.3.1 Stationary Orbit Initialization. To provide a means of formation installation utilizing ROEs, sets of initial conditions to allow for stationary relative orbits is derived using period matching and methods of J_2 invariance.

1.1.3.2 Guidance and Maneuver. As an application of the ROEs, a guidance algorithm is proposed to modify the orbit using osculating ROEs. The

purpose of this study is to introduce the concept and applicability of controls to osculating ROEs.

II. Background

The relative motion between two bodies is not a new concept. More than likely, the mapping of the motion of one object compared to that of another is a daily occurrence. Walking side by side, driving on a highway, running along a track; the examples are endless. Luckily, rather than free will driving the motion of one body, the differential equations of orbital mechanics determine the relative trajectories. While the assumption of Keplerian motion greatly simplifies the governing laws, various perturbations can increase the complexity of the dynamical models. This background will provide an overview of the past and current state of the art. Section 2.1 will provide historical examples of relative motion applications. Sections 2.2 to 2.4 will provide the basic background and reference frames needed to understand the mathematics in the classical ROE expressions. Finally, Section 2.5 will discuss the impact of the non-circular chief and the J_2 perturbation on relative satellite motion.

2.1 Relative Satellite Motion Throughout History

2.1.1 Historical Examples. Between June of 1983 and August of 2005, a total of 57 shuttle missions utilized one or more forms of close proximity operations successfully [9]. The objectives of these operations vary from formation maintenance to final docking with a desired chief. Prior to these maneuvers, experiments to validate the ability of a human eye to track and maintain manual control of a docking sequence were performed on Mercury missions. Following the Mercury Program, Gemini set forth and established a solid foundation for the future of human rendezvous. Goodman states that the most significant accomplishments of the Gemini Program with respect to rendezvous operations included high and low orbit coelliptic rendezvous, orbital night and day docking, optical measurement rendezvous, conjunctive countdown for the maneuver from both chief and deputy perspective, and multiple rendezvous operations while staying in a propellant budget [9]. The Apollo Program established rendezvous operations as methodical techniques, using several missions to practice lunar landing. As a side note, the idea of lunar rendezvous was not a new thought at this

time; one of the first accounts of relative motion model development is Hill's [10] lunar equations: his attempt to describe relative motion in the Earth-Moon-Sun system.

Moving the focus to that of formation flying, the size, cost, and complexity of many classes of missions can be greatly reduced by utilizing a number of smaller satellites. Using multiple satellites allows multi-tasking within the formation. In the event of a catastrophic failure in one of the deputy satellites within the formation, adjustments can be made to compensate for the loss. [3]. Examples of formation flight include the Orion program as a proof of concept for GPS based relative navigation, and the ESA Cluster mission for magnetospheric studies. Stationkeeping requirements for formation control tend to be on a low order of required thrust. This has led to direct development of electric thrusters utilizing electromagnetic as well as electrostatic forces [11]. A formation design will specify initial conditions in such a way to satisfy the mission requirements. For example, a circular in-plane formation will be bounded by specifying the in-track and cross-track states as a function of the radial states. While specifying these values limits the the initial degrees of freedom (in this case, only having two initial conditons to choose), the motion is deterministically known and the free initial conditions can be used to set the period and phasing of the deputy [11].

2.1.2 Model Development. Whether having been applied to rendezvous operations or to the control of a formation, the idea of relative motion models has been widely used throughout the history of the space program. The history of model development in this field is an interesting study in various attempts at first order linearizations, linearized state transition matrices, incorporating various orbital perturbations, and increasing model fidelity. In fact, the history of model development can almost be seen as a survey of the state transition matrices derived over the years. The idea of propagation of an initial state to a desired time through deterministic dynamics is quite popular in both theory and practice. The popularity is of course due to accuracy without time-consuming and computationally expensive numerical

integration. The initiation of a state transition matrix depends on the linearization inherent in the model. Moreover, the independent variable used in the propagation is of extreme importance. For example, if time is used then certain states may be poorly represented near perigee without the appropriate time step; however, if true anomaly is used, complicating definite integrals will show themselves. A brief survey on the properties of state transition matrices can be found in Appendix A. Despite the broad definitions of these models, Carter [12] proposes three classifications of linearized models

1. Inertial or rotating reference frames
2. Linearizing the central force field to introduce a gradient to the equations of motion, or linearizing orbital parameters
3. Nominal reference orbit

Although proving more abstract to view initially, the rotating frame is employed the most often as a means to visualize system behavior in the vicinity of the chief. More specifically, the linearization of an inverse square gravity term (μ/r^2) yields the most well known relative motion model in the field: Clohessy and Wiltshire [4], which is discussed in great detail in Section 2.3. Limitations of this model are a result of the linearizations made to derive the closed form solution. Constraints such as a circular chief, proximity assumptions, and unperturbed motion limit the long term applications of the model. The circular chief was expanded to second-order truncation by Karlgaard and Lutze using the method of multiple scales in spherical coordinates [13] with significant increase in accuracy over HCW.

The circular chief assumption is highly limiting, most paramount in that a pure circular orbit is not plausible. For missions involving vehicle servicing or sample return [6], the chief orbit is most often not circular. A dominant downside to relaxing the circular chief assumption is the transition from a time-invariant system to a time-varying system, in that a spacecraft's dynamic rates are explicit functions of time. Realizing the future impact, in the decade following the Clohessy-Wiltshire publica-

tion, an independent effort was undertaken by Lawden [14] along with Tschauner and Hempel [15]. Tschauner and Hempel were pursuing the closed-form solution for an arbitrary elliptic chief, while Lawden was attempting to describe the primer vector with respect to optimal trajectories. The two models proved to be nearly identical, but cumbersome with the inclusion of the below integral [12]

$$I = \int \frac{d\theta}{\sin^2 \theta (1 + e \cos \theta)^2} \quad (2.1)$$

where θ is the true anomaly of the chief. The integral in Eq.(2.1) is obviously singular for true anomalies of integer π multiples. Carter later transformed this integral to the form [16]

$$J = \int \frac{\cos \theta d\theta}{(1 + e \cos \theta)^3} \quad (2.2)$$

which remains nonsingular. More recently, in 2002 Yamanaka and Ankersen [6] used basic orbital mechanics relations to provide a solution to this integral as a function of orbital angular momentum. The Yamanaka-Ankersen model will be discussed in more depth further in Section 3.1.2.

Alfriend and Yan contend [17] that for the nearly thirty years following the Tschauner-Hempel and Lawden derivations, little work was done in the field. Some work such as Carter’s reformulation of the singular integral [16] was performed, but it was not until the concept of satellite formation flight was popularized in the late 1990s and early 2000s that the quest for model fidelity was pursued. The quest for high fidelity in the model is a direct consequence of desired long term accuracy. Most often, the unperturbed Keplerian orbit assumption is made to soften the mathematics. However, for low Earth orbits (LEO), air drag and oblateness impact the orbit significantly (See Sections 2.5.1 and 2.5.2 for specifics on the impact on relative motion).

A dominating perturbation to consider for relative motion is the J_2 effect. Making the assumption of a circular chief, Schweighart and Sedwick [7] incorporated an orbit averaged J_2 modification to the classic HCW model that captures the effects very

well. The HCW equations have also been further modified to include both linear [18] and quadratic [19] drag effects. Chen and Jing have recently developed differential equations including both air drag and J_2 on the arbitrary elliptical chief [20] using Lagrangian dynamics, but has no closed form solution.

Modeling the elliptical chief is significantly more challenging than the circular, reinforced by the fact that the Chen-Jing model does not have a closed form solution. In recent literature, the concept of orbital element differences to describe the relative motion has come to light. Rather than expressing the trajectory in Cartesian coordinates (x, y, z) , the more intuitive idea of using the difference in the chief and deputy classical or non-singular orbital elements can be used to propagate to a future state. Alfriend has shown that relative motion theories using these states tends to higher accuracy than using a Cartesian or curvilinear frame [21]. In this manner, the complexity of the model increases significantly if the instantaneous orbital elements are used, and is simplified if the model operates in mean orbital element space. Schaub makes use of this in [22] with the propagation existing in mean orbital element space. Hamel and Lafontaine [23] derive a time-varying state space form using these differences, but rely on an estimated time of flight solution. Gim and Alfriend [8] derive a state transition matrix that propagates either the initial Cartesian conditions or the initial orbital element differences to a desired time using either the mean or osculating J_2 effect. The GA model is of significant importance to the analytical investigation in this study and is described in depth in Section 3.1.1.

There do exist approaches to mapping the relative motion other than solving ordinary differential equations. For example, Wiesel applies Floquet theory in [5] to the relative motion problem. In this work, Wiesel incorporates all zonal harmonics to the HCW model and produces a model with two modes that are linear in time, and completely describes the solution by a periodic vector and a periodic modal matrix. As another example, work done by Kolenen and Kasdin [24] introduces eccentricity as a perturbation to the linearized HCW model using Hamiltonian mechanics. Another non-traditional solution is that of Vadali [25] and Sengupta, Vadali, and Alfriend [26]

in which the motion of both the chief and deputy are normalized by their respective radii and projected onto a unit sphere. Following the projection, spherical trigonometry reveals an exact kinematic relation, and is found to be accurate for relative ranges of up to approximately 160 km [17].

In a most recent effort at the Air Force Institute of Technology (AFIT), Kirk Johnson [27] applied a "Virtual Chief" method to the relative motion problem. A circular virtual chief on an orbit known *a priori* whose orbital elements are identical to those of the chief with the exception of the zero eccentricity is propagated. The motion of the physical chief and deputy are propagated in accordance with HCW dynamics with respect to the virtual reference. The coupling of linearization errors of both the chief and deputy with respect to the HCW propagation introduced significant error when compared to two body dynamics. However, the possibility of retaining higher-order terms in the set-up of the model may increase the accuracy of the model. Johnson also proposed in his thesis a set of six parameters that defined the motion of the VC trajectory with respect to geometry, drift, phasing, periodicity, and skewness. As a side study to this thesis, the conversion of these parameters to ROEs under a circular assumption is presented in Appendix E.

Linearizations made also impact the physical space of the model; for example, an initial condition on relative displacement for one model does not necessarily correspond to an initial condition for numerical integration. Therefore, initial condition matching has also populated the literature surrounding this topic. Of particular interest is the concept of creating a bounded, periodic relative orbit by specifying initial conditions. The problem resulting from this is an initial condition in one linearized model does not necessarily correspond to the same condition in another linearized model. Inalhan, Tillerson, and How present an algorithm to initialize the velocity space as a function of position at any point in the orbit [28]. Gurfil has recently adapted the periodicity problem in terms of energy matching [29], which allows velocity to be extracted from a quadratic expression. In Schaub's text [30], an in-depth discussion is made concerning period matching and J_2 invariant relative orbits. From

this brief survey, the overarching method of initial condition matching is in the form of maintaining equal periods between the two orbits. In some cases this may relax to equal semi-major axes; however, in the presence of the J_2 disturbance, short-period oscillations in the chief and deputy semi-major axes will modify the period. Moreover, in the presence of atmospheric drag, the decay of the orbit's energy will also challenge energy matching between the chief and the deputy.

2.2 *Coordinate Frames*

Now being familiar with the importance and applicability of relative satellite motion, it is now necessary to introduce the environment which the majority of models describe.

2.2.1 Inertial Reference Frame. A geocentric reference frame will be used for the purpose of the current study. The Earth-centered-inertial frame originating from the center of the Earth is the frame of choice. Seen in Fig. 2.1, the \hat{I} vector is in the direction of the vernal equinox, the \hat{K} vector is vertical through the north pole, and the \hat{J} vector is orthogonal eastward to \hat{I} and lies in the Equatorial plane. Serving as one of the most common frames in orbital mechanics, it is deemed “inertial enough.” Slight changes occur in the location of the vernal equinox and in the equatorial plane; however, specification of a certain epoch often implies an inertial system.

2.2.2 Local Vertical-Local Horizontal. The majority of the relative motion models studied express their solution in the local-vertical, local-horizontal (LVLH) frame. This is a frame that assumes the satellite is a point mass and rotates at the same angular rate as the satellite in its orbit. For example, a LVLH frame attached to an unperturbed circular chief will rotate exactly at the mean motion, while a LVLH frame attached to an unperturbed non-circular chief will rotate at the time derivative of the true anomaly. Another term for this frame, and used interchangeably throughout this study, is the RIC (radial, in-track, cross-track) frame. The radial

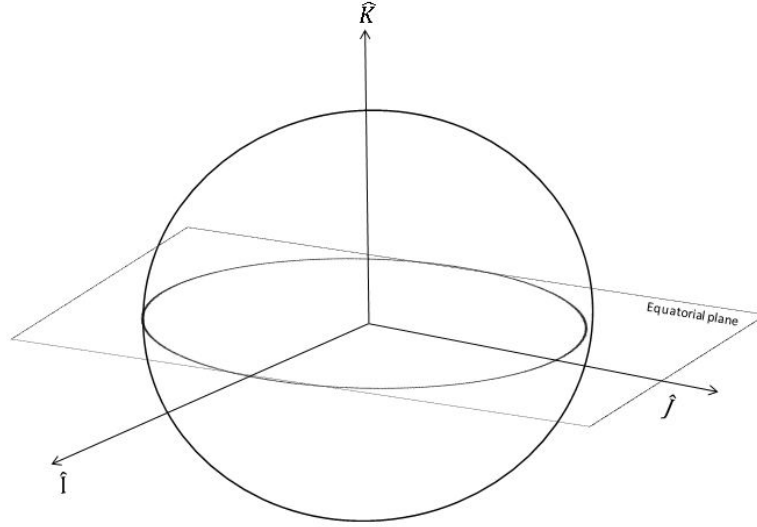


Figure 2.1: Earth Centered Inertial Reference Frame

($\hat{\mathbf{o}}_r$) axis is in the direction of the position vector from the center of the Earth to the satellite, positive outward. The cross-track ($\hat{\mathbf{o}}_h$) axis is parallel to the orbital angular momentum vector in the orbit normal direction. The in-track ($\hat{\mathbf{o}}_\theta$) axis completes the orthogonal set. Equation 2.3 expresses the LVLH vectors mathematically, following Schaub [22].

$$\begin{aligned}
 \hat{\mathbf{o}}_r &= \vec{\mathbf{r}}/r \\
 \hat{\mathbf{o}}_h &= \vec{\mathbf{h}}/h \\
 \hat{\mathbf{o}}_\theta &= \hat{\mathbf{o}}_h \times \hat{\mathbf{o}}_r
 \end{aligned} \tag{2.3}$$

where $\vec{\mathbf{r}}$ is the position vector from the center of the central body to the chief, $\vec{\mathbf{h}}$ is the specific angular momentum vector ($\vec{\mathbf{h}} = \vec{\mathbf{r}} \times \dot{\vec{\mathbf{r}}}$), and the unbolded scalars are the 2-norm of the respective vectors. Figure 2.2 provides a visualization of the reference frame

The location of the deputy in the relative LVLH frame must now be discussed. The chief, although constantly moving and rotating, is kept at the origin of the frame. The position vector from the chief to the deputy is denoted as ρ , and its

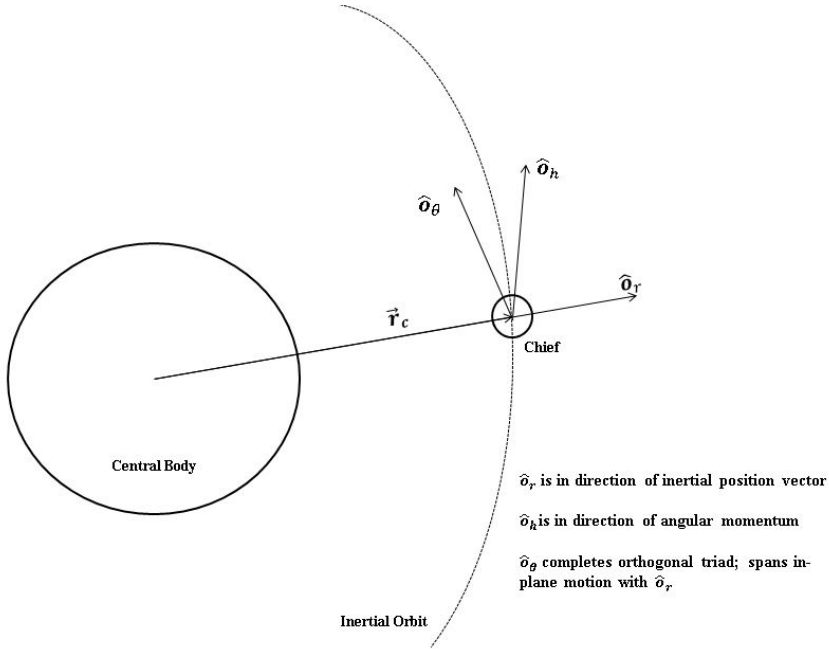


Figure 2.2: Local Vertical Local Horizontal Reference Frame

time derivative as $\dot{\rho}$. The Cartesian components of the relative position and velocity vectors are expressed in the radial (x), in-track (y), and cross-track (z) directions. For this study, the following notation in Eq. 2.4 is used for the relative position vector

$$\vec{\rho} = \begin{pmatrix} x \\ y \\ z \end{pmatrix} \quad (2.4)$$

The relative velocity vector is presented similarly, only using scalar relative velocity components where the relative position states are. Figure 2.3 provides a visualization of the deputy's location relative to the chief. It is important now to note that even though a time history of a relative orbit will show movement around the origin, the deputy is in reality not orbiting around the chief. The central body remains the source of the primary gravitational force field.

2.2.3 Curvilinear Reference Frame. Similar to the LVLH frame described in 2.2.2, the curvilinear frame is nearly identical in form. The Gim-Alfriend model uses

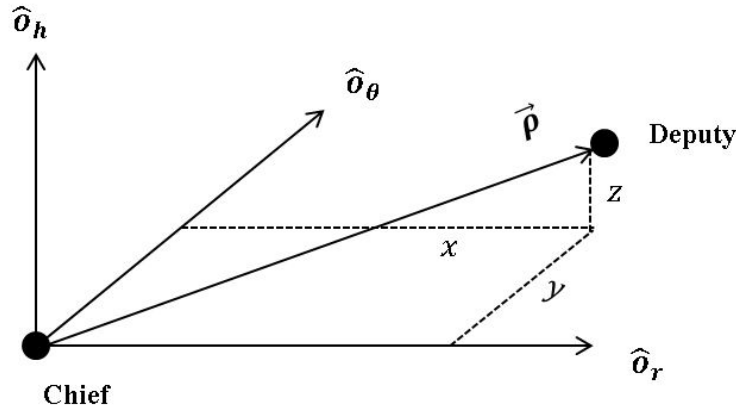


Figure 2.3: Relative Position Vector in the LVLH Frame

curvilinear coordinates to obtain more accurate results [8]. The calculated states still represent the same physical phenomenon, and may still be used for ROE substitution. The x coordinate is taken as the difference in radii between the chief and the deputy, the y and z coordinates are taken as curvilinear distances along and perpendicular to an instantaneous imaginary circle on the reference orbital plane. In this sense, the relative position vector can be thought to “bend” along the trajectory.

2.3 The Clohessy-Wiltshire Model

The most famous relative motion model is that of Clohessy and Wiltshire [4]. As the HCW model is the basis for the relative orbit element realization, the following section presents a beginning to end derivation and trend analysis as discussed in Vallado [31].

2.3.1 Derivation. To begin the derivation of the HCW model, a problem statement is first defined. It is desired to determine the analytical solution for the relative motion of the deputy with respect to a circular chief. The inertial chief and deputy position vectors are denoted as \vec{r}_c and \vec{r}_d , respectively. The inertial relative

range vector (${}^i\vec{\rho}$) is now

$${}^i\vec{\rho} = \vec{r}_d - \vec{r}_c \quad (2.5)$$

If one desires to obtain the equations of motion, the inertial relative acceleration vector is needed (Eq. 2.6)

$${}^i\ddot{\vec{\rho}} = \ddot{\vec{r}}_d - \ddot{\vec{r}}_c \quad (2.6)$$

Assuming unperturbed Keplerian two-body motion, the individual accelerations are well known and can be represented as Eq. 2.7

$$\ddot{\vec{r}} = -\frac{\mu\vec{r}}{r^3} \quad (2.7)$$

Now, substituting Eq. 2.7 in Eq. 2.6, the differential equation becomes

$${}^i\ddot{\vec{\rho}} = -\frac{\mu\vec{r}_d}{r_d^3} + \frac{\mu\vec{r}_c}{r_c^3} \quad (2.8)$$

Having the basic set-up, there is now a need to simplify the system. Using the law of cosines, the magnitude of the deputy's inertial position vector is then found as

$$r_d^2 = r_c^2 + \rho^2 + 2\vec{r}_c \cdot {}^i\vec{\rho} \quad (2.9)$$

Substituting Eq. 2.9 into a form similar to the two-body acceleration

$$\frac{\vec{r}_d}{r_d^3} = \frac{\vec{r}_c + {}^i\vec{\rho}}{(r_c^2 + \rho^2 + 2\vec{r}_c \cdot {}^i\vec{\rho})^{\frac{3}{2}}} \quad (2.10)$$

Now is where the second assumption (the first being unperturbed Keplerian motion) is made. It is assumed that the relative position vector is much smaller than the position vector of the chief. Therefore, $\rho^2 \ll r_c^2$. Applying this assumption to Eq. 2.10 and simplifying, Eq. 2.11 falls out

$$\frac{\vec{r}_d}{r_d^3} = \frac{\vec{r}_c + {}^i\vec{\rho}}{r_c^3} \frac{1}{\left(1 + \frac{2\vec{r}_c \cdot {}^i\vec{\rho}}{r_c^2}\right)^{\frac{3}{2}}} \quad (2.11)$$

A binomial expansion of the form

$$(1+x)^n = \sum_{k=0}^{\infty} \binom{n}{k} x^k = 1 + nx + \frac{n(n-1)x^2}{2!} + \dots \quad (2.12)$$

is then applied to the denominator of Eq. 2.11, and truncated at the first term to arrive at

$$\left(1 + \frac{2\vec{r}_c \cdot {}^i\vec{\rho}}{r_c^2}\right)^{-3/2} = 1 - \frac{3}{2} \frac{(2\vec{r}_c \cdot {}^i\vec{\rho})}{r_c^2} \quad (2.13)$$

Substituting Eq. 2.13 and substituting in Eq. 2.11,

$$\frac{\vec{r}_d}{r_d^3} = \frac{\vec{r}_c + {}^i\vec{\rho}}{r_c^3} \left(1 - \frac{3}{2} \frac{(2\vec{r}_c \cdot {}^i\vec{\rho})}{r_c^2}\right) \quad (2.14)$$

Taking Eq. 2.14 and substituting in Eq. 2.8

$$\begin{aligned} {}^i\ddot{\vec{\rho}} &= -\frac{\mu\vec{r}_d}{r_d^3} + \frac{\mu\vec{r}_c}{r_c^3} \\ &= -\mu \left(\frac{\vec{r}_c + {}^i\vec{\rho}}{r_c^3} \left(1 - \frac{3}{2} \frac{(2\vec{r}_c \cdot {}^i\vec{\rho})}{r_c^2}\right) \right) + \frac{\mu\vec{r}_c}{r_c^3} \end{aligned} \quad (2.15)$$

Noting opposite signs and simplifying, we arrive at

$${}^i\ddot{\vec{\rho}} = -\frac{\mu}{r_c^3} \left(-\frac{3}{2} \frac{\vec{r}_c}{r_c} \frac{2\vec{r}_c \cdot {}^i\vec{\rho}}{r_c} + {}^i\vec{\rho} \right) \quad (2.16)$$

It is now noted that the inertial position vector can be expressed in the LVLH frame from the dot products in Eq. 2.16. This follows mathematically as

$$\begin{aligned} -\frac{3}{2} \frac{\vec{r}_c}{r_c} \frac{2\vec{r}_c \cdot {}^i\vec{\rho}}{r_c} &= -3\hat{o}_r (\hat{o}_r \cdot {}^i\vec{\rho}) \\ &= -3x\hat{o}_r \end{aligned} \quad (2.17)$$

After substitution, we arrive at

$${}^i\ddot{\vec{\rho}} = -\frac{\mu}{r_c^3} (-3x\hat{o}_r + {}^i\vec{\rho}) \quad (2.18)$$

As this is the inertial acceleration, and the desired solution is in the LVLH frame, the transport theorem is now applied. For completion, the transport theorem is

$${}^i \frac{d}{dt}(\cdot) = {}^b \frac{d}{dt}(\cdot) + \omega^{bi} \times (\cdot) \quad (2.19)$$

where the superscript b denotes a non-inertial reference frame, and the superscript i denoted an inertial frame. Because this is an acceleration, the transport theorem is applied twice to yield, among others, the well known Coriolis and centripetal terms. The full transport theorem is expressed as

$${}^i \ddot{\vec{r}} = {}^b \ddot{\vec{r}} + \dot{\vec{\omega}} \times \vec{r} + 2\vec{\omega} \times \dot{\vec{r}} + \vec{\omega} \times (\vec{\omega} \times \vec{r}) \quad (2.20)$$

Assuming a circular chief, the angular velocity of the LVLH frame with respect to the inertial frame is the mean motion of the chief. That is, $\vec{\omega} = \sqrt{\frac{\mu}{r^3}} \hat{o}_h = n \hat{o}_h$ and $\dot{\vec{\omega}} = \vec{0}$. Applying Eq. 2.20 and the angular velocity to Eq. 2.18, the final vector equation of motion is found as

$$\ddot{\vec{\rho}} = -n^2(\vec{\rho} - 3x\hat{o}_r) + 2(ny\hat{o}_r - n\dot{x}\hat{o}_\theta) + \ddot{x}\hat{o}_r + \ddot{y}\hat{o}_\theta \quad (2.21)$$

Expressing the $\vec{\rho}$ vector in component form

$$\ddot{x}\hat{o}_r + \ddot{y}\hat{o}_\theta + \ddot{z}\hat{o}_h = -n^2((x-3x)\hat{o}_r + y\hat{o}_\theta + z\hat{o}_h) + 2(ny\hat{o}_r - n\dot{x}\hat{o}_\theta) + \ddot{x}\hat{o}_r + \ddot{y}\hat{o}_\theta \quad (2.22)$$

And finally collecting the vector components, the set of three linear, coupled, ordinary differential equations is found as

$$\begin{aligned} 0 &= \ddot{x} - 2n\dot{y} - 3n^2x \\ 0 &= \ddot{y} + 2n\dot{x} \\ 0 &= \ddot{z} + n^2z \end{aligned} \quad (2.23)$$

It is worth noting that if an external force is present, the left-hand side of zeros in Eq. 2.23 are replaced by more specific expressions. Finally, to place the differential equations in a more comfortable matrix form, the system above can be expressed in state-space form as

$$\begin{pmatrix} \dot{x} \\ \dot{y} \\ \dot{z} \\ \ddot{x} \\ \ddot{y} \\ \ddot{z} \end{pmatrix} = \begin{bmatrix} 0 & 0 & 0 & 1 & 0 & 0 \\ 0 & 0 & 0 & 0 & 1 & 0 \\ 0 & 0 & 0 & 0 & 0 & 1 \\ 3n^2 & 0 & 0 & 0 & 2n & 0 \\ 0 & 0 & 0 & -2n & 0 & 0 \\ 0 & 0 & -n^2 & 0 & 0 & 0 \end{bmatrix} \begin{pmatrix} x \\ y \\ z \\ \dot{x} \\ \dot{y} \\ \dot{z} \end{pmatrix} \quad (2.24)$$

Having the familiar form of $\dot{X} = AX$, basic concepts of linear systems can be used to find the closed-form solutions in Section 2.3.2.

Without replicating the derivation, Schaub [30] presents the coupled, non-linear system of differential equations as

$$\begin{aligned} \ddot{x} - 2\dot{f} \left(\dot{y} - y \frac{\dot{r}_c}{r_c} \right) - x\dot{f}^2 - \frac{\mu}{r_c^2} &= -\frac{\mu}{r_d^3} (r_c + x) \\ \ddot{y} + 2\dot{f} \left(\dot{x} - x \frac{\dot{r}_c}{r_c} \right) - y\dot{f}^2 &= -\frac{\mu}{r_d^3} y \\ \ddot{z} &= -\frac{\mu}{r_d^3} z \end{aligned} \quad (2.25)$$

where f is the true anomaly of the chief. This system remains valid for arbitrarily large orbits with a non-circular chief. However, making the same assumptions as earlier (circular chief, close proximity, first order truncation) this model does in fact yield the same linear time-invariant set given in Eq. 2.24 (the HCW model).

Finally, we can change the variables to a curvilinear frame via the following

$$\begin{aligned} x &= \delta r \\ y &= r_c \delta \theta \end{aligned} \quad (2.26)$$

where δr and $\delta\theta$ are differential displacements in the radial and angular directions. The HCW equations can be expressed as

$$\begin{aligned} 0 &= \delta\ddot{r} - 2nr_c\delta\dot{\theta} - 3n^2\delta r \\ 0 &= r_c\delta\ddot{\theta} + 2n\delta\dot{r} \\ 0 &= \ddot{z} + n^2z \end{aligned} \tag{2.27}$$

The use of curvilinear coordinates is often found to be more accurate as the system will naturally bend the in-track vector along the orbital path [30].

2.3.2 Solving the HCW Differential Equations. Now having a system of linear, time-invariant ordinary differential equations (LTI ODEs), fundamental properties of linear systems can be applied to find the solution to Eq. 2.24. The first fundamental principle (applied without proof) is that the solution to the unforced system of LTI ODEs

$$\dot{\mathbf{x}} = A\mathbf{x} \tag{2.28}$$

where A is the plant matrix, and \mathbf{x} is the vector of states, is of the form

$$\mathbf{x}(t) = \Phi(t - t_0)\mathbf{x}_0 \tag{2.29}$$

where $\Phi(t - t_0)$ is termed the state transition matrix (STM). As STMs form a significant foundation for this study, a brief survey is provided in Appendix A. To find $\Phi(t - t_0)$, the matrix exponential is used

$$\begin{aligned} \Phi(t - t_0) &= e^{A(t-t_0)} \\ \Phi(t - t_0) &= (s\mathbf{1} - A)^{-1} \end{aligned} \tag{2.30}$$

with s being the Laplace variable. Substituting in the plant matrix from Eq. 2.24, the STM is expressed as

$$\Phi(t - t_0) = \mathfrak{L}^{-1} \begin{bmatrix} s & 0 & 0 & -1 & 0 & 0 \\ 0 & s & 0 & 0 & -1 & 0 \\ 0 & 0 & s & 0 & 0 & -1 \\ -3n^2 & 0 & 0 & s & -2n & 0 \\ 0 & 0 & 0 & -2n & s & 0 \\ 0 & 0 & -n^2 & 0 & 0 & s \end{bmatrix}^{-1} \quad (2.31)$$

where \mathfrak{L}^{-1} is the inverse Laplace transform. Without replicating the matrix algebra, Eq. 2.31 reduces to a very elegant solution of the form

$$\Phi(t - t_0) = \begin{bmatrix} 4 - 3 \cos \theta & 0 & 0 & \frac{\sin \theta}{n} & \frac{2}{n}(1 - \cos \theta) & 0 \\ 6(\sin \theta - \theta) & 1 & 0 & \frac{2}{n}(\cos \theta - 1) & \frac{4}{n} \sin \theta - \frac{3\theta}{n} & 0 \\ 0 & 0 & \cos \theta & 0 & 0 & \frac{\sin \theta}{n} \\ 3n \sin \theta & 0 & 0 & \cos \theta & 2 \sin \theta & 0 \\ 6n(\cos \theta - 1) & 0 & 0 & -2 \sin \theta & 4 \cos \theta - 3 & 0 \\ 0 & 0 & -n \sin \theta & 0 & 0 & \cos \theta \end{bmatrix} \quad (2.32)$$

where $\theta = n(t - t_0)$. The state at any time is now a linear combination of the initial conditions. Often in the literature (for example, [32]), the HCW Φ matrix is partitioned into four 3×3 matrices, as the following

$$\Phi(t - t_0) = \begin{bmatrix} \Phi_{rr} & \Phi_{rv} \\ \Phi_{vr} & \Phi_{vv} \end{bmatrix} \quad (2.33)$$

where the subscripts r and v correspond to position and velocity, respectively. Having a complete closed form solution to the LTI ODEs, the system behavior can now be investigated in Section 2.3.3.

2.3.3 System Behavior. In this section, only a brief survey is given on the system behavior of the HCW equations. This is a direct consequence of the ROEs completely describing the trajectory. As such, to avoid duplicate derivatons, only top-level system qualities are detailed, and the more mathematical derivations are detailed in Section 2.4.

The most elegant fallout is the geometry of the in-plane motion of the deputy relative to the chief. It will later be shown that the radial and in-track trajectory is a 2:1 ellipse. That is, the in-track motion oscillates at twice the magnitude of the radial with an orthogonal phasing. The ellipse is centered at a constant radial displacement, but an in-track displacement that may drift if certain initial conditions are not met. Examining Eq. 2.32, the only secular terms are in the $\dot{y}(t)$ equation is

$$\textit{Secular Term} = (-6nx_0 - 3\dot{y}_0)t \quad (2.34)$$

and to eliminate the drift in the in-track direction, Eq. 2.34 must be null, implying

$$\dot{y}_0 = -2nx_0 \quad (2.35)$$

which will produce a 2:1 ellipse centered at a constant radial and in-track displacement.

The cross-track (z) motion is completely uncoupled from the radial and in-track motion in the linearized case. The result of this uncoupling is that any cross-track displacement will simply superimpose an oscillatory motion on the in-plane trajectory in the cross-track direction. Vallado [31] summarizes of the effect of initial conditions on the motion, detailed below

1. The deputy will progress further in-track if beginning in a lower orbit ($x_0 < 0$). For unperturbed motion, a lower orbit implies a higher-energy orbit. The deputy will move at a greater relative velocity than the chief and move ahead in-track

2. The deputy will regress further in-track if beginning in a higher orbit ($x_0 > 0$). For unperturbed motion, a higher orbit implies a lower-energy orbit. The deputy will move at a lower relative velocity than the chief and move behind in-track
3. As the initial radial displacement is increased, the relative motion trajectory will increase. As shown later in the ROE development the size of the relative orbit is determined by the radial displacement, and the velocities in the radial and in-track direction.
4. The ellipse can be centered at a constant displacement and the relative orbit made periodic if the initial condition $\dot{y}_0 = -2nx_0$ is enforced.
5. For a fixed radial displacement, any in-track displacement will produce the same relative motion, as the deputy will still be in the same orbit at the same energy.
6. A cross-track displacement will simply superimpose oscillations over the in-plane motion.

Now, having a solid foundation for the HCW motion, the relative orbit elements can now be derived and shown as a practical parameterization of the model.

2.4 The Relative Orbit Element Realization

Taking the results from Section 2.3, the relative orbit elements are now derived. Being that the ROEs are the basis of this study, great care is taken in their derivation following the results of Lovell [33].

2.4.1 Derivation. The ROEs are a set of six parameters that describe the relative motion in the LVLH frame for the circular chief. The six ROEs are the semi-major axis (a_e), the radial displacement (x_d), the in-track displacement (y_d), the in-plane phasing (β), the maximum cross-track amplification (z_{max}), and the out-of-plane phasing (ψ). The derivation will be divided into the ROEs describing the in-plane and the out-of-plane motion.

2.4.1.1 *In-Plane ROEs.* The two ROEs most easily derived are the radial and in-track displacements. Examining the HCW expressions for the motion in these two directions

$$\begin{aligned} x &= \frac{\dot{x}_0}{n} \sin \theta - \left(3x_0 + \frac{2\dot{y}_0}{n} \right) \cos \theta + \left(4x_0 + \frac{2\dot{y}_0}{n} \right) \\ y &= \left(6x_0 + \frac{4\dot{y}_0}{n} \right) \sin \theta + \frac{2\dot{x}_0}{n} \cos \theta - (6nx_0 + 3\dot{y}_0)t + \left(y_0 - \frac{2\dot{x}_0}{n} \right) \end{aligned} \quad (2.36)$$

it remains obvious that the x expression is oscillatory with the exception of an offset term, and that the y expression is oscillatory with the exception of an offset and a secular term. These offsets are defined as the radial and in-track displacements such that

$$\begin{aligned} x_d &= \left(4x_0 + \frac{2\dot{y}_0}{n} \right) \\ y_d &= -(6nx_0 + 3\dot{y}_0)t + \left(y_0 - \frac{2\dot{x}_0}{n} \right) \end{aligned} \quad (2.37)$$

Letting the constant term $(y_0 - \frac{2\dot{x}_0}{n}) = y_{d0}$, and recognizing that the expression for y_d is a linear combination of x_d , it is then found that the displacements can be written as

$$\begin{aligned} x_d &= 4x_0 + \frac{2\dot{y}_0}{n} \\ y_d &= y_{d0} - \frac{3}{2}nx_d(t - t_0) \end{aligned} \quad (2.38)$$

To determine the magnitude of the oscillatory in-plane motion, one can apply the Hamonic Addition Theorem (or the linear combination of trigonometric functions), which states that a function written as

$$f = A \sin \theta + B \cos \theta \quad (2.39)$$

can be written in the following two manners

$$\begin{aligned} f &= \sqrt{A^2 + B^2} \sin \left(\theta + \tan^{-1} \left(\frac{B}{A} \right) \right) \\ f &= -\sqrt{A^2 + B^2} \cos \left(\theta + \tan^{-1} \left(\frac{A}{-B} \right) \right) \end{aligned} \quad (2.40)$$

Applying Eq. 2.40 to the radial motion in Eq. 2.36, and letting $A = \frac{\dot{x}_0}{n}$ and $B = -(3x_0 + \frac{2\dot{y}_0}{n})$, we see that

$$x = -\sqrt{\left(\frac{\dot{x}_0}{n}\right)^2 + \left(3x_0 + \frac{2\dot{y}_0}{n}\right)^2} \cos \left(\theta + \tan^{-1} \left(\frac{\frac{\dot{x}_0}{n}}{(3x_0 + \frac{2\dot{y}_0}{n})} \right) \right) + x_d \quad (2.41)$$

For simplicity, the constant phasing parameter β_0 can now be defined as

$$\beta_0 = \tan^{-1} \frac{\frac{\dot{x}_0}{n}}{(3x_0 + \frac{2\dot{y}_0}{n})} \quad (2.42)$$

Rewriting the radial motion using $C = \sqrt{\left(\frac{\dot{x}_0}{n}\right)^2 + \left(3x_0 + \frac{2\dot{y}_0}{n}\right)^2}$ such that

$$x = -C \cos(\theta + \beta_0) \quad (2.43)$$

The argument in the cosine function can also be reduced using $\beta = \theta + \beta_0$, providing the final radial expression

$$x = -C \cos \beta \quad (2.44)$$

Having a simplified expression for the radial motion, the in-track motion can be simplified in the same manner. Applying Eq. 2.40 to the in-track expression, and letting $A = (6x_0 + \frac{4\dot{y}_0}{n})$ and $B = (\frac{2\dot{x}_0}{n})$, it follows that

$$y = 2\sqrt{\left(\frac{\dot{x}_0}{n}\right)^2 + \left(3x_0 + \frac{2\dot{y}_0}{n}\right)^2} \sin \left(\theta + \tan^{-1} \left(\frac{\frac{\dot{x}_0}{n}}{(3x_0 + \frac{2\dot{y}_0}{n})} \right) \right) \quad (2.45)$$

Substituting the phase and dummy magnitudes,

$$y = 2C \sin \beta \quad (2.46)$$

Thus it follows that the in-track motion oscillates orthogonal to the radial motion at twice the magnitude. This corresponds to the definition of a 2:1 ellipse with the semi-major axis on the in-track axis. The in-plane ROEs have now been described and are summarized below, removing the subscripts other than on the initial ROEs:

$$\begin{aligned} a_e &= 2\sqrt{\left(\frac{\dot{x}}{n}\right)^2 + \left(3x + \frac{2\dot{y}}{n}\right)^2} \\ x_d &= 4x + \frac{2\dot{y}}{n} \\ y_d &= y_{d0} - \frac{3}{2}nx_d(t - t_0) \\ \beta &= \theta + \tan^{-1}\left(\frac{\dot{x}}{3nx + 2\dot{y}}\right) = \theta + \beta_0 \end{aligned} \quad (2.47)$$

where $\theta = n(t - t_0)$. The transformation to Cartesian position coordinates was also found, while the velocity coordinates are simply the time derivatives

$$\begin{aligned} x &= -\frac{a_e}{2} \cos \beta + x_d \\ y &= a_e \sin \beta + y_d \\ \dot{x} &= \frac{a_e n}{2} \sin \beta \\ \dot{y} &= a_e n \cos \beta - \frac{3n}{2}x_d \end{aligned} \quad (2.48)$$

2.4.1.2 Out-of-Plane ROEs. As the out-of-plane motion is uncoupled from the in-plane, only two parameters (other than the mean motion and time) are needed to fully describe the motion. Examining the cross-track position

$$z = z_0 \cos \theta + \frac{\dot{z}_0}{n} \sin \theta \quad (2.49)$$

it is fairly obvious the motion is solely sinusoidal with no offset. Directly applying the Harmonic Addition Theorem to Eq. 2.49, and letting $A = \frac{\dot{z}_0}{n}$ and $B = z_0$, the cross-track motion is written as

$$z = \sqrt{\left(\frac{\dot{z}_0}{n}\right)^2 + z_0^2} \sin\left(\theta + \tan^{-1}\left(\frac{z_0}{\frac{\dot{z}_0}{n}}\right)\right) \quad (2.50)$$

Similar to the in-plane motion, initial and current phase angles (ψ_0, ψ) can be defined such that

$$\begin{aligned} \psi_0 &= \tan^{-1} \frac{z_0 n}{\dot{z}} \\ \psi &= \theta + \psi_0 \end{aligned} \quad (2.51)$$

and the cross track motion reduces to

$$z = \sqrt{\left(\frac{\dot{z}_0}{n}\right)^2 + z_0^2} \sin \psi \quad (2.52)$$

The z motion has now been reduced to a simple sinusoid, with an amplitude of

$$z_{max} = \sqrt{\left(\frac{\dot{z}_0}{n}\right)^2 + z_0^2} \quad (2.53)$$

The cross-track motion can now be specified as

$$z = z_{max} \sin \psi \quad (2.54)$$

Consequently, the two ROEs describing the cross-track motion can be described as

$$\begin{aligned} z_{max} &= \sqrt{\left(\frac{\dot{z}_0}{n}\right)^2 + z_0^2} \\ \psi &= \theta + \psi_0 = \theta + \tan^{-1}\left(\frac{z_0 n}{\dot{z}}\right) \end{aligned} \quad (2.55)$$

where $\theta = n(t - t_0)$. The inverse transformation to Cartesian coordinates is

$$\begin{aligned} z &= z_{max} \sin \psi \\ \dot{z} &= z_{max} n \cos \psi \end{aligned} \tag{2.56}$$

2.4.2 System Behavior. The time evolution of the relative orbit elements is of significant importance to this study. The linear time invariant system effected by the HCW assumptions yields an elegant time history for the ROEs. However, when this parameterization is applied to a perturbed environment or an elliptical chief, there is no reason to expect the response to remain the same.

Immediately from the expressions for the radial and in-track motion, the expression for a_e remains constant over time. Also from the radial motion, the radial displacement remains constant over time. The in-track motion will drift at a rate of

$$\begin{aligned} \dot{y}_d &= -\frac{3n}{2}x_d \\ &= -\frac{3n}{2}x_{d0} \end{aligned} \tag{2.57}$$

which can now be utilized for a boundedness condition. If $x_{d0} = 0$, Eq. 2.57 reduces to zero, and the relative ellipse will remain stationary. The phase angle β increases linearly with time from the initial state β_0 by an amount proportional to the mean motion of the chief. The cross-track ROEs follow a similar analysis. The maximum cross-track amplification remains at a fixed value, and the cross-track phasing behaves similarly to the in-plane phasing.

The significance of the ROE parameterization is that the relative motion of the deputy can be found as an instantaneous elliptical path that is centered at $(x_d, y_d, 0)$ [33]. If the relative orbit is drifting, it will drift linearly as specified by the expression for y_d . The phase angle β is related to the angular position to the deputy in the relative orbit. The cross-track motion intersects the LVLH frame of the chief when

the phasing is an integer multiple of π , and it takes on the value of z_{max} and $-z_{max}$ when the sine function is maximized ($\psi = \pi/2, 3\pi/2$, respectively).

If the angle $\gamma = \psi - \beta$ is used as the constant phase difference between the cross-track and in-plane motion, then the cross-track expressions can be written as

$$\begin{aligned} z &= z_{max} \sin(\gamma + \beta) \\ \dot{z} &= z_{max} n \cos(\gamma + \beta) \end{aligned} \tag{2.58}$$

and the only time-varying ROEs are β and y_d , both of which change linearly with time.

2.4.3 Summary. To summarize the ROEs, analytical expressions for the time history is provided as detailed in Lovell [33], as well as the Cartesian conversion. The ROEs can be converted from Cartesian coordinates as

$$\begin{aligned} a_e &= 2\sqrt{\left(\frac{\dot{x}}{n}\right)^2 + \left(3x + \frac{2\dot{y}}{n}\right)^2} \\ x_d &= 4x + \frac{2\dot{y}}{n} \\ y_d &= y - \frac{2\dot{x}}{n} \\ \beta &= \tan^{-1}\left(\frac{\dot{x}}{3nx + 2\dot{y}}\right) \\ z_{max} &= \sqrt{\left(\frac{\dot{z}}{n}\right)^2 + z^2} \\ \psi &= \tan^{-1}\left(\frac{nz}{\dot{z}}\right) \end{aligned} \tag{2.59}$$

The set \mathbf{R} is now defined for future use as $\mathbf{R} = [a_e, x_d, y_d, \beta, z_{max}, \psi]$. The time evolution of the ROEs is

$$\begin{aligned}
a_e &= a_{e0} \\
x_d &= x_{d0} \\
y_d &= y_{d0} - \frac{3n}{2}x_d t \\
\beta &= \beta_0 + nt \\
z_{max} &= z_{max0} \\
\psi &= \psi_0 + nt
\end{aligned} \tag{2.60}$$

The Cartesian conversion is

$$\begin{aligned}
x &= -\frac{a_e}{2} \cos \beta + x_d \\
y &= a_e \sin \beta + y_d \\
z &= z_{max} \sin \psi \\
\dot{x} &= \frac{a_e}{2} n \sin \beta \\
\dot{y} &= a_e n \cos \beta - \frac{3}{2} n x_d \\
\dot{z} &= z_{max} n \cos \psi
\end{aligned} \tag{2.61}$$

A visualization of the the in-plane ROEs is provided in Fig. 2.4 with β^* serving as the physical interpretation of the phase angle.

A visualization of the out-of-plane ROEs is provided in Fig. 2.5 with γ^* serving as the in-plane physical interpretation of the relative ascending node.

2.5 Theoretical Impacts of Eccentricity and J_2 on the Relative Trajectory

Before delving into the analytical and numeric results, the following sections present the actual impacts expected in the analytics. The effect of chief eccentricity is explored. The J_2 perturbation is initially surveyed, and its application as a perturbing

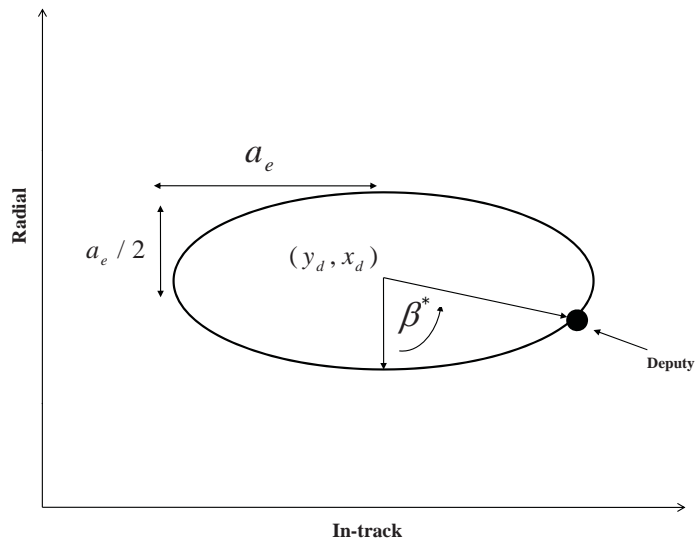


Figure 2.4: Visualization of the In-Plane Relative Orbit Using ROEs

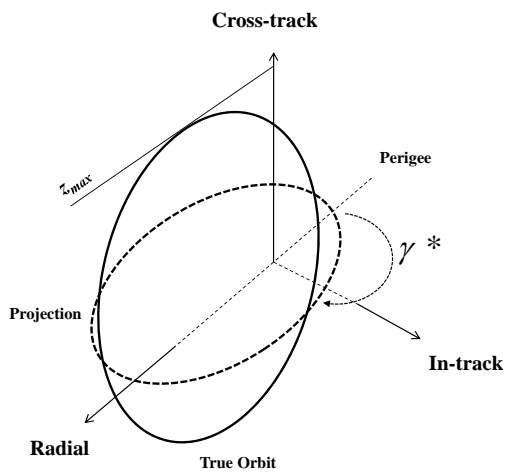


Figure 2.5: Visualization of the Out-of-Plane Relative Orbit Using ROEs

force on relative motion detailed. It should be noted that the combination of both eccentricity and J_2 will induce non-linear combinations of the impacts described in this section.

2.5.1 The Impact of a Non-Circular Chief Orbit on Relative Motion. Jiang, et. al. [34] investigated the unperturbed first-order relative motion to a significant degree using algebraic methods. It was concluded that the radial/in-track projection of the orbit may have no more than one self-intersection per orbit, and that the in-track/cross-track and radial/cross-track may intersect no more than two times per orbit. Another significant conclusion made is that the general three-dimensional motion is only planar for degenerate, unrealistic cases. The relative motion was found to rest on three quadric surfaces: a hyperboloid of one-sheet, an elliptic cone, or an elliptic cylinder. Sengupta [35] utilizes the solution to the Tschauner and Hempel equations and expands the in-track and cross-track components as a Fourier series to examine the effects of eccentricity. Using both true anomaly and time as independent variables, Sengupta expands the motion using Cauchy residue theory to be functions of constants, a dominant harmonic, size parameters, and high-order harmonics. Sengupta notes five significant eccentricity effects due to the expansion using true anomaly:

1. The presence of high-order harmonics in the motion is the primary mode of the deviation from the 2×1 trajectory.
2. The amplitude of the primary harmonic is scaled by the eccentricity, which results in a cross-track expansion and in-track decrease as eccentricity is increased.
3. A phase shift is induced to the sinusoids of the HCW including terms of (e^2, e^4, e^6, \dots) . Ignoring the higher order eccentricity terms yields the original phase.
4. Constant terms displace the center of the relative orbit, and is dependent on the initial in-plane and out-of-plane phasing.

5. The relative orbit plane is skewed by the higher order harmonics. Most notably, the plane of symmetry of the cross-track motion that is normal to the in-track trajectory is skewed as a function of the eccentricity.

Sengupta's expansion in time exhibits the same quantitative effects as the true anomaly expansion.

2.5.2 The Impact of the J_2 Perturbation.

2.5.2.1 Background on the J_2 Perturbation. Motion about a spherical central body dictates a constant attraction at a given range with no regard to angular location. This spherical, point-mass assumption leads to an inverse square gravity field. Oblateness effects such as the equatorial will dramatically modify the gravitational attraction, and for an arbitrary body the differential specific gravitational potential acting on a point A can be expressed as [30]

$$dV = -\frac{Gdm}{s} \quad (2.62)$$

with G as the universal gravitational constant, dm as a differential mass on the body, and s is the magnitude of the position vector between the differential mass and A . Following the introduction of Legendre polynomials, it is well documented that the gravitational potential field on a body can be expressed as ([30], [31])

$$V = -\frac{Gm}{r} - \frac{G}{r} \sum_{k=1}^{\infty} \int \int \int_B \left(\frac{\rho}{r}\right)^k P_k(\cos \gamma) dm \quad (2.63)$$

where r is the norm of the position vector from the body centroid to the point A , ρ is the norm of the position vector from the body centroid to the dm , γ is angle between ρ and r , and P_k is the Legendre polynomial such that

$$P_{n+1}(\nu) = \frac{2n+1}{n+1} \nu P_n(\nu) - \frac{n}{n+1} P_{n-1}(\nu) \quad (2.64)$$

The Legendre polynomials have zero mean and are orthogonal to one another.

A change of coordinates from Cartesian to spherical will result in an infinite series that expresses the gravitational potential in terms of spherical harmonics. Rather than expressing it as Eq. 2.63, the gravitational potential can eventually be written as

$$V(r, \phi) = -\frac{\mu}{r} \left(1 - \sum_{k=2}^{\infty} \left(\frac{r_{eq}}{r} \right)^k J_k P_k(\sin \phi) \right) \quad (2.65)$$

where J_k is the zonal gravitational harmonic, r_{eq} is the equatorial radius, and ϕ locates the position vector vertically from the equatorial plane. Determination of the zonal harmonics is typically done via an estimation algorithm extracted from observations. The value for the J_2 harmonic has a value of 1082.63×10^{-6} [30].

Now, using the classical orbital elements $a, e, i, \Omega, \omega, M_0$, numerous partial derivatives and extensive use of Lagrangian mechanics will yield Lagrange's planetary equations, presented in Eq. 2.66 using Schaub's [30] notation but placed in matrix form.

$$\begin{bmatrix} \dot{\Omega} \\ \dot{i} \\ \dot{\omega} \\ \dot{a} \\ \dot{e} \\ \dot{M}_0 \end{bmatrix} = \begin{bmatrix} 0 & \frac{1}{nab \sin i} & 0 & 0 & 0 & 0 \\ -\frac{1}{nab \sin i} & 0 & \frac{\cos i}{nab \sin i} & 0 & 0 & 0 \\ 0 & \frac{\cos i}{nab \sin i} & 0 & 0 & \frac{b}{na^3 e} & 0 \\ 0 & 0 & 0 & 0 & 0 & \frac{2}{na} \\ 0 & 0 & -\frac{b}{na^3 e} & 0 & 0 & \frac{b^2}{na^4 e} \\ 0 & 0 & 0 & -\frac{2}{na} & -\frac{b^2}{na^4 e} & 0 \end{bmatrix} \begin{bmatrix} \frac{\partial R}{\partial \Omega} \\ \frac{\partial R}{\partial i} \\ \frac{\partial R}{\partial \omega} \\ \frac{\partial R}{\partial a} \\ \frac{\partial R}{\partial e} \\ \frac{\partial R}{\partial M_0} \end{bmatrix} \quad (2.66)$$

where a and b are the semi-major and semi-minor axes, and R is the the disturbance potential, which is now known from the spherical harmonic gravitational potential in Eq. 2.65. Truncating the disturbance potential at the dominant second harmonic, R becomes

$$R(\mathbf{r}) = -\frac{J_2 \mu}{2 r} \left(\frac{r_{eq}}{r} \right)^2 (3 \sin^2 \phi - 1) \quad (2.67)$$

A change of variables ($\sin \phi = \sin(\omega + \nu) \sin i$) then allows to disturbance potential to be written as

$$R(\mathbf{r}) = -\frac{J_2 \mu}{2 r} \left(\frac{r_{eq}}{r} \right)^2 (3(\sin(\omega + \nu) \sin i)^2 - 1) \quad (2.68)$$

Taking the gradient of Eq. 2.68, the osculating time rates of the orbital elements can be found from the matrix multiplication in Eq. 2.66. The J_2 perturbation induces both short and long term periodic effects, in addition to secular drift rates. For relative motion, it is typically assumed that the differences in the short and long term variations in the chief and deputy are negligible. Thus, it is the secular time rate that is the primary perturbation in relative motion. An orbit-average of Lagrange's planetary equations using the J_2 disturbance yields the following mean orbital element drift rates in Eq. (2.69 [31]).

$$\begin{aligned}
\dot{\bar{\Omega}} &= -\frac{3}{2} J_2 n \left(\frac{r_{eq}}{p} \right)^2 \cos i \\
\dot{\bar{i}} &= 0 \\
\dot{\bar{\omega}} &= \frac{3}{4} J_2 n \left(\frac{r_{eq}}{p} \right)^2 (5 \cos^2 i - 1) \\
\dot{\bar{a}} &= 0 \\
\dot{\bar{e}} &= 0 \\
\dot{\bar{M}}_0 &= \frac{3}{4} J_2 n \left(\frac{r_{eq}}{p} \right)^2 \sqrt{1 - e^2} (3 \cos^2 i - 1) + n
\end{aligned} \tag{2.69}$$

where the barred quantities indicate mean elements.

The resulting orbit averaged COEs make intuitive sense. Using conservation of energy arguments, the semi-major axis can be shown to vary only periodically [31]. Inherent in the construction of spherical harmonics is the assumption of an axially symmetric central body; this implies that the angular momentum about the polar axis is a constant. If the inclination varied secularly from J_2 , at one point this term would equate to zero, which also directly implies that the eccentricity can only vary periodically.

2.5.2.2 Effect on Relative Motion. Short period effects of J_2 induce small oscillations in the orbit elements, but do not contribute to the orbital drift [30], as errors from short period can be expected on the order of 50-100 m [31] and nearly

identical between the chief and deputy. The long period effect is the rotation of apsides and will have a near negligible difference between the chief and the deputy for close proximity operations.

To better understand what effects will occur from the perturbations, the linear transformation from orbital elements to the Hill frame (presented in [30]) is examined. The radial displacement is merely the difference in the two orbital radii. From the two-body trajectory relation, the orbital radii are functions of a , e , and true anomaly. Using mean orbital elements, the mean change in the radial direction will be unaffected by a and e oscillations, but will be impacted by the mean anomaly difference (which obviously corresponds to a true anomaly difference) [30]. The in-track and cross-track motions are functions of the chief's orbital radius, inclination, and true latitude, and also are functions of the differences in the true latitude, inclination, and right ascension of the ascending node. Greater variations are to be expected in these components as the mean rates impact this motion significantly.

Schweighart [36] provides a well-rounded discussion concerning where the J_2 effect would manifest itself in the relative trajectory, but it is primarily for circular reference orbits. The variance in the ascending node modifies the amplitude of the cross-track motion. Schweighart compares the cross-track relation to a "scissoring effect" [36] in that as the scissors are opened, the intersection of the blade tips quickly moves towards the handle, but opening further decreases the rate of the intersection. The blades correspond to the orbital planes and their movement due to secular drift in the ascending node. The rotation of the apsides moves the location of closest approach, modifying the period and minima locations of the radial and in-track components. This change impacts the periodicity of the radial and in-track motion in addition to modifying the period of the reference orbit. A similar effect is found from the secular change of the mean anomaly which also modifies the period of the reference orbit.

The orbital element rate of the mean anomaly and argument of perigee can be collapsed to a drift in the mean argument of latitude ($\dot{\theta} = \dot{M} + \dot{\omega}$). The difference

between the two $\dot{\theta}$ values will result in in-plane angular deviation. The differences in $\dot{\Omega}$ will lead to cross-track amplification. To maintain a static relative orbit, initial conditions can be made to construct invariant orbits based on equating the secular drift of the latitude and ascending node.

III. Description of Applied Models and Methodology

As a means to provide clarity on the state transition matrices and models applied throughout the remainder of this study, the following sections will present in detail the methodology and results of the applied models. The Gim-Alfriend, Yamanaka-Ankersen, Schweighart-Sedwick, and numerically integrated truth model will be discussed in detail. The application of each model to this study is then discussed. The processes used to perform the operational mapping, stationary orbit initialization, and the guidance algorithm are also discussed.

3.1 Applied Models

The following section details the propagation in the Gim-Alfriend, Yamanaka-Ankersen, and Schweighart-Sedwick relative motion models. The Gim-Alfriend and Yamanaka-Ankersen systems are presented in closed form, while the Schweighart-Sedwick system is given initially as a set of differential equations that are later solved by the author.

3.1.1 Gim-Alfriend. The Gim-Alfriend model [8] is a geometric method to determine the relative motion dynamics to include both chief eccentricity and the J_2 effect. The model uses the non-singular orbital elements defined as the set $\mathbf{e} = (a, \theta, i, q_1, q_2, \Omega)^T$, where a is the semi-major axis, i is the inclination, θ is the argument of latitude, and Ω is the right ascension of the ascending node. The parameters q_1 and q_2 are defined as

$$\begin{aligned} q_1 &= e \cos \omega \\ q_2 &= e \sin \omega \end{aligned} \tag{3.1}$$

where e is the eccentricity, and ω is the argument of periapsis. Using the argument of true latitude and the $q_{(\cdot)}$ parameters avoids singularities as true anomaly and the argument of perigee are undefined for circular orbits. For higher accuracy, the use of curvilinear coordinates is used as discussed in Section 2.2.3.

The GA model provides a STM to propagate the Cartesian initial conditions forward using either osculating or mean orbital elements. Using the GA verbiage, the propagation goes as

$$\mathbf{X}(t) = [A(t) + \alpha B(t)]\delta\mathbf{e}(t) \quad (3.2)$$

where A is the unperturbed transformation from orbital elements to Cartesian coordinates, B is transformation from orbital elements to Cartesian coordinates containing J_2 terms, α is equal to $3J_2R_e^2$, R_e is the radius of the Earth, and $\delta\mathbf{e}(t)$ is the instantaneous orbital element differences ($\delta\mathbf{e} = \mathbf{e}_d - \mathbf{e}_c$). The vector $\delta\mathbf{e}(t)$ is propagated as

$$\delta\mathbf{e}(t) = \phi_e(t, t_0)\delta\mathbf{e}(t_0) \quad (3.3)$$

where ϕ_e is the state transition matrix for orbital element differences. The propagation from Cartesian initial conditions to the current Cartesian state is thus

$$\begin{aligned} \mathbf{X}(t) &= \Phi_{J_2}(t, t_0)\mathbf{X}(t_0) \\ \Phi_{J_2} &= [A(t) + \alpha B(t)]\phi_e(t, t_0)[A(t_0) + \alpha B(t_0)]^{-1} \end{aligned} \quad (3.4)$$

This is the point at which the model splits between the use of osculating orbital elements and mean orbital elements. If mean orbital elements are used, the Φ_{J_2} state transition matrix is expressed as $\bar{\Phi}_{J_2}$ such that

$$\begin{aligned} \mathbf{X}(t) &= \bar{\Phi}_{J_2}(t, t_0)\mathbf{X}(t_0) \\ \bar{\Phi}_{J_2} &= [\bar{A}(t) + \alpha\bar{B}(t)]\bar{\phi}_e(t, t_0)[\bar{A}(t_0) + \alpha\bar{B}(t_0)]^{-1} \end{aligned} \quad (3.5)$$

In Eq. 3.5, \bar{A} is equivalent to A ; however, osculating elements invoke a different angular velocity and $\bar{B} \neq B$.

If osculating elements are to be used, the propagation goes as

$$\begin{aligned} \mathbf{X}(t) &= \Phi_{J_2}(t, t_0)\mathbf{X}(t_0) \\ \Phi_{J_2} &= [A(t) + \alpha B(t)]D(t)\bar{\phi}_e(t, t_0)D^{-1}(t_0)[A(t_0) + \alpha B(t_0)]^{-1} \end{aligned} \quad (3.6)$$

where the D matrix is the Jacobian of the osculating orbital elements with respect to the mean orbital elements. That is

$$D(t) = \frac{\partial \mathbf{e}_{osc}}{\partial \mathbf{e}_{mean}} \quad (3.7)$$

which includes the short and long period oscillations in the osculating classical orbital elements. The members of these matrices are entirely too cumbersome to list here and are detailed in the appendices of [8].

Assumptions inherent in the GA model are close proximity between the chief and deputy, equivalent drag effects, and the only perturbation to Keplerian motion is the J_2 effect.

3.1.2 Yamanaka-Ankersen. The Yamanaka-Ankersen (YA) model provides a state transition matrix mapping Cartesian initial conditions to a current Cartesian state [6]. The model remains as a first order linearization, but presents a closed form solution. Following a derivation similar to the HCW construction, the differential equations of relative motion as presented in the YA verbiage are

$$\begin{bmatrix} \ddot{x} \\ \ddot{y} \\ \ddot{z} \end{bmatrix} = \begin{bmatrix} -k\omega^{3/2}x + 2\omega\dot{z} + \dot{\omega}z + \omega^2x \\ -k\omega^{3/2}y \\ 2k\omega^{3/2}z - 2\omega\dot{x} - \dot{\omega}x + \omega^2z \end{bmatrix} + \mathbf{a}_f + \mathbf{a}_{cd} + \mathbf{a}_{dd} \quad (3.8)$$

where ω is the angular rate of the chief, x, y, z are the Cartesian relative motion coordinates, $k = \mu/h^{3/2}$, \mathbf{a}_f is an applied force, and $\mathbf{a}_{cd}, \mathbf{a}_{dd}$ are the perturbing forces on the chief and deputy. The Cartesian coordinates differ from the reference frame explained in Section 2.2.2. The previous development has x, y, z representing the radial, in-track, and cross-track motion; compared to this, the YA model places its x, y, z as the in-track, negative cross-track, and negative radial. Later, matrices of 1's and 0's will be used for model agreement. Assuming unforced and unperturbed

conditions, the differential equations can be simplified as

$$\begin{aligned}
\rho x'' - 2e \sin \theta x' - e \cos \theta x &= 2\rho z' - 2e \sin \theta z \\
\rho y'' - 2e \sin \theta y' &= -y \\
\rho z'' - 2e \sin \theta z' - (3 + e \cos \theta)z &= -2\rho x' + 2e \sin \theta x
\end{aligned} \tag{3.9}$$

where the prime superscript indicates differentiation with respect to the true anomaly of the chief, θ is the true anomaly of the chief, and $\rho = 1 + e \cos \theta$. A solution is derived that contains the same integral as Eq. 2.2, which was historically left in integral form until the Yamanaka-Ankersen development. The YA proposal is that constant angular momentum allows the time rate of change of the true anomaly to be expressed as

$$\frac{d\theta}{dt} = k^2 \rho^2 \tag{3.10}$$

which eventually yields the expression

$$k^2(t - t_0) = J(\theta) \tag{3.11}$$

where $J(\theta)$ is the integral from Eq. 2.2. Following a geometric interpretation of the relative motion and some matrix algebra to prove existence and uniqueness, a solution algorithm is proposed. Beginning with initial conditions in the LVLH frame, a transformation to a "tilde" space is made. The tilde space is non-physical and is transformed from LVLH space through multiplication by the eccentricity, true anomaly, and the integral J . These initial tilde conditions are then transformed into a set of "psuedoinitial" conditions that can then be propagated forward in the same space. The "psuedoinitial" conditions are found by evaluating the inverse of the STM evaluated at the initial time. These conditions can then be propagated forward in tilde space. The out-of-plane motion does not require the "psuedoinitial" transformation and is propagated solely in the tilde state.

Assumptions inherent in the YA model are close proximity between the chief and deputy, equivalent drag effects, and unperturbed Keplerian motion.

3.1.3 Schweighart-Sedwick.

3.1.3.1 Model Description. The Schweighart-Sedwick (SS) model [36] is perhaps one of the most applicable modes of this study. The SS system assumes a circular reference orbit, just as the assumption inherent in the ROE derivation. However, an orbit average of the J_2 perturbation is included as a perturbing force. The model is presented in closed form with initial conditions enforced to bound the orbit. Therefore, the SS model presents a method of initialization for a periodic orbit.

The derivation of the equations of motion is rather intuitive. The J_2 effect is inserted as an acceleration to a Newtonian second law formulation. Higher order terms are linearized with respect to the reference orbit, and a priori corrections are made to the reference orbit to account for the perturbation (including period matching, nodal drift correction, and cross-track motion correction). The model uses this to derive a set of constant coefficient, linear, ordinary differential equations that have a form rather similar to the HCW differential equations. The solutions presented in [37] are given in closed form. However, the desire is to express the ROEs as a function of any initial condition. The differential equations are derived as

$$\begin{aligned}
 \ddot{x} - 2ncy - (5c^2 - 2)n^2x &= 0 \\
 \ddot{y} + 2ncx &= 0 \\
 \ddot{z} + (3c^2 - 2)n^2z &= 0
 \end{aligned}
 \tag{3.12}$$

where x, y, z are the radial, in-track, and cross-track coordinates, n is the mean motion of the chief, and c is a constant incorporating the J_2 effect. For this study, Eq. 3.12 will be solved in closed form without enforcing initial conditions. The SS model

provides a periodic orbit of the following form (from [37])

$$\begin{aligned}
x &= x_0 \cos \theta + \frac{g}{2c} y_0 \sin \theta \\
y &= -\frac{2c}{g} x_0 \sin \theta + y_0 \cos \theta \\
z &= r\Phi \sin(\alpha - \gamma) \\
\Phi &= \Phi_0 \cos \gamma_0 \sec \gamma \\
\gamma &= \tan^{-1}(\epsilon + \tan \gamma_0)
\end{aligned} \tag{3.13}$$

where θ is a modified time-varying in-plane phasing, α is a modified orbital frequency, Φ is related to the cross-track amplification, γ is a cross-track phasing, and ϵ is a frequency related to the change in cross-track phasing. The various constants and coefficient definitions can be found in [37]. The values are primarily functions of the reference orbit inclination and are first order in J_2 . The in-plane phasing and initial conditions of HCW are slightly dampened, and the cross-track motion operates as a function of angular differences rather than the simple, uncoupled harmonic oscillator. The differential equations in Eq. 3.12 will be solved later.

Assumptions inherent in the SS model are close proximity between the chief and deputy, equivalent drag effects, a circular chief or orbit, and the only perturbation to Keplerian dynamics is the J_2 effect.

3.1.4 Numerically Integrated Truth Model. To construct a foundation for comparison of the true motion for both Keplerian and perturbed motion, a numerical integration is employed in Matlab using the ode45 function (a one-step solution using the Dormand-Prince pair of the Runge-Kutta family of integrators). Initial inputs selected are the chief orbital elements $[a, e, i, \omega, \Omega, M]^T$ and the initial LVLH displacement ($\vec{\rho}$) and velocity ($\dot{\vec{\rho}}$). This section will describe the equations of motion for the J_2 case, and it is noted that the unperturbed motion can be simply obtained by setting J_2 to zero. Given the chief satellite orbital elements, a standard two-body formulation will yield the inertial position and velocity of the chief. The inertial position and

velocity of the deputy are then found through the following rotation

$${}^i\vec{r}_d = \mathbf{R}^{io}\vec{\rho} + {}^i\vec{r}_c \quad (3.14)$$

where the rotation matrix \mathbf{R}^{io} rotates a vector from the LVLH or orbital frame to the inertial frame, and is defined as

$$\mathbf{R}^{io} = \begin{bmatrix} \hat{o}_r & \hat{o}_\theta & \hat{o}_h \end{bmatrix} \quad (3.15)$$

whose column-vector components have been previously defined in Eq. 2.3. The inertial velocity of the deputy requires a Coriolis term in the rotation and is found as

$$\dot{{}^i\vec{r}}_d = \dot{{}^i\vec{r}}_c + \mathbf{R}^{io} \left(\dot{\vec{\rho}} + \vec{\omega}^{oi} \times \vec{\rho} \right) \quad (3.16)$$

with f having been previously defined as the chief true anomaly, and $\vec{\omega}^{oi}$ is the angular velocity of the orbital LVLH frame with respect to the inertial frame. Now having the inertial position and velocity of the chief and deputy, initial conditions are known for the integration. Simultaneous integration of Eq. 3.17 for both the chief and deputy allow for their states to be known at any time.

$$\ddot{\vec{r}} = -\frac{\mu}{r^3} + \nabla \mathbf{R}(\vec{r})_{J_2} \quad (3.17)$$

where $\mathbf{R}(\vec{r})_{J_2}$ is the J_2 disturbing function. Knowing the state at a time t , the relative position vector can be found as

$$\vec{\rho} = \mathbf{R}^{oi} (\vec{r}_d - \vec{r}_c) \quad (3.18)$$

where $\mathbf{R}^{oi} = \mathbf{R}^{ioT}$ and rotates from the inertial to the orbital LVLH frame. The relative velocity requires a cross term and is found as

$$\dot{\vec{\rho}} = \mathbf{R}^{oi} \left(\dot{\vec{r}}_d - \dot{\vec{r}}_c + \vec{\omega}^{io} \times (\vec{r}_d - \vec{r}_c) \right) \quad (3.19)$$

The J_2 effect, however, modifies the angular velocity of the LVLH frame slightly. Rather than just having its three-component as the time rate of the true anomaly, the angular velocity using mean orbital elements is found from Gim and Alfriend [8] as

$$\vec{\omega}^{oi} = \begin{pmatrix} \dot{\Omega} \sin \theta \sin i \\ \dot{\Omega} \cos \theta \sin i \\ \dot{\theta} + \dot{\Omega} \cos i \end{pmatrix} \quad (3.20)$$

where the mean orbital element time rates are detailed in Eq. 2.69.

Note that as expected for unperturbed motion, the time rates of the perturbed orbital elements are nulled and the angular velocity vector becomes

$$\vec{\omega}^{oi} = \begin{pmatrix} 0 \\ 0 \\ \dot{f} \end{pmatrix} \quad (3.21)$$

and Eq. 3.17 reduces to

$$\ddot{\vec{r}} = -\frac{\mu}{r^3} \quad (3.22)$$

and the previously mentioned rotations remain the same.

If it is desired to examine the relative motion outside the linearized regime the analytical models allow, the numerically integrated truth model allows for the selection of initial orbital elements for both the chief and deputy and the forward propagation.

3.2 Methodology

The following section details how the relative motion models are applied to the three phases of this study. The general transformations and propagations to derive the ROE expressions are described. Applications of ROEs are then described to include initialization of a bounded relative orbit based on ROEs, and a proposed guidance and navigation algorithm.

3.2.1 *Analytical Expressions for the Relative Orbit Elements.* Currently, expressions for the ROEs are known for the unperturbed circular chief. It is now desired to examine the behavior of the ROEs for a perturbed, circular chief and an unperturbed, elliptical chief. There is a further sub-division in this study between Cartesian and geometric representations. Let the transformation from Cartesian space to ROE space be denoted as

$$\begin{aligned}\mathbf{R}(t) &= \begin{bmatrix} a_e(t) & x_d(t) & y_d(t) & \beta(t) & z_{max}(t) & \psi(t) \end{bmatrix} \\ &= \Lambda(\mathbf{X})\end{aligned}\tag{3.23}$$

where \mathbf{X} is the Cartesian relative position and velocity states, and Λ represents a series of non-linear operations on the states. The analytical instantaneous states of the Yamanaka-Ankersen and Schweighart-Sedwick models will be substituted as the argument in the Λ transformation. The inverse transformation is now defined as $\mathbf{X} = \Lambda^{-1}\mathbf{R}(t)$. Consequently, this allows propagation of the initial relative orbit elements to any time following the transformation. The direct state substitution is employed for the unperturbed elliptical chief using the YA model; however, the cross-track motion of the Schweighart-Sedwick motion allows for a more intuitive expression for the out-of-plane relative orbit elements.

Expressing the states in terms of orbital element differences is a study investigated solely for the perturbed circular chief. The primary reasoning for this restriction is for the perturbed or two-body elliptical chief, the ROE expressions become exceedingly unwieldy. However, if the initial circular assumption is made in the linearized mapping between the Hill frame and orbital element differences [30], changes in the resulting expressions resulting from J_2 can be obtained rather elegantly. The perturbed orbital element differences will be taken from the Gim-Alfriend model. A chain rule approach will also be taken to examine the time rates of the circular ROEs under the J_2 effect.

3.2.2 Applications of Osculating Relative Orbit Elements. The following sections briefly detail the methodology in describing the applications of osculating ROEs.

3.2.2.1 Initialization of Relative Orbit Elements for Periodic Trajectories. Several methods exist (for example, Sabol [3], Schaub [30], and Sengupta [38]) to set the initial conditions of a formation to induce a stationary trajectory. The definition used in this study for a stationary orbit is that of a relative trajectory that repeats itself. For ideal Keplerian motion, the fundamental requirement for a static relative trajectory is equal periods for each body in the formation. This constraint equates to $\delta a = 0$ for unperturbed motion. Although the constraint remains the same, chief eccentricity complicates the expression when converted to Cartesian coordinates. Considering the J_2 perturbed environment, movement of the perigee and nodal regression modify the periodicity of the orbit. Schaub proposes a algorithm [30] for J_2 invariance that results in selection of either the differential inclination, eccentricity, or semi-major axes between the chief and deputy, and the initial differential ascending node, perigee, and mean anomalies calculated. Moreover, because of the first-order approximation of the J_2 invariance algorithm, there is slight long-term drift.

Initial conditions for the unperturbed elliptical chief will be transformed from the Cartesian LVLH frame to ROE conditions using an equal periodicity condition. The conditions will be validated using the Yamanaka-Ankersen derived ROEs. Bounding the perturbed circular orbit will use the Cartesian conditions set in the Schweighart-Sedwick model converted to ROE space. Validation will be used via the Schweighart-Sedwick derived ROEs.

3.2.2.2 Guidance and Navigation. Estimation of relative orbit elements also carries with it the connotation of guidance. As a means of showing the applicability of the ROEs, the eccentric ROE derivation will be used to determine an instantaneous impulse that can be used to control docking, rendezvous, and guidance. Expressions will be derived to numerically solve a set of non-linear equations for the

necessary velocity change to yield a desired end state. Assuming that the desired maneuver is a solvable problem, the calculated post-burn ROEs will be compared with the desired maneuver, along with the resulting trajectories.

IV. Osculating Relative Orbit Elements

The following sections detail the mathematical derivations necessary to obtain analytical expressions for the relative orbit elements with an eccentric chief and a perturbed circular chief. Section 4.1 details the derivation for the elliptical chief. Section 4.2 derives the closed form expressions of the J_2 perturbed osculating ROEs. Finally, Sec.4.3 details areas of applications for the ROEs using a guidance and navigation algorithm and, in addition, analytical expressions to initialize a bounded relative orbit.

4.1 The Non-Circular Chief

4.1.1 State Propagation. Yamanaka and Ankersen presents an algorithm for calculating relative satellite motion [6]. Before detailing the matrix multiplication, the verbiage used in the YA model is now introduced as

$$\begin{aligned}
 \rho &= 1 + e \cos \theta \\
 s &= \rho \sin \theta \\
 c &= \rho \cos \theta \\
 s' &= \cos \theta + e \cos 2\theta \\
 c' &= -(\sin \theta + e \sin 2\theta) \\
 J &= \frac{h}{p^2}(t - t_0)
 \end{aligned} \tag{4.1}$$

Here, θ is the true anomaly of the chief, p is the semi-latus rectum of the chief's orbit, and h is the chief orbital angular momentum. Given in [6], the in-plane motion can be propagated as

$$\begin{bmatrix} \tilde{x} \\ \tilde{z} \\ \tilde{v}_x \\ \tilde{v}_z \end{bmatrix} = \begin{bmatrix} 1 & -c \left(1 + \frac{1}{\rho}\right) & s \left(1 + \frac{1}{\rho}\right) & 3\rho^2 J \\ 0 & s & c & (2 - 3esJ) \\ 0 & 2s & 2c - e & 3(1 - 2esJ) \\ 0 & s' & c' & -3e(s'J + \frac{s}{\rho^2}) \end{bmatrix} \begin{bmatrix} \bar{x}_0 \\ \bar{z}_0 \\ \bar{v}_{x0} \\ \bar{v}_{z0} \end{bmatrix} \tag{4.2}$$

It is very important to note that the terms x, z, v_x, v_y terms are reported here using the YA LVLH frame. A conversion will be made later for model agreement. For the moment, the 4×4 matrix in Eq. 4.2 is denoted as Φ , such that $\tilde{X}_{ip} = \Phi \bar{X}_{ip0}$, with the in-plane YA states used as arguments in the unbolded vector X_{ip} . The tilde and bar accents denote transformed coordinates; however, the transformation is not a rotation but can be shown to be a product of matrix multiplication. Letting the Cartesian to tilde space transformation be denoted by \mathbf{H} , and the tilde to Cartesian transformation as \mathbf{H}^{-1} , the matrices are found by inspection of the YA model as

$$\mathbf{H} = \begin{bmatrix} \rho & 0 & 0 & 0 \\ 0 & \rho & 0 & 0 \\ -es & 0 & \frac{1}{k^2\rho} & 0 \\ 0 & -es & 0 & \frac{1}{k^2\rho} \end{bmatrix} \quad (4.3)$$

$$\mathbf{H}^{-1} = \begin{bmatrix} \frac{1}{\rho} & 0 & 0 & 0 \\ 0 & \frac{1}{\rho} & 0 & 0 \\ k^2es & 0 & k^2\rho & 0 \\ 0 & k^2es & 0 & k^2\rho \end{bmatrix}$$

such that

$$\begin{aligned} \tilde{X} &= \mathbf{H}X \\ X &= \mathbf{H}^{-1}\tilde{X} \end{aligned} \quad (4.4)$$

The barred coordinates are a function of the tilde coordinates. Allowing the transformation denoted by \mathbf{L} such that $\bar{X} = \mathbf{L}\tilde{X}$, the matrix \mathbf{L} is expressed as

$$\mathbf{L} = \frac{1}{1 - e^2} \begin{bmatrix} 1 - e^2 & 3es \left(\frac{1}{\rho} + \frac{1}{\rho^2} \right) & -es \left(1 + \frac{1}{\rho} \right) & -ec + 2 \\ 0 & -3s \left(\frac{1}{\rho} + \frac{e^2}{\rho^2} \right) & s \left(1 + \frac{1}{\rho} \right) & c - 2e \\ 0 & -3 \left(\frac{c}{\rho} + e \right) & c \left(1 + \frac{1}{\rho} \right) + e & -s \\ 0 & 3\rho + e^2 - 1 & -\rho^2 & es \end{bmatrix} \quad (4.5)$$

The final matrix multiplication for the in-plane motion then becomes

$$\begin{aligned}
X_{ip}(t) &= \mathbf{H}^{-1}(t)\tilde{X}_{ip}(t) \\
X_{ip}(t) &= \mathbf{H}^{-1}(t)\Phi(t, t_0)\bar{X}_{ip0} \\
X_{ip}(t) &= \mathbf{H}^{-1}(t)\Phi(t, t_0)\mathbf{L}(t_0)\tilde{X}_{ip0} \\
X_{ip}(t) &= \mathbf{H}^{-1}(t)\Phi(t, t_0)\mathbf{L}(t_0)\mathbf{H}(t_0)X_{ip0}
\end{aligned} \tag{4.6}$$

There now exists a single state transition matrix to propagate the initial conditions to a desired time for the in-plane motion. Using the YA defined STM, the out of plane motion is found more simply as a propagation in YA tilde coordinates. Letting the out-of-plane tilde to Cartesian transformation be denoted as \mathbf{H}_1 , the propagation goes as

$$X_{op} = \mathbf{H}_1^{-1}(t)\Phi_{op}(t, t_0)\mathbf{H}_1(t_0)X_{op0} \tag{4.7}$$

with the matrices defined as

$$\begin{aligned}
\Phi_{op}(t, t_0) &= \begin{bmatrix} c & s \\ -s & c \end{bmatrix}_{\theta-\theta_0} \\
\mathbf{H}_1^{-1}(t) &= \frac{1}{\rho\theta-\theta_0} \begin{bmatrix} \frac{1}{\rho} & 0 \\ k^2 e s & k^2 \rho \end{bmatrix} \\
\mathbf{H}_1(t_0) &= \begin{bmatrix} \rho & 0 \\ -e s & \frac{1}{k^2 \rho} \end{bmatrix}_{\theta-\theta_0}
\end{aligned} \tag{4.8}$$

where $\theta-\theta_0$ indicates that values in the matrix are calculated at the difference between the initial and current true anomaly of the chief. However, the Yamanaka-Ankersen model uses a coordinate system that does not agree with the nomenclature already established in the current study. The YA model labels its x, y, z coordinates as in-track, negative cross-track, and negative radial, counter to the current study's usage of x, y, z as radial, in-track, cross-track (X_{ROE}). This requires a multiplication of the initial conditions and end-state by a matrix of ones and zeros. Labeling this

'agreement' matrix as \mathbf{U} such that $X_{ROE} = \mathbf{U}X_{ya}$, the in-plane and out-of-plane portions are found by inspection as

$$\mathbf{U}_{ip} = \begin{bmatrix} 0 & -1 & 0 & 0 \\ 0 & 0 & 0 & -1 \\ 1 & 0 & 0 & 0 \\ 0 & 0 & 1 & 0 \end{bmatrix} \quad (4.9)$$

$$\mathbf{U}_{op} = \begin{bmatrix} -1 & 0 \\ 0 & -1 \end{bmatrix}$$

This conversion in matrix form is now seen as

$$\begin{bmatrix} x \\ y \\ \dot{x} \\ \dot{y} \end{bmatrix}_{ROE} = \begin{bmatrix} 0 & -1 & 0 & 0 \\ 0 & 0 & 0 & -1 \\ 1 & 0 & 0 & 0 \\ 0 & 0 & 1 & 0 \end{bmatrix} \begin{bmatrix} x \\ z \\ \dot{x} \\ \dot{z} \end{bmatrix}_{YA} \quad (4.10)$$

$$\begin{bmatrix} z \\ \dot{z} \end{bmatrix}_{ROE} = \begin{bmatrix} -1 & 0 \\ 0 & -1 \end{bmatrix} \begin{bmatrix} y \\ \dot{y} \end{bmatrix}$$

The final propagation in the nomenclature of the current study now goes as

$$\begin{aligned} X_{ip}(t) &= \mathbf{U}_{ip}\mathbf{H}^{-1}(t)\Phi(t, t_0)\mathbf{L}(t_0)\mathbf{H}(t_0)\mathbf{U}_{ip}^T X_{ip}(t_0) \\ X_{op}(t) &= \mathbf{U}_{op}\mathbf{H}_1^{-1}(t)\Phi_{op}(t, t_0)\mathbf{H}_1(t_0)\mathbf{U}_{op}^T X_{op0} \end{aligned} \quad (4.11)$$

where $X_{ip}(t) = [x \ y \ \dot{x} \ \dot{y}]^T$ and $X_{op}(t) = [z \ \dot{z}]^T$. The x, y, z triplet now denotes radial, in-track, and cross-track coordinates. Condensing Eq. 4.11, the expression can be written as

$$\begin{aligned} X_{ip}(t) &= \bar{\Phi}_{ip}(t, t_0)X_{ip}(t_0) \\ X_{op}(t) &= \bar{\Phi}_{op}(t, t_0)X_{op0} \end{aligned} \quad (4.12)$$

where $\bar{\Phi}_{ip}(t, t_0)$ is a 4×4 matrix propagating the in-plane trajectory, and $\bar{\Phi}_{op}(t, t_0)$ is a 2×2 matrix propagating the out-of-plane trajectory. Now having the state propagation, the relative orbit elements can now be solved for analytically.

4.1.2 Analytical Derivation of Relative Orbit Elements for the Unperturbed Noncircular Chief. Now we can derive the ROEs for the noncircular chief using the full matrix multiplication of Eq. 4.11. For now, the derivation will not make any assumptions on initial conditions (In Section 4.1.3, a perigee epoch assumption will be enforced and justified). To avoid cumbersome equations, the components of the state transition matrices in Eq. 4.11 will be expressed for the in-plane motion as

$$\begin{bmatrix} x \\ y \\ \dot{x} \\ \dot{y} \end{bmatrix} = \begin{bmatrix} A_{11} & \dots & \dots & A_{14} \\ \vdots & \ddots & & \vdots \\ \vdots & & \ddots & \vdots \\ A_{41} & \dots & \dots & A_{44} \end{bmatrix} \begin{bmatrix} x_0 \\ y_0 \\ \dot{x}_0 \\ \dot{y}_0 \end{bmatrix} \quad (4.13)$$

and for the out of plane motion as

$$\begin{bmatrix} z \\ \dot{z} \end{bmatrix} = \begin{bmatrix} C_{11} & C_{12} \\ C_{21} & C_{22} \end{bmatrix} \begin{bmatrix} z_0 \\ \dot{z}_0 \end{bmatrix} \quad (4.14)$$

The analytical expressions for the parameters $A_{11}, A_{12}, \dots, C_{22}$ can be found in Appendix C. However, it is important to note that the full expressions are very cumbersome and are extremely tedious to present analytically. Those components presented in the Appendix utilize an assumption of a perigee initial condition and epoch time of $t_0 = 0$. This is not without loss of applicability as is noted in Section 4.1.3. The following derivations are performed using generic A_{ij} components and is valid for both the full and assumed expressions.

4.1.2.1 *Initial ROE Propagation in lieu of the State Vector.* The

in-plane initial conditions expressed in terms of ROEs are

$$\begin{bmatrix} x_0 \\ y_0 \\ \dot{x}_0 \\ \dot{y}_0 \end{bmatrix} = \begin{bmatrix} -\frac{a_{e0}}{2} \cos \beta_0 + x_{d0} \\ a_{e0} \sin \beta_0 + y_{d0} \\ \frac{a_{e0}}{2} n \sin \beta_0 \\ a_{e0} n \cos \beta_0 - \frac{3}{2} n x_{d0} \end{bmatrix} \quad (4.15)$$

With respect to the ROEs, the non-phasing terms can be separated from the angular terms by inspection as

$$\begin{bmatrix} -\frac{a_{e0}}{2} \cos \beta_0 + x_{d0} \\ a_{e0} \sin \beta_0 + y_{d0} \\ \frac{a_{e0}}{2} n \sin \beta_0 \\ a_{e0} n \cos \beta_0 - \frac{3}{2} n x_{d0} \end{bmatrix} = \begin{bmatrix} -\frac{\cos \beta_0}{2} & 1 & 0 \\ \sin \beta_0 & 0 & 1 \\ \frac{n}{2} \sin \beta_0 & 0 & 0 \\ n \cos \beta_0 & -\frac{3n}{2} & 0 \end{bmatrix} \begin{bmatrix} a_{e0} \\ x_{d0} \\ y_{d0} \end{bmatrix} \quad (4.16)$$

Rewriting the initial Cartesian vector as Eq. 4.16 and substituting in Eq. 4.13, the in-plane state can be written as

$$\begin{bmatrix} x \\ y \\ \dot{x} \\ \dot{y} \end{bmatrix} = \begin{bmatrix} (A_{12} \sin \beta_0 - \frac{A_{11} \cos \beta_0}{2} + A_{14} n \cos \beta_0 + \frac{A_{13} n \sin \beta_0}{2}) & (A_{11} - \frac{3nA_{14}}{2}) & A_{12} \\ (A_{22} \sin \beta_0 - \frac{A_{21} \cos \beta_0}{2} + A_{24} n \cos \beta_0 + \frac{A_{23} n \sin \beta_0}{2}) & (A_{21} - \frac{3nA_{24}}{2}) & A_{22} \\ (A_{32} \sin \beta_0 - \frac{A_{31} \cos \beta_0}{2} + A_{34} n \cos \beta_0 + \frac{A_{33} n \sin \beta_0}{2}) & (A_{31} - \frac{3nA_{34}}{2}) & A_{32} \\ (A_{42} \sin \beta_0 - \frac{A_{41} \cos \beta_0}{2} + A_{44} n \cos \beta_0 + \frac{A_{43} n \sin \beta_0}{2}) & (A_{41} - \frac{3nA_{44}}{2}) & A_{42} \end{bmatrix} \begin{bmatrix} a_{e0} \\ x_{d0} \\ y_{d0} \end{bmatrix} \quad (4.17)$$

For simplicity, each component of Eq. 4.17 will be assigned to parameter B_{ij} to form the time varying matrix $\mathbf{B}(t)$ such that

$$\begin{bmatrix} x \\ y \\ \dot{x} \\ \dot{y} \end{bmatrix} = \mathbf{B}(t) \begin{bmatrix} a_{e0} \\ x_{d0} \\ y_{d0} \end{bmatrix} \quad (4.18)$$

Similar to the initial set-up of the in-plane motion, the out-of-plane state can be expressed as a function of the initial ROEs using the conversion

$$\begin{aligned} z_0 &= z_{max0} \sin \psi_0 \\ \dot{z}_0 &= z_{max0} n \cos \psi_0 \end{aligned} \quad (4.19)$$

Substituting Eq. 4.19 in Eq. 4.14, the cross-track state can be found as

$$\begin{bmatrix} z \\ \dot{z} \end{bmatrix} = \begin{bmatrix} C_{11} & C_{12} \\ C_{21} & C_{22} \end{bmatrix} \begin{bmatrix} z_{max0} \sin \psi_0 \\ z_{max0} n \cos \psi_0 \end{bmatrix} \quad (4.20)$$

Factoring out the z_{max0} term and multiplying the resulting inner matrices, a single multiplication can be found as

$$\begin{bmatrix} z \\ \dot{z} \end{bmatrix} = \begin{bmatrix} C_{11} \sin \psi_0 + C_{12} n \cos \psi_0 \\ C_{21} \sin \psi_0 + C_{22} n \cos \psi_0 \end{bmatrix} z_{max0} \quad (4.21)$$

and assigning each component of the matrix in Eq. 4.21 the parameter D_{ij} , the cross-track motion is now propagated as

$$\begin{bmatrix} z \\ \dot{z} \end{bmatrix} = \mathbf{D}(t) z_{max0} \quad (4.22)$$

4.1.2.2 State Substitution as Arguments in the Relative Orbit Element Expressions. Having expressions for the state as a function of initial ROEs, the propagated ROEs can now be found. The relative semi-major axis is found as

$$a_e = 2 \sqrt{\left(\frac{\dot{x}}{n}\right)^2 + \left(3x + \frac{2\dot{y}}{n}\right)^2} \quad (4.23)$$

Expanding the above expression becomes a rather tedious process. To gather enough information to observe the impact of the coefficients on the initial conditions, the expression for a_e is squared, expanded, and grouped according to the initial ROEs.

Foregoing the extensive algebra, the highly coupled end result is found as

$$a_e = \sqrt{\alpha_1 a_{e0}^2 + \alpha_2 x_{d0}^2 + \alpha_3 y_{d0}^2 + \alpha_4 x_{d0} y_{d0} + \alpha_5 a_{e0} x_{d0} + \alpha_6 a_{e0} y_{d0}} \quad (4.24)$$

where the values for the time-varying α coefficients are listed in Appendix C. Moreover, the derivations are given in further detail in Appendix B.

In contrast to the relative semi-major axis, the radial displacement is a linear combination of two Cartesian states. Expressing the radial displacement as

$$x_d = 4x + 2\frac{\dot{y}}{n} \quad (4.25)$$

state substitution yields after grouping like terms

$$x_d = \sigma_1 a_{e0} + \sigma_2 x_{d0} + \sigma_3 y_{d0} \quad (4.26)$$

where the values for the time-varying σ coefficients are listed in Appendix C.

Very similar to the radial-displacement and expressing y_d as $y_d = y - \frac{2\dot{x}}{n}$, the in-track displacement is also found as a function of time-varying coefficients as

$$y_d = \Sigma_1 a_{e0} + \Sigma_2 x_{d0} + \Sigma_3 y_{d0} \quad (4.27)$$

with the Σ expressions listed in Appendix C.

The in-plane phasing angle is expressed as

$$\beta = \tan^{-1} \left(\frac{\dot{x}}{3nx + 2\dot{y}} \right) \quad (4.28)$$

which in reality is the ratio of the two parenthetical components of the semi-major axis function. The in-plane phasing is found as

$$\beta = \tan^{-1} \left(\frac{B_{31} a_{e0} + B_{32} x_{d0} + B_{33} y_{d0}}{(3nB_{11} + 2B_{41}) a_{e0} + (3nB_{12} + 2B_{42}) x_{d0} + (3nB_{13} + 2B_{43}) y_{d0}} \right) \quad (4.29)$$

where the B coefficients have previously been defined from Eq. 4.17.

The out-of-plane phasing angle ψ is nonlinear in the arctangent function. The expression for ψ is

$$\psi = \tan^{-1} \left(\frac{nz}{\dot{z}} \right) \quad (4.30)$$

and after substitution it is found as

$$\psi = \tan^{-1} \left(\frac{nD_{11}}{D_{21}} \right) \quad (4.31)$$

where the D_{ij} terms are obtained from Eq. 4.22. The final ROE to examine is the cross-track amplification. Using the conversion

$$z_{max} = \sqrt{\left(\frac{\dot{z}}{n} \right)^2 + z^2} \quad (4.32)$$

which is found as a time-varying value as

$$z_{max} = z_{max0} \sqrt{\left(\frac{D_{21}}{n} \right)^2 + D_{11}^2} \quad (4.33)$$

To provide a summarization of the osculating ROEs with an eccentric chief, the following list is provided

$$\begin{aligned}
a_e &= \sqrt{\alpha_1 a_{e0}^2 + \alpha_2 x_{d0}^2 + \alpha_3 y_{d0}^2 + \alpha_4 x_{d0} y_{d0} + \alpha_5 a_{e0} x_{d0} + \alpha_6 a_{e0} y_{d0}} \\
\begin{bmatrix} x_d \\ y_d \end{bmatrix} &= \begin{bmatrix} \sigma_1 & \sigma_2 & \sigma_3 \\ \Sigma_1 & \Sigma_2 & \Sigma_3 \end{bmatrix} \begin{bmatrix} a_{e0} \\ x_{d0} \\ y_{d0} \end{bmatrix} \\
\beta &= \tan^{-1} \left(\frac{B_{31} a_{e0} + B_{31} x_{d0} + B_{33} y_{d0}}{(3nB_{11} + 2B_{41}) a_{e0} + (3nB_{12} + 2B_{42}) x_{d0} + (3nB_{13} + 2B_{43}) y_{d0}} \right) \\
\psi &= \tan^{-1} \left(\frac{nD_{11}}{D_{21}} \right) \\
z_{max} &= z_{max0} \sqrt{\left(\frac{D_{21}}{n} \right)^2 + D_{11}^2}
\end{aligned} \tag{4.34}$$

with the time-varying coefficients $\alpha_i, \sigma_i, \Sigma_i, B_{ij}$, and D_{ij} detailed in Appendix C.

4.1.3 Perigee Epoch Simplification. The time-varying coefficients of Eq. 4.34 are extremely cumbersome. To simplify the complicated coefficients, it is now assumed that the epoch time is equivalently zero ($t_0 = 0$), and that the true anomaly of the chief at epoch is perigee ($\theta_0 = 0$). The implication of this assumption is not in immediate disfavor of the model. From a deterministic standpoint and employment of a state transition matrix, knowledge of the state at any one time allows knowledge of the state any other time. For example, consider a set of relative navigation data at a time t that yields a relative state $X(t)$. From the fundamentals of state transition matrices given in Appendix A, the state at perigee at time t_p can be found as $X(t_p) = \Phi(t_p, t)X(t) = \Phi^{-1}(t, t_p)X(t)$, and the model reinitialized to $t = 0$ at the perigee time for model agreement presents little difficulty. The only spatial limitations on the initial conditions are those limited by the degree of accuracy in the linearization assumptions in the model.

The actual enforcement of the initial condition assumption allows for the \mathbf{L} and \mathbf{H} of Eq. 4.4 and Eq. 4.5 transformations to greatly simplify. However, the nature

of the derivation demands that the general form of Eq. 4.34 remains the same. The coefficients simplify significantly and are detailed in Appendix C.

4.1.4 Numerical Examples. To demonstrate the applicability of the osculating parameterization, the following numerical examples will demonstrate the accuracy of the method when applied to numerical integration of two-body (Keplerian) motion. The relative states are calculated analytically using the ROE parameterization and compared to the resulting integration. Stationary (repeating relative orbits) examples of varying eccentricity are given, followed by a drifting example. The stationary relative orbits are found using the conditions detailed in Appendix F. Initial conditions are given in the form $\mathbf{R}_0 = [a_{e0} \ x_{d0} \ y_{d0} \ \beta_0 \ z_{max0} \ \psi_0]$ with units of (km,rad) where appropriate, and the chief orbital elements are given in the form $\mathbf{e}_{c0} = [a \ e \ i \ \omega \ \Omega \ M_0]$ with units of (km,rad) as well.

4.1.4.1 Low-Eccentricity, Stationary Relative Orbit. Given the following initial conditions

$$\begin{aligned} \mathbf{R}_0 &= [3.4890 \ 0.1 \ 0.5 \ 0 \ 0.5 \ 0] \\ \mathbf{e}_{c0} &= [10000 \ 0.01 \ 0.5236 \ 0 \ 0 \ 0] \end{aligned} \tag{4.35}$$

The three-dimensional propagation using osculating ROEs as compared to the integration is shown in Fig. 4.1 By immediate inspection, the three-dimensional trajectory using the YA dynamics compares well with the numerical integration. Little skewness is observed in the out-of-plane motion, and the projected in-plane resembles a closed irregular conic.

Figure 4.2 provides a display of the in-plane ROEs as calculated through the derived equations compared to the HCW prediction. The x-axis is labeled as orbit fraction and represents the current time in the orbit divided by the nominal chief period. The ROEs for a circular chief predict a constant a_e and x_d ; however, using the eccentric chief parameterization shows a periodic a_e that coincidentally intersects

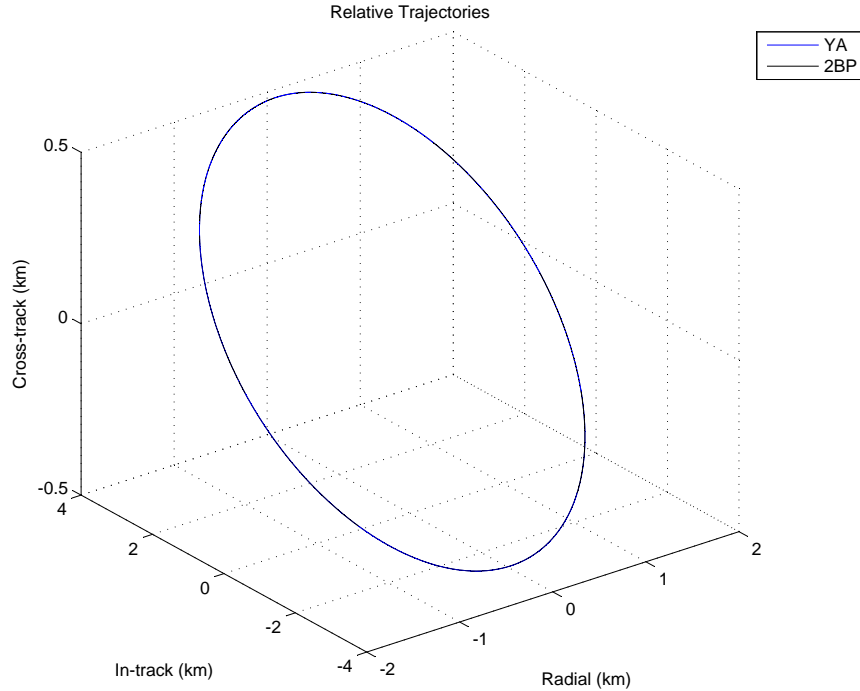


Figure 4.1: Three-Dimensional Relative Trajectory using Osculating ROEs Compared to Numerical Integration with Chief Eccentricity of 0.01

the HCW semi-major axis at perigee. The same condition is true for the radial displacement with a HCW coexistence at perigee. Using the HCW realization would introduce drift in this case, but the eccentricity effects yield a bounded trajectory. An energy argument logically provides that the periods are no longer matched with the added eccentricity. The in-plane phasing shows little deviation from the linear prediction of HCW.

Figure 4.3 provides the out-of-plane ROEs; the amplitude is slightly perturbed, reaching a minimum at apogee, and osculating the HCW value at perigee. The maximum out-of-plane error between the HCW realization and the eccentric chief value is on the order of 0.01 km. These observations imply that using the circular ROEs for low eccentricity may be a favorable trade-off between model complexity and accuracy.

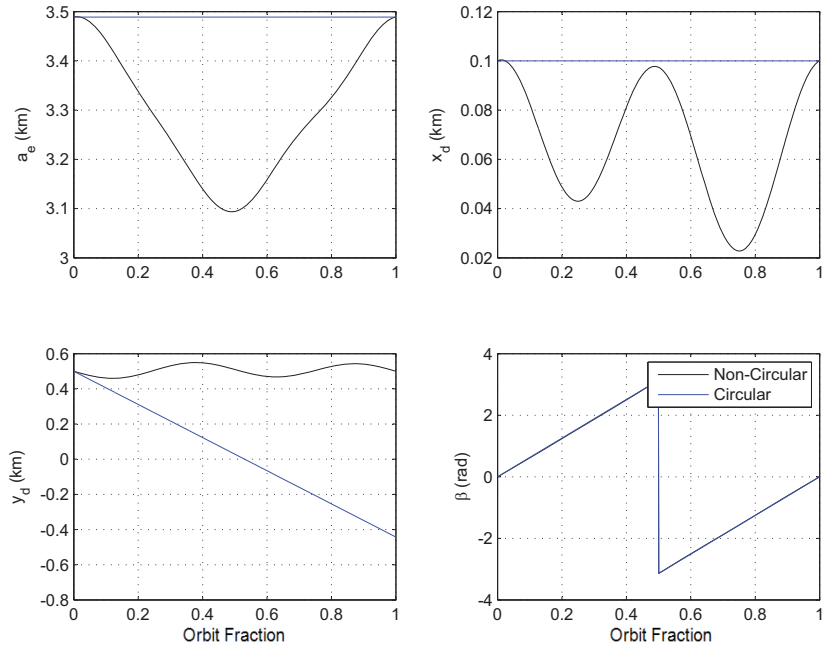


Figure 4.2: In-Plane Osculating Relative Orbit Elements with Chief Eccentricity of 0.01

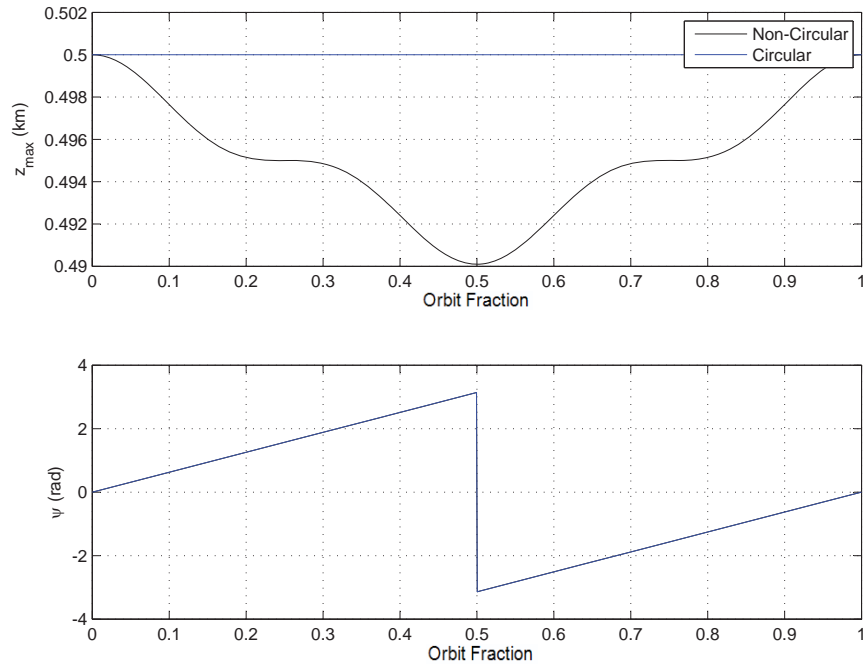


Figure 4.3: Out-of-Plane Osculating Relative Orbit Elements with Chief Eccentricity of 0.01

4.1.4.2 *Medium-Eccentricity, Stationary Relative Orbit.* Given the following initial conditions

$$\begin{aligned} \mathbf{R}_0 &= \begin{bmatrix} 1.3462 & 0.5 & 0.5 & 0 & 0.5 & 0 \end{bmatrix} \\ \mathbf{e}_{c0} &= \begin{bmatrix} 12000 & 0.3 & 0.5236 & 0 & 0 & 0 \end{bmatrix} \end{aligned} \quad (4.36)$$

The three-dimensional propagation using osculating ROEs as compared to the integration is shown in Fig. 4.4 The propagation compared with the numerical integration

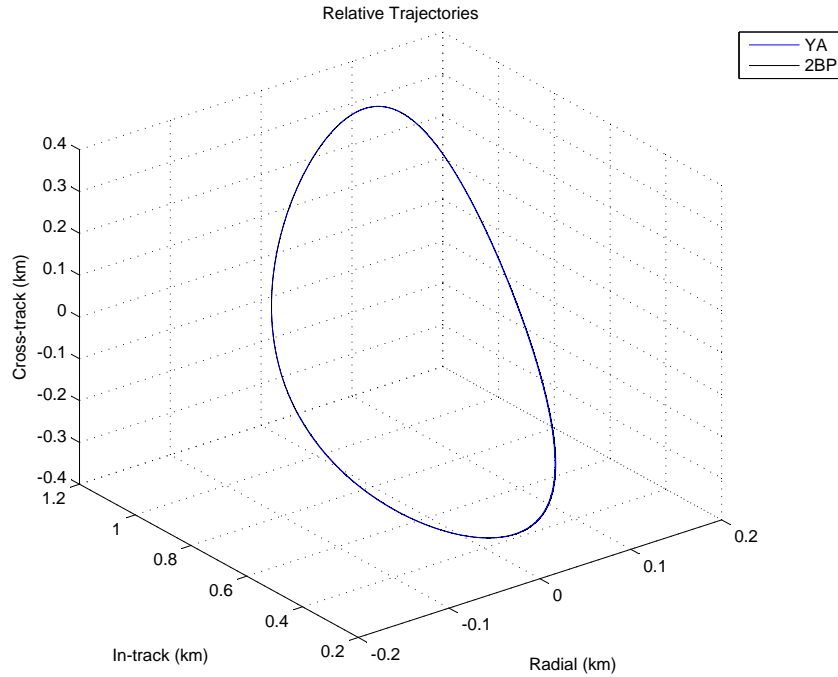


Figure 4.4: Three-Dimensional Relative Trajectory using Osculating ROEs Compared to Numerical Integration with Chief Eccentricity of 0.3

is near exact. There are additional frequencies manifesting in the cross-track motion, skewing the trajectory. The projection still remains a closed conic, with a shape that is also skewed by additional harmonics.

Figure 4.5 provides the in-plane ROEs compared to the expected HCW values. Immediate equality is noted again at perigee due to the absence of radial velocity. The addition of eccentricity accelerated the HCW drift rate when compared to the eccentric motion. The semi-major axis now becomes more of an indication of the

magnitude of the radial and in-track oscillations, which have significant less phase than the circular counterpart.

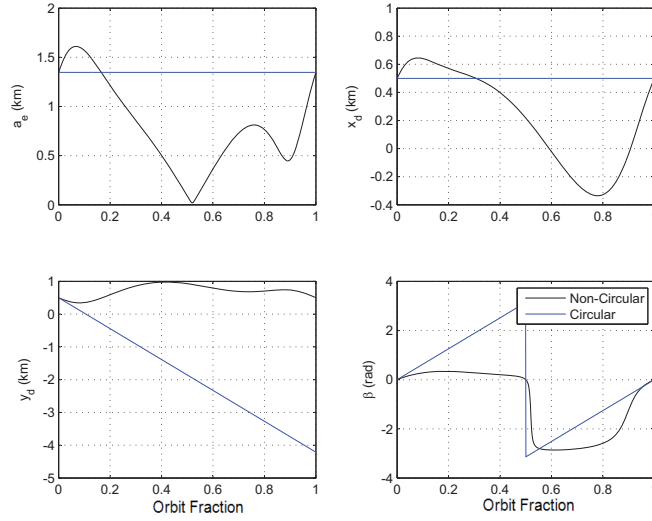


Figure 4.5: In-Plane Osculating Relative Orbit Elements with Chief Eccentricity of 0.3

The eccentricity effects seen in Fig. 4.6 decrease the magnitude of the cross-track motion on the order of 0.25 km. The cross-track phasing lags with respect to the HCW, showing the variance in the orbital angular momentum in comparison to the circular assumption.

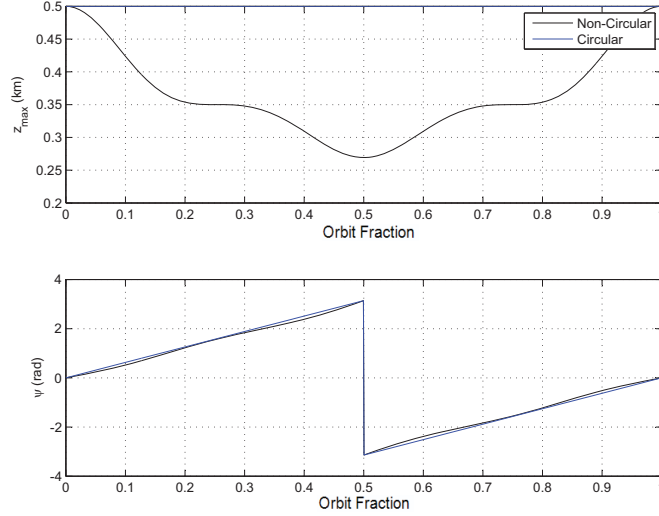


Figure 4.6: Out-of-Plane Osculating Relative Orbit Elements with Chief Eccentricity of 0.3

4.1.5 Physical Interpretation of the Osculating Relative Orbit Elements for the Unperturbed Non-Circular Chief. For the circular chief, the ROEs elegantly describe the geometry of the relative motion. When applied to the current scenario, the physical significance of the ROEs encroaches a mathematical abstract. The effects of chief eccentricity were detailed in Section 2.5.1, but can also be observed in time-response of the newly derived ROEs.

Focusing solely on the radial and in-track motion, the in plane projection of the relative trajectory is found now as the locus of points (x, y) such that

$$\left(\frac{x(t) - x_d(t)}{a_e(t)}\right)^2 + \left(\frac{y(t) - y_d(t)}{2a_e(t)}\right)^2 = 1 \quad (4.37)$$

This implies directly that the position (x, y) is the solution to Eq. 4.37 given the ROE parameterization $R(t)$. This describes the motion of a 2×1 ellipse whose center is translating in the plane according to the trajectory of (x_d, y_d) . The semi-major axis of the instantaneous ellipse is time-varying according to the function $a_e(t)$. Moreover, as the ellipse may intersect with the true trajectory at multiple points, the location

described at time t can be located through the phasing angle β . Figure 4.7 provides a visualization of this application, where E denotes the osculating ellipse, and $R(t)$ is the ROE parameterization at time t . This description fits perfectly with the idea of

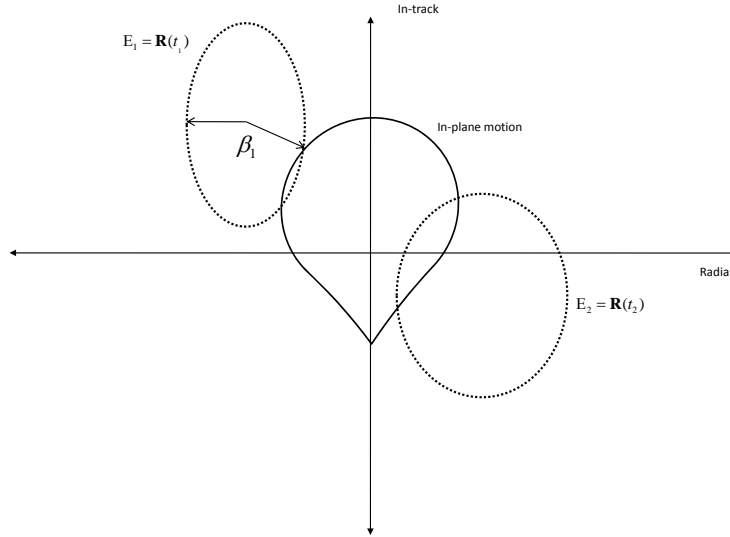


Figure 4.7: In-Plane Relative Orbit Element Characterization for the Eccentric Chief

an osculating relative orbit. If at a time t , the calculated ROE space were initialized, the osculating ellipse entirely describes the relative trajectory if the chief eccentricity were not present. However, the inclusion of the eccentricity terms yields a different response on the true trajectory, and the osculating ellipse simply coincides with the instantaneous position terms as a function of the parameterization. An interesting note is that when the orbit is bounded, as the chief approaches the initial conditions, the osculating ellipse becomes coplanar with the HCW ellipse.

The motion of the osculating ellipse, termed by the author as the osculational translation, is also an indication of the offset of the ROE parameterization from the true solution. The osculating semi-major axis scales the magnitude and places the in-plane components with respect to the phasing, and the offsets compensate for the remainder of any deviation. A typical plot of the osculational translation is found in

Fig. 4.8 where the (x_d, y_d) trajectory the center of the given osculating ellipse. (This

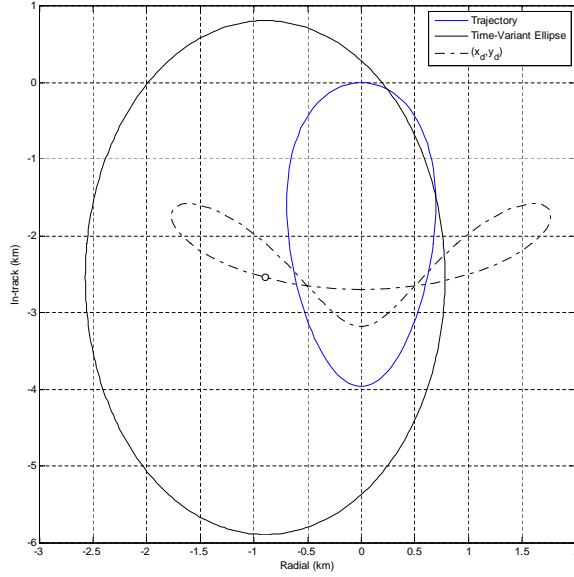


Figure 4.8: Osculational Translation

example was generated using a chief with 9000 km semi-major axis, 0.3 eccentricity, 15 degree inclination, and all other orbital elements as zero, with a Cartesian LVLH initial condition of $[\rho, \dot{\rho}]^T = [0, 0.005, 0.001, 0.001, 0, 0.001]^T$ (km, km/s).

The cross-track motion is far less complicated for this unperturbed case. The out-of-plane motion remains uncoupled but is attenuated from the HCW solution as a function of the eccentricity as

$$z(t) = z_{max0} Z(t) \sin \psi(t) \quad (4.38)$$

The form of Eq. 4.38 shows the HCW cross-track maximum, but is modified by the product $Z(t) \sin \psi(t)$. This will be referred to as the cross-track attenuation, and forces a dampening in amplitude and skewness. Figure 4.9 provides an example of the cross-track motion normalized by the HCW expected maximum (using the same initial conditions as the previous example). Inspection of Fig. 4.9 reveals extrema

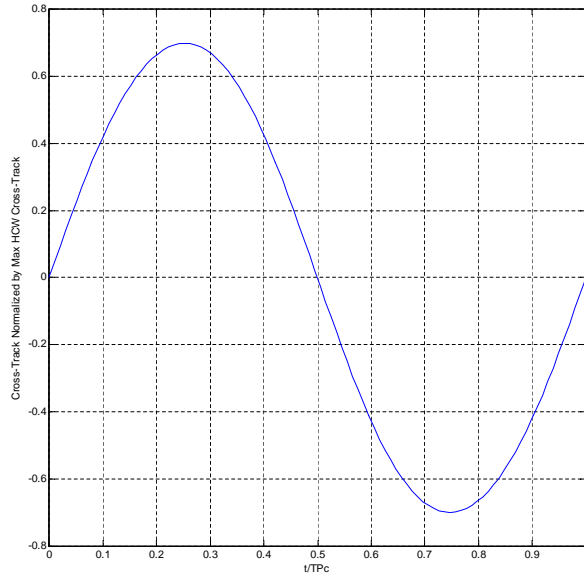


Figure 4.9: Cross-Track Attenuation

values of the attenuation, showing an actual maximum amplification. This will occur when the cross-track phasing is orthogonal to the in-plane motion ($\psi = 0$). This shows a highly-coupled relationship with the true-anomaly and mean motion of the chief, and also indicates a maxima on an elliptical cylinder containing the entirety of the stationary trajectory, or of an instantaneous elliptic cylinder containing the instantaneous motion of the drifting trajectory. In addition, the cross-track phasing simply provides directionality to the magnitude.

At any point in the trajectory, the instantaneous ellipse shows the behavior of the HCW realization. This means that if the model were initialized at any time t , the osculating ellipse is the HCW realization using the relative state at t as its initial conditions. It has been demonstrated that the eccentric ROEs equate to the circular ROEs at perigee. This is resulting from the fact that for any closed orbit, the velocity at perigee is purely tangential with no radial component. At each other point in the relative trajectory, the chief has a radial component that skews the ideal 2×1 ellipse. The idea of the osculating ellipse becomes a mathematical abstract to describe the

resulting relative trajectory, as in this sense the geometric parameterization is now a locus of solutions to a time variant ellipse . Although the physical significance of the ROEs tends to break down, the parameters still describe certain properties. The following details the physical properties of the eccentric ROEs

- The parameter a_e does describe the semi-major axis of the in-plane projection of the HCW trajectory if the model were initiated at at time t with initial conditions $x(t), y(t)$. However, it also helps determine the instantaneous maximum amplitude of the radial ($a_e(t)/2$) and in-track motion ($a_e(t)$).
- The parameters x_d and y_d do detail the center of the osculating ellipse. However, in the eccentric ROE scenario, they describe the offset of the radial and in-track motion.
- The angles β and ψ remain as indications of the in-plane and cross-track phasing frequencies, but lose true physical interpretation.
- The parameter z_{max} indicates the instantaneous maximum magnitude of the cross-track motion.

4.2 The Perturbed, Circular Chief

4.2.1 *Relative Orbit Elements for the Perturbed, Circular Chief Using Geometrical Insight and Linearized Mapping.* It has been shown that relaxation of the circular assumption complicates the physical interpretation of the ROEs. However, their applicability to low eccentricity references orbits still holds. The focus of this study now moves to how the equatorial bulge of the psuedo-spherical Earth impacts the circular development.

4.2.1.1 *Derivation of Relative Orbit Elements for the Unperturbed Circular Chief using Orbital Element Differences.* As a means to gain expectations for the behavior of the relative geometry, an analytical exercise is first performed, using the Gim-Alfriend mapping between Cartesian and orbital element differences [8]

$$\mathbf{X}(t) = (A(t) + \alpha B(t)) \delta \mathbf{e}(t) \quad (4.39)$$

Where $\delta \mathbf{e}(t) = \mathbf{e}_d - \mathbf{e}_c$ are the orbital element differences at a time t . To gather a more intuitive understanding, the restriction is made to work in mean orbital element space. The unperturbed portion A from condenses to

$$A = \begin{bmatrix} 1 & 0 & 0 & -R \cos \theta & -R \sin \theta & 0 \\ 0 & 0 & 0 & V_t \sin \theta & -V_t \cos \theta & 0 \\ 0 & R & 0 & 0 & 0 & R \cos i \\ -\frac{3V_t}{2R} & 0 & 0 & 2V_t \cos \theta & 2V_t \sin \theta & 0 \\ 0 & 0 & R \sin \theta & 0 & 0 & -R \sin i \cos \theta \\ 0 & 0 & V_t \cos \theta & 0 & 0 & V_t \sin \theta \end{bmatrix} \quad (4.40)$$

while the mean perturbed \bar{B} portion from [8] reduces to

$$\bar{B} = \begin{bmatrix} 0 & 0 & 0 & 0 & 0 & 0 \\ 0 & 0 & 0 & \frac{(5 \cos^2 i - 1)(-n \sin \theta)}{4R} & \frac{(5 \cos^2 i - 1)(n \cos \theta)}{4R} & 0 \\ 0 & 0 & 0 & 0 & 0 & 0 \\ \frac{7n \cos^2 i}{4R^2} & 0 & \frac{n \sin i \cos i}{2R} & 0 & 0 & 0 \\ 0 & 0 & 0 & 0 & 0 & 0 \\ -\frac{7n \cos \theta \sin i \cos i}{4R^2} & 0 & -\frac{2n \cos \theta \sin^2 i}{4R} & 0 & 0 & 0 \end{bmatrix} \quad (4.41)$$

At this point, it is desired to express the unperturbed relative orbit elements as functions of the unperturbed orbital element differences; this is achieved by setting α equal to zero in Eq. 4.39. Also inserting the circular assumption, the state transformation becomes

$$\begin{bmatrix} x \\ \dot{x} \\ y \\ \dot{y} \\ z \\ \dot{z} \end{bmatrix} = \begin{bmatrix} 1 & 0 & 0 & -a \cos \theta & -a \sin \theta & 0 \\ 0 & 0 & 0 & na \sin \theta & -na \cos \theta & 0 \\ 0 & a & 0 & 0 & 0 & a \cos i \\ -\frac{3n}{2} & 0 & 0 & 2na \cos \theta & 2na \sin \theta & 0 \\ 0 & 0 & a \sin \theta & 0 & 0 & -a \sin i \cos \theta \\ 0 & 0 & na \cos \theta & 0 & 0 & na \sin \theta \end{bmatrix} \begin{bmatrix} \delta a \\ \delta \theta \\ \delta i \\ \delta q_1 \\ \delta q_2 \\ \delta \Omega \end{bmatrix} \quad (4.42)$$

where θ is now the argument of true latitude, V_t is the tangential velocity (mean motion for this specific example), and all other variables are previously defined. This can be expanded and substituted into the ROE expressions with easy verification to find

$$\begin{aligned} a_e &= 2a \sqrt{(\delta q_1)^2 + (\delta q_2)^2} = 2ae_d \\ x_d &= \delta a \\ y_d &= a\delta\theta + a\delta\Omega \cos i - 2a(\delta q_1 \sin \theta - \cos \theta \delta q_2) \\ \beta &= \tan^{-1} \left(\frac{\delta q_1 \sin \theta - \delta q_2 \cos \theta}{\delta q_1 \cos \theta + \delta q_2 \sin \theta} \right) \\ z_{max} &= a \sqrt{(\delta i)^2 + (\delta \Omega \sin i)^2} \\ \psi &= \tan^{-1} \left(\frac{\delta i \sin \theta - \delta \Omega \cos \theta \sin i}{\delta i \cos \theta + \delta \Omega \sin \theta \sin i} \right) \end{aligned} \quad (4.43)$$

Immediately, it is noted that the boundedness condition of $x_d = 0$ easily extends to orbital element different space as $\delta a = 0$ (the equal period condition). Also of note is that the non-constant values (y_d, β, ψ) remain the same. As a direct fallout, these expressions are near identical to parameters developed by Schaub [30]. When the expression given in Eq. 4.43 for z_{max} is divided by the semi-major axis, the resulting expression is given by Schaub as the angle between the orbit planes of the deputy and the chief. This implies that the z_{max}/a is a spherical tilt angle between the two orbit planes for very small orbital element differences. The inquisitive response to this is how the J_2 perturbation will affect these expressions.

4.2.1.2 Osculating Relative Orbit Elements from the J_2 Effect using Orbital Element Differences: An Analytical Approach. The objective now is to derive the mean effects of J_2 on the relative orbit elements. Using the mean secular J_2 time rates, the following linear relationships are developed based on the secular drift in the orbital elements

$$\begin{aligned}
\delta a &= \delta a_0 \\
\delta q_1 &= q_1 = q_{10} \cos(\dot{\omega}\Delta t) - q_{20} \sin(\dot{\omega}\Delta t) \\
&= e_d \cos \omega(t) \\
\delta q_2 &= q_2 = q_{10} \sin(\dot{\omega}\Delta t) + q_{20} \cos(\dot{\omega}\Delta t) \\
&= e_d \sin \omega(t) \\
\delta \Omega &= \delta \Omega_0 + \delta \dot{\Omega} \Delta t \\
\delta \theta &= \delta \theta_0 + \delta \dot{\theta} \Delta t \\
\delta i &= \delta i_0
\end{aligned} \tag{4.44}$$

where e_d is the eccentricity of the deputy. Direct state substitution can now be used to examine the effect on the unperturbed ROEs. Beginning with the relative semi-major

axis

$$\begin{aligned}
a_e &= 2a\sqrt{(\delta q_1)^2 + (\delta q_2)^2} \\
&= 2a\sqrt{(e_d \cos(\omega(t)))^2 + (e_d \sin(\omega(t)))^2} \\
\bar{a}_{eJ_2} &= 2ae_d
\end{aligned} \tag{4.45}$$

This implies that even under J_2 the mean relative semi-major axis of the relative formation remains equivalent to the unperturbed case. Similarly, the radial displacement is nominally found as $x_d = \delta a$, and assuming mean secular rates, this value remains unchanged under the perturbation; thus,

$$\bar{x}_{dJ_2} = \delta a \tag{4.46}$$

The in-track displacement is effected by the perturbation. Substituting state expressions into the y_d component of Eq. 4.43, it is found that

$$\bar{y}_{dJ_2} = a\delta\theta(t) + a\delta\Omega(t) \cos i - 2ae_d (\sin \theta \cos \omega_d - \cos \theta \sin \omega_d) \tag{4.47}$$

Substituting Eq. 4.44 into Eq. 4.47, using the definition of the true latitude ($\theta = \omega + \nu$) and using a double-angle trigonometric identity yields,

$$\begin{aligned}
\bar{y}_{dJ_2} &= a\delta\theta_0 + a(\delta\dot{\omega} + \delta\dot{\nu}) \Delta t + a(\delta\Omega_0 + \delta\dot{\Omega}\Delta t \cos i) + 2ae_d \sin(\omega_d - \theta) \\
&= a(\delta\theta_0 + \delta\Omega_0) + a(\delta\dot{\omega} + \delta\dot{\nu} + \delta\dot{\Omega} \cos i) \Delta t + 2ae_d \sin(\omega_d - \theta)
\end{aligned} \tag{4.48}$$

Immediately it is observed the same constant offset term based on the initial argument of latitude and ascending node is present. A periodic term arises that induces an oscillation at a frequency of the difference between the deputy perigee and chief true latitude. The additional term to the in-track offset is the inclusion of the perigee and ascending node rates. Secular drift in track is manifest in this condition, which implies that $\delta\dot{\theta} = \delta\dot{\omega} + \delta\dot{\nu} = -\delta\Omega \cos i$ will limit the in-track drift. Finishing the in-plane

motion with the perturbed phasing angle and substituting the perturbed states

$$\begin{aligned}\bar{\beta}_{J_2} &= \tan^{-1} \left(\frac{\delta q_1 \sin \theta - \delta q_2 \cos \theta}{\delta q_1 \cos \theta + \delta q_2 \sin \theta} \right) \\ \beta &= \tan^{-1} \left(\frac{\sin(\theta - \omega_d)}{\cos(\theta - \omega_d)} \right) \\ \bar{\beta}_{J_2} &= (\theta - \omega_d)\end{aligned}\tag{4.49}$$

This is the identical expression for the unperturbed motion; however, the argument of perigee term now has a secular drift from the J_2 effect, implying that the frequency of the phasing goes as

$$\dot{\bar{\beta}}_{J_2} = \dot{\theta} + \dot{\omega}_d\tag{4.50}$$

Letting $\dot{\theta}$ for the circular chief be expressed as $n + \dot{\omega}$, the in-plane phasing frequency is found as

$$\dot{\bar{\beta}}_{J_2} = n - \delta\dot{\omega}\tag{4.51}$$

where $\delta\dot{\omega} = \dot{\omega}_d - \dot{\omega}_c$.

Focusing in the cross-track direction, the maximum amplitude is found as just a slight modification of the unperturbed form as

$$\bar{z}_{maxJ_2} = a \sqrt{(\delta i_0)^2 + (\delta\dot{\Omega} \sin i_0 \Delta t)^2}\tag{4.52}$$

Thus, there is a secular drift in the cross-track direction. This can be eliminated if the ascending node rates ($\delta\dot{\Omega}$) are matched. If not, the cross-track magnitude will increase in time at a nearly first order rate. However, for a chief with zero inclination, the cross-track amplitude will remain constant. Finally, the cross-track phasing is found as

$$\bar{\psi}_{J_2} = \tan^{-1} \left(\frac{\delta i \sin \theta - \cos \theta \sin i \delta\dot{\Omega} \Delta t}{\cos \theta \delta i + \sin \theta \sin i \delta\dot{\Omega} \Delta t} \right)\tag{4.53}$$

Summarizing, analytical expressions for the mean response of the ROEs for a circular chief are

$$\begin{aligned}
\bar{a}_{eJ_2} &= 2ae_d \\
\bar{x}_{dJ_2} &= \delta a \\
\bar{y}_{dJ_2} &= a(\delta\theta_0 + \delta\Omega_0 \cos i) + a(\delta\dot{\omega} + \delta\dot{\nu} + \delta\dot{\Omega} \cos i) \Delta t + 2ae_d \sin(\omega_d - \theta) \\
\bar{\beta}_{J_2} &= (\theta - \omega_d) \\
\bar{z}_{maxJ_2} &= a\sqrt{(\delta i_0)^2 + (\delta\dot{\Omega} \sin i_0 \Delta t)^2} \\
\bar{\psi}_{J_2} &= \tan^{-1} \left(\frac{\delta i \sin \theta - \cos \theta \sin i \delta\dot{\Omega} \Delta t}{\delta i \cos \theta + \sin \theta \sin i \delta\dot{\Omega} \Delta t} \right)
\end{aligned} \tag{4.54}$$

These equations illustrate the importance of matching the drift rates of the chief and deputy ascending nodes and arguments of perigee for formation keeping.

4.2.1.3 Osculating Relative Orbit Elements from the J_2 Effect using Orbital Element Differences: An Analytical Jacobian Approach. As a primarily analytical exercise, one can also look at how the ROEs will change as a function of time using a perturbation approach to verify the previous section's state substitution. Let the solution vector \mathbf{X} equate to the six ROEs, and let the state vector $\delta\mathbf{e}$ equal to the non-singular orbital element differences between the chief and deputy. To examine the effect of J_2 on the ROEs, we perform the following Jacobian operation

$$\frac{\partial \mathbf{X}}{\partial t} = \frac{\partial \mathbf{X}}{\partial \delta \mathbf{e}} \frac{\partial \delta \mathbf{e}}{\partial t} \tag{4.55}$$

where

$$\frac{\partial \mathbf{X}}{\partial \delta \mathbf{e}} = \begin{bmatrix} \frac{\partial a_e}{\partial \delta a} & \cdots & \frac{\partial a_e}{\partial \delta \Omega} \\ \vdots & \ddots & \vdots \\ \frac{\partial \psi}{\partial \delta a} & \cdots & \frac{\partial \psi}{\partial \delta \Omega} \end{bmatrix} \tag{4.56}$$

The partials in Eq. 4.56 can be found by taking partials of Eq. 4.43 with respect to the orbital element differences. For this exercise, only the spatial ROEs will be

examined, while the phasing angles are left for future work. The mean secular J_2 rates are used. The time rate of the orbital element differences is expressed as

$$\begin{bmatrix} \frac{\partial \delta a}{\partial t} \\ \frac{\partial \delta \theta}{\partial t} \\ \frac{\partial \delta i}{\partial t} \\ \frac{\partial \delta q_1}{\partial t} \\ \frac{\partial \delta q_2}{\partial t} \\ \frac{\partial \delta \Omega}{\partial t} \end{bmatrix} = \begin{bmatrix} 0 \\ \delta \dot{\theta} \\ 0 \\ \dot{q}_{1d} \\ \dot{q}_{2d} \\ \delta \dot{\Omega} \end{bmatrix} \quad (4.57)$$

The resulting matrix math needed is then

$$\frac{\partial \mathbf{X}}{\partial \delta \mathbf{e}} = \begin{bmatrix} \frac{\partial a_e}{\partial \delta a} & \cdots & \frac{\partial a_e}{\partial \delta \Omega} \\ \vdots & \ddots & \vdots \\ \frac{\partial \psi}{\partial \delta a} & \cdots & \frac{\partial \psi}{\partial \delta \Omega} \end{bmatrix} \begin{bmatrix} 0 \\ \delta \dot{\theta} \\ \dot{q}_{1d} \\ \dot{q}_{2d} \\ 0 \\ \delta \dot{\Omega} \end{bmatrix} \quad (4.58)$$

As a result, only the second through fourth and sixth columns of $\frac{\partial \mathbf{X}}{\partial \delta \mathbf{e}}$ are necessary. The semi-major axis a_e and radial displacement are found as functions of solely a , e_d , and δa ; thus, partials of these expressions with respect to any other variable is zero. Directly a_e and x_d remain constant—that is,

$$\begin{aligned} \frac{\partial a_e}{\partial t} &= 0 \\ \frac{\partial x_d}{\partial t} &= 0 \end{aligned} \quad (4.59)$$

However, examining the in-track displacement and cross-track amplification, the relationship is less linear. The resulting expressions become

$$\begin{aligned}\frac{\partial y_d}{\partial t} &= \frac{\partial y_d}{\partial \delta \theta} \dot{\delta \theta} + \frac{\partial y_d}{\partial \delta q_1} \dot{q}_{1d} + \frac{\partial y_d}{\partial \delta q_2} \dot{q}_{2d} + \frac{\partial y_d}{\partial \delta \Omega} \dot{\delta \Omega} \\ \frac{\partial z_{max}}{\partial t} &= \frac{\partial z_{max}}{\partial \delta \theta} \dot{\delta \theta} + \frac{\partial z_{max}}{\partial \delta q_1} \dot{q}_{1d} + \frac{\partial z_{max}}{\partial \delta q_2} \dot{q}_{2d} + \frac{\partial z_{max}}{\partial \delta \Omega} \dot{\delta \Omega}\end{aligned}\quad (4.60)$$

Immediately from Eq. 4.43, each partial of y_d exists, while only the partial of z_{max} with respect to $\delta \Omega$ is non-zero. The gradient of y_d is found as

$$\begin{aligned}\frac{\partial y_d}{\partial \delta \theta} &= a \\ \frac{\partial y_d}{\partial \delta q_1} &= -2a \sin \theta \\ \frac{\partial y_d}{\partial \delta q_2} &= 2a \cos \theta \\ \frac{\partial y_d}{\partial \delta \Omega} &= a \cos i\end{aligned}\quad (4.61)$$

while for z_{max} we find

$$\frac{\partial z_{max}}{\partial \delta \Omega} = -\frac{a^2 \delta \Omega \sin^2 i}{z_{max}} \quad (4.62)$$

Combining the above results, the time rate for y_d is now

$$\begin{aligned}\frac{\partial y_d}{\partial t} &= a \dot{\delta \theta} - 2a \sin \theta \dot{q}_{1d} + 2a \cos \theta \dot{q}_{2d} + a \cos i \dot{\delta \Omega} \\ &= a \left(\dot{\delta \theta} + 2 (\dot{q}_{2d} \cos \theta - \dot{q}_{1d} \sin \theta) + \dot{\delta \Omega} \cos i \right)\end{aligned}\quad (4.63)$$

and for the z_{max} time rate

$$\frac{\partial z_{max}}{\partial t} = -\frac{a^2 \delta \Omega \sin^2 i}{z_{max}} \dot{\delta \Omega} \quad (4.64)$$

And if we express $\delta \Omega = \dot{\delta \Omega} \Delta t$, Eq. 4.64

$$\frac{\partial z_{max}}{\partial t} = -\frac{a^2}{z_{max}} \sin^2 i (\dot{\delta \Omega})^2 \Delta t \quad (4.65)$$

Although not in exact agreement, this expression shows the same trend in the z_{max} parameter when compared to Eq. 4.54. Equation 4.65 shows a linear time-rate, while Eq. 4.54 shows a relationship on the order of $\sqrt{\Delta t^2}$. The two expressions appear to have time rates on the same order of magnitude.

4.2.2 *Relative Orbit Elements for the Perturbed, Circular Chief Developed by the Schwieghart-Sedwick Differential Equations with Arbitrary Initial Conditions.*

The following section details the development of the ROEs from solving the differential equations and setting arbitrary initial conditions. From Eq. 3.12, the radial and in-track motion is still uncoupled from the cross-track as in the HCW model. Placing the in-plane system in matrix form as [36]

$$\begin{bmatrix} x \\ y \\ \dot{x} \\ \dot{y} \end{bmatrix} = \begin{bmatrix} 0 & 0 & 1 & 0 \\ 0 & 0 & 0 & 1 \\ (5c^2 - 2)n^2 & 0 & 0 & 2nc \\ 0 & 0 & -2nc & 0 \end{bmatrix} \begin{bmatrix} \dot{x} \\ \dot{y} \\ \ddot{x} \\ \ddot{y} \end{bmatrix} \quad (4.66)$$

This linear system can be solved using a number of different tools. The approach taken by this author is the matrix exponential. The resulting state transition matrix found via $\Phi(t, t_0) = e^{A(t-t_0)}$ is

$$\Phi_{ss} = \begin{bmatrix} \frac{B^2 - \sigma \cosh(K_1 \Delta t)}{K_2} & 0 & \frac{(-B^2 + \sigma) \sinh(K_1 \Delta t)}{(-K_2)^{3/2}} & \frac{B - B \cosh(K_1 \Delta t)}{K_2} \\ -\frac{B\sigma(K_2 \Delta t + \sqrt{-K_2} \sinh(K_1 \Delta t))}{K_2^2} & 1 & \frac{B(\cosh(K_1 \Delta t) - 1)}{K_2} & -\frac{K_2 \sigma \Delta t + B^2 \sqrt{-K_2} \sinh(K_1 \Delta t)}{K_2^2} \\ \frac{-K_2 \sigma \sinh(K_1 \Delta t)}{(-K_2)^{3/2}} & 0 & \cosh(K_1 \Delta t) & \frac{-K_2 B \sinh(K_1 \Delta t)}{(-K_2)^{3/2}} \\ \frac{B\sigma(\cosh(K_1 \Delta t) - 1)}{K_2} & 0 & \frac{BK_2 \sinh(K_1 \Delta t)}{(-K_2)^{3/2}} & \frac{-\sigma + B^2 \cosh(K_1 \Delta t)}{K_2} \end{bmatrix} \quad (4.67)$$

such that $[x, y, \dot{x}, \dot{y}]^T = \Phi_{ss}(t, t_0)[x_0, y_0, \dot{x}_0, \dot{y}_0]^T$, where the constants are defined as

$$\begin{aligned}
\Delta t &= (t - t_0) \\
K_1 &= \sqrt{-B^2 + \sigma} \\
K_2 &= B^2 - \sigma = -K_1^2 \\
B &= 2nc \\
\sigma &= (5c^2 - 2)n^2 \\
c &= \sqrt{1 + s} \\
s &= \frac{3J_2 R_e^2}{8r^2} (1 + 3 \cos(2i))
\end{aligned} \tag{4.68}$$

There now exists a closed form solution of the SS differential equations regardless of initial conditions.

4.2.2.1 Deriving the In-Plane Relative Orbit Elements. Focusing on the in-plane motion, the state can be expressed linearly at any time as $X(t) = \Phi(t, t_0)X_0$. From Eq. 4.16, the initial Cartesian conditions were found as functions of the initial ROEs by the following relation

$$\begin{bmatrix} x_0 \\ y_0 \\ \dot{x}_0 \\ \dot{y}_0 \end{bmatrix} = \begin{bmatrix} -\frac{\cos \beta_0}{2} & 1 & 0 \\ \sin \beta_0 & 0 & 1 \\ \frac{n}{2} \sin \beta_0 & 0 & 0 \\ n \cos \beta_0 & -\frac{3n}{2} & 0 \end{bmatrix} \begin{bmatrix} a_{e0} \\ x_{d0} \\ y_{d0} \end{bmatrix} \tag{4.69}$$

Allowing the product of time-varying matrix in Eq. 4.69 with the STM in Eq. 4.67 to be expressed as $\mathbf{J}(t)$, the instantaneous ROEs are found as $\mathbf{R}(t) = \Lambda(\mathbf{J}(t)R_{i0})$, where Λ is the transformation from Cartesian to ROE space, and $R_{i0} = [a_{e0} \ x_{d0} \ y_{d0}]^T$ is the initial in-plane spatial ROEs. Now knowing the necessary operations, the only remaining issue is the algebraic derivation. For simplicity, it is desired to express the

in-plane relative position in the following form

$$\begin{aligned} x &= C_1 + \zeta_{x1} \cosh \theta + \zeta_{x2} \sinh \theta \\ y &= C_2 + \zeta_{y1} \cosh \theta + \zeta_{y2} \sinh \theta + \varphi \Delta t \end{aligned} \quad (4.70)$$

The expression in Eq. 4.70 is the $\mathbf{X} = \mathbf{J}(t)R_{i0}$ function. Performing the matrix multiplication and grouping like terms, the constants in Eq. 4.70 are found as

$$\begin{aligned} C_1 &= x_{d0} \left(\frac{B^2}{K_2} - \frac{3Bn}{2K_2} \right) + a_{e0} \left(\frac{B \cos \beta_0}{K_2} - \frac{B^2 \cos \beta_0}{2K_2} \right) \\ C_2 &= y_{d0} + a_{e0} \left(\sin \beta_0 - \frac{Bn \sin \beta_0}{2K_2} \right) \\ \zeta_{x1} &= x_{d0} \left(\frac{3Bn}{2K_2} - \frac{\sigma}{K_2} \right) + a_{e0} \left(-\frac{B \cos \beta_0}{K_2} + \frac{\sigma \cos \beta_0}{2K_2} \right) \\ \zeta_{x2} &= \frac{a_{e0}n \sin \beta_0}{2\sqrt{-K_2}} \\ \zeta_{y1} &= \frac{a_{e0}Bn \sin \beta_0}{2K_2} \\ \zeta_{y2} &= x_{d0} \left(\frac{3B^2n}{2(-K_2)^{3/2}} - \frac{B\sigma}{(-K_2)^{3/2}} \right) + a_{e0} \left(-\frac{B^2 \cos \beta_0}{(-K_2)^{3/2}} + \frac{B\sigma \cos \beta_0}{2(-K_2)^{3/2}} \right) \\ \varphi &= x_{d0} \left(-\frac{B\sigma}{K_2} + \frac{3n\sigma}{2K_2} \right) + a_{e0} \left(-\frac{\sigma \cos \beta_0}{K_2} + \frac{B\sigma \cos \beta_0}{2K_2} \right) \\ \theta &= K_1 \Delta t \end{aligned} \quad (4.71)$$

Also from Eq. 4.70, time derivatives provide the relative velocities to be

$$\begin{aligned} \dot{x} &= \dot{\theta} (\zeta_{x1} \sinh \theta + \zeta_{x2} \cosh \theta) \\ \dot{y} &= \dot{\theta} (\zeta_{y1} \sinh \theta + \zeta_{y2} \cosh \theta) + \varphi \end{aligned} \quad (4.72)$$

where $\dot{\theta} = K_1$.

Having condensed forms of the relative trajectory expressions, the in-plane portion of the Λ transformation is now possible. Beginning with the semi-major axis a_e ,

define the following two variables

$$\begin{aligned}
a_{e1} &= \frac{\dot{x}}{n} \\
&= \frac{\dot{\theta}}{n} (\zeta_{x2} \cosh \theta + \zeta_{x1} \sinh \theta) \\
a_{e2} &= 3x + 2\frac{\dot{y}}{n} \\
&= 3(C_1 + \zeta_{x1} \cosh \theta + \zeta_{x2} \sinh \theta) + \frac{2\dot{\theta}}{n} (\zeta_{y2} \cosh \theta + \zeta_{y1} \sinh \theta)
\end{aligned} \tag{4.73}$$

such that the final expression for a_e becomes by simple substitution

$$a_e = 2\sqrt{a_{e1}^2 + a_{e2}^2} \tag{4.74}$$

which is seen as the combination of hyperbolic trigonometric functions at a frequency of $\dot{\theta}$.

The in-plane displacements along the radial and in-track directions can be written as a linear combination. Using the expressions from Eq. 2.59

$$\begin{aligned}
x_d &= 4x + \frac{2\dot{y}}{n} \\
y_d &= y - \frac{2\dot{x}}{n}
\end{aligned} \tag{4.75}$$

Substitution of Eq. 4.70 and Eq. 4.72 and grouping terms according to the trigonometric terms, it is observed that

$$\begin{bmatrix} x_d \\ y_d \end{bmatrix} = \begin{bmatrix} 4\zeta_{x1} + \frac{2\dot{\theta}\zeta_{y2}}{n} & 4\zeta_{x2} + \frac{2\dot{\theta}\zeta_{y1}}{n} \\ \zeta_{y1} - \frac{2\dot{\theta}\zeta_{x2}}{n} & \zeta_{y2} - \frac{2\dot{\theta}\zeta_{x1}}{n} \end{bmatrix} \begin{bmatrix} \cosh \theta \\ \sinh \theta \end{bmatrix} + \begin{bmatrix} 4C_1 \\ C_2 + \varphi\Delta t \end{bmatrix} \tag{4.76}$$

The in-plane phasing is finally found as

$$\beta = \tan^{-1} \left(\frac{\dot{x}}{3nx + 2\dot{y}} \right) \tag{4.77}$$

and using the previously defined variables a_{e1} and a_{e2} from Eq. 4.73, we find

$$\beta = \tan^{-1} \left(\frac{a_{e1}}{a_{e2}} \right) \quad (4.78)$$

4.2.2.2 Out-of-Plane Relative Orbit Elements. Schweighart and Sedwick [37] further defined the cross-track motion for the circular satellite under the J_2 perturbation. The cross-track motion is described in [37] as

$$z(t) = A(t) \sin(B(t)t - C(t)) \quad (4.79)$$

where Schweighart denotes $A(t)$ as the time-varying cross-track magnitude, $B(t)$ as the orbital frequency (which is modified under J_2), and $C(t)$ as a phasing angle. Expressed as functions, these parameters are

$$\begin{aligned} A(t) &= r\eta \\ B(t) &= nk \\ k &= c + l \cos^2 i \\ l &= \frac{3J_2 R_e^2}{2r^2} \end{aligned} \quad (4.80)$$

An immediate comparison can be made to the ROE expression for the cross-track motion

$$z(t) = z_{max} \sin \psi \quad (4.81)$$

such that it is evident that

$$\begin{aligned} z_{max}(t) &= A(t) \\ \psi(t) &= B(t)t - C(t) \end{aligned} \quad (4.82)$$

The time-varying magnitude $A(t)$ is found as the product of the circular reference orbit's radius and the spherical angle (η) resulting from the combination of differences between the ascending nodes and inclinations of the chief and deputy. For small

angles, this has already been found earlier in Eq. 4.43 as z_{max}/r and is equal to

$$\eta = \sqrt{(\Delta i)^2 + (\Delta\Omega \sin^2 i)^2} \quad (4.83)$$

and develops according to

$$\eta = \eta_0 \cos \gamma_0 \sec \gamma \quad (4.84)$$

where γ is the cross-track phasing angle, expressed for small angles as [37]

$$\gamma = \cot^{-1} \left(\frac{\Delta i}{\Delta\Omega \sin i} \right) \quad (4.85)$$

Using the proposed parameterization in Eq. 4.82, and assuming $t_0 = 0$, the angle γ is equal to and opposite ψ at epoch. That is

$$\psi_0 = -\gamma_0 \quad (4.86)$$

which is given by Schweighart and Sedwick as

$$\gamma_0 = -\tan^{-1} \left(\frac{\dot{z}_0}{z_0} \frac{1}{n(k-b)} \right) \quad (4.87)$$

where $b = l \sin^2 i$. This immediately implies from Eq. 4.86

$$\psi_0 = \tan^{-1} \left(\frac{\dot{z}_0}{z_0} \frac{1}{n(k-b)} \right) \quad (4.88)$$

The cross-track phasing is then given as

$$\psi = nkt + \psi_0 \quad (4.89)$$

Turning the attention to the cross-track amplification, the expression for $A(t)$ is given as

$$\begin{aligned} A(t) &= r\eta \\ &= r\eta_0 \cos \gamma_0 \sec \gamma \end{aligned} \quad (4.90)$$

Utilizing $z_{max} = A(t)$ and making the substitutions $z_{max0} = r\eta_0$ and $\psi_0 = -\gamma_0$, we arrive at

$$A(t) = z_{max0} \cos \psi_0 \sec \gamma \quad (4.91)$$

where γ is defined in [37] as

$$\gamma = \tan^{-1} (nbt + \tan \gamma_0) \quad (4.92)$$

Finally, from Eq. 4.82, the cross-track amplification is found as

$$z_{max}(t) = z_{max0} \cos \psi_0 \sec \gamma \quad (4.93)$$

such that the cross-track motion is then defined as

$$z(t) = z_{max0} \cos \psi_0 \sec \gamma \sin \psi(t) \quad (4.94)$$

Utilizing the trigonometric identity

$$\begin{aligned} \sec(\arctan(x)) &= \frac{1}{\cos(\arctan(x))} \\ &= \frac{1}{\frac{1}{\sqrt{1+x^2}}} \\ &= \sqrt{1+x^2} \end{aligned} \quad (4.95)$$

and substituting in Eq. 4.94, the final form of the cross-track motion is then found as

$$z(t) = z_{max}(t) \sin \psi(t) \quad (4.96)$$

where

$$z_{max}(t) = z_{max0} \cos \psi_0 \sqrt{1 + (bnt - \tan \psi_0)^2} \quad (4.97)$$

4.2.2.3 *Summary of the Relative Orbit Elements for the J_2 Perturbed, Circular Chief for Arbitrary Initial Conditions.* The following provides a summary of the ROEs for the circular chief perturbed by J_2 .

$$\begin{aligned}
a_e &= 2\sqrt{a_{e1}^2 + a_{e2}^2} \\
\begin{bmatrix} x_d \\ y_d \end{bmatrix} &= \begin{bmatrix} 4\zeta_{x1} + \frac{2\dot{\theta}\zeta_{y2}}{n} & 4\zeta_{x2} + \frac{2\dot{\theta}\zeta_{y1}}{n} \\ \zeta_{y1} - \frac{2\dot{\theta}\zeta_{x2}}{n} & \zeta_{y2} - \frac{2\dot{\theta}\zeta_{x1}}{n} \end{bmatrix} \begin{bmatrix} \cosh \theta \\ \sinh \theta \end{bmatrix} + \begin{bmatrix} 4C_1 \\ C_2 + \varphi\Delta t \end{bmatrix} \\
\beta &= \tan^{-1} \left(\frac{a_{e1}}{a_{e2}} \right) \\
z_{max}(t) &= z_{max0} \cos \psi_0 \sqrt{1 + (bnt - \tan \psi_0)^2} \\
\psi &= nkt + \psi_0
\end{aligned} \tag{4.98}$$

These expressions have been developed for arbitrary initial conditions and are not dependent on velocity states initialized to bound the relative orbit.

4.2.3 *Numerical Examples and Deviations from the Clohessy-Wiltshire Assumptions.* As the primary assumption in the HCW realization is a circular chief, examining the effects on the HCW ROEs from J_2 is very appropriate. The stationary relative orbits are found using the conditions detailed in Appendix F. The following numerical examples will demonstrate the deviation of the model from HCW. Initial conditions are given in the form $\mathbf{R}_0 = [a_{e0} \ x_{d0} \ y_{d0} \ \beta_0 \ z_{max0} \ \psi_0]$ with units of (km,rad) where appropriate, and the chief orbital elements are given in the form $\mathbf{e}_{c0} = [a \ e \ i \ \omega \ \Omega \ M_0]$ with units of (km,rad) as well.

4.2.3.1 *Relative Orbit Elements at for a Low Altitude Chief with Low Inclination.* Given the following initial conditions

$$\begin{aligned}
\mathbf{R}_0 &= [11.89 \ 0.01 \ 0.05 \ 0 \ 1 \ 0.5] \\
\mathbf{e}_{c0} &= [7000 \ 0 \ 0.1745 \ 0 \ 0 \ 0]
\end{aligned} \tag{4.99}$$

Figure 4.10 provides a visualization of the in-plane ROEs. Initial conditions for bounded motion have been used. The expressions for these initial conditions are derived in App. F. Of immediate note is these initial conditions supplied to the HCW model yield a drifting trajectory (evident in y_d). There are variations on the order of 10^1 meters in the expressions for a_e , x_d , and y_d ; however, the in-plane phasing differs only slightly from the expected motion.

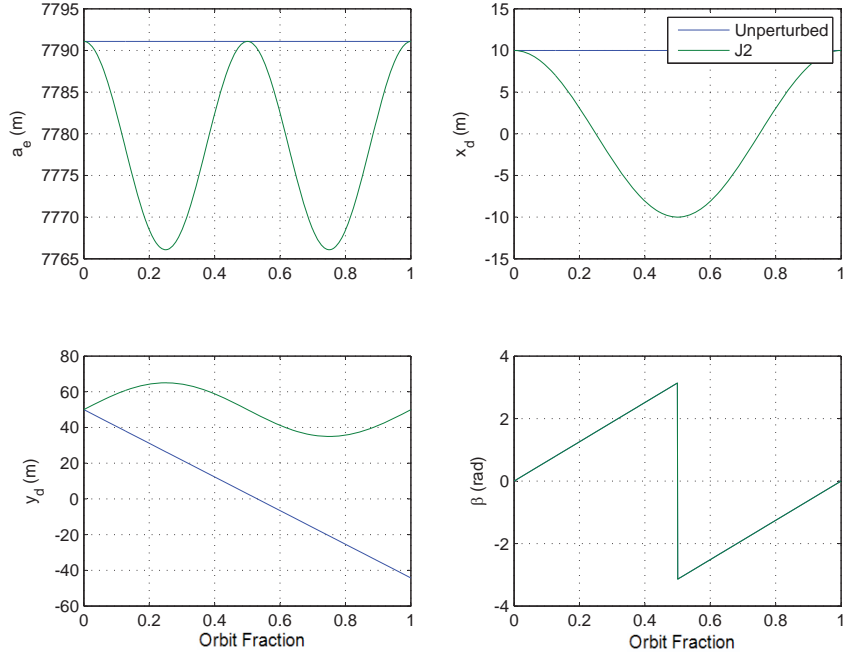


Figure 4.10: In-Plane Osculating Relative Orbit Elements for J_2 Perturbed, Low Altitude Circular Chief

Figure 4.11 provides a visualization of the out-of-plane ROEs. The cross-track amplification decreases nearly linear, but at low, near negligible rate. This again is due to the bounding condition. Differential drift rates will induce perturbations to the orbital angular momenta of both the chief and deputy and modify the action of the cross-track motion. The short term effect of the cross-track variation is near negligible, but long term projections will be error prone.

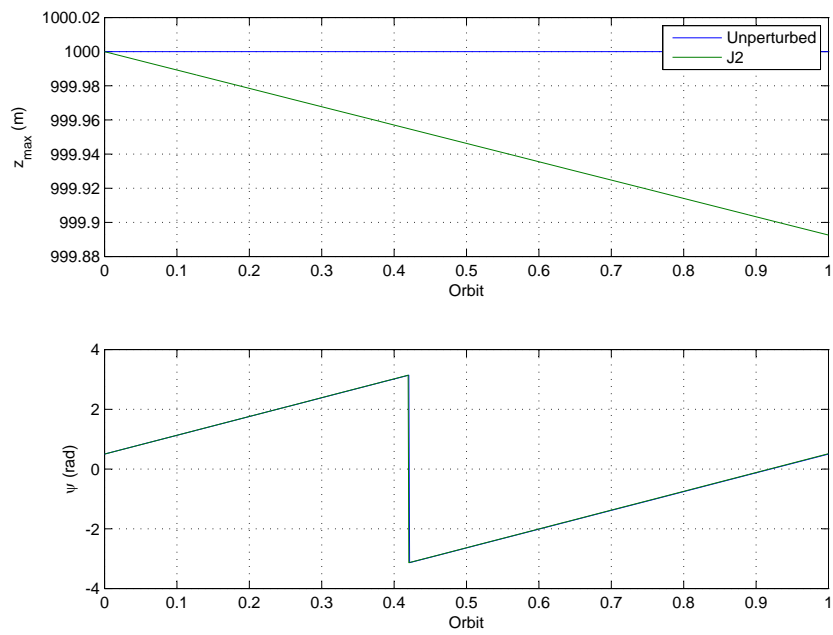


Figure 4.11: Out-of-Plane Osculating Relative Orbit Elements for J_2 Perturbed, Low Altitude Circular Chief

4.3 Applications of Osculating Relative Orbit Elements

4.3.1 Guidance and Navigation.

4.3.1.1 *Derivation.* Having analytical expressions for the osculating ROEs, one can examine the effect of an impulsive burn in any of the directions in the orbital plane of the chief. The derivation begins by assuming that a single, impulsive burn is possible and can be oriented in such a way that the burn acts entirely in the radial, in-track, and/or cross-track directions. The derivation follows similarly to that in [33], and focuses primarily on the idea of a single burn. Assuming knowledge of the ROE state at the time the burn (tb) occurs, and letting the subscript pb indicate the desired post-burn value, the expressions can be written as

$$\begin{bmatrix} a_{e_{pb}} \\ x_{d_{pb}} \\ y_{d_{pb}} \\ \beta_{pb} \\ z_{max_{pb}} \\ \psi_{pb} \end{bmatrix} = \begin{bmatrix} a_{e_{tb}} \\ x_{d_{tb}} \\ y_{d_{tb}} \\ \beta_{tb} \\ z_{max_{tb}} \\ \psi_{tb} \end{bmatrix} + \begin{bmatrix} \Delta a_e \\ \Delta x_d \\ \Delta y_d \\ \Delta \beta \\ \Delta z_{max} \\ \Delta \psi \end{bmatrix} \quad (4.100)$$

where the Δ values indicate the contribution to the ROE provided by the impulse. If the relative velocity is known at $t = t_b$, then an instantaneous burn would yield the following expressions for the Δ components

$$\begin{bmatrix} \Delta a_e \\ \Delta x_d \\ \Delta y_d \\ \Delta \beta \\ \Delta z_{max} \\ \Delta \psi \end{bmatrix} = \begin{bmatrix} 2\sqrt{\left(\frac{\Delta \dot{x}}{n}\right)^2 + \left(3x_{tb} + 2\frac{\Delta \dot{y}}{n}\right)^2} \\ 4x_{tb} + \frac{2\Delta \dot{y}}{n} \\ y_{tb} - \frac{2\Delta \dot{x}}{n} \\ \tan^{-1}\left(\frac{\Delta \dot{x}}{3nx_{tb} + 2\Delta \dot{y}}\right) \\ \sqrt{\left(\frac{\Delta \dot{z}}{n}\right)^2 + (z_{tb})^2} \\ \tan^{-1}\left(\frac{nz_{tb}}{\Delta \dot{z}}\right) \end{bmatrix} \quad (4.101)$$

where the Δ values are expressed as

$$\begin{bmatrix} \Delta \dot{x} \\ \Delta \dot{y} \\ \Delta \dot{z} \end{bmatrix} = \begin{bmatrix} \dot{x} + \Delta V_x \\ \dot{y} + \Delta V_y \\ \dot{z} + \Delta V_z \end{bmatrix} \quad (4.102)$$

One can then make the substitution using the Cartesian to ROE conversion such that

$$\begin{aligned} x_{tb} &= -\frac{a_{e-} \cos \beta_-}{2} + x_{d-} \\ y_{tb} &= a_{e-} \sin \beta_- + y_{d-} \\ z_{tb} &= z_{max-} \sin \psi_- \end{aligned} \quad (4.103)$$

where the minus subscript indicates the state immediately before the burn. Substitution into Eq. 4.101 yields dependence entirely on the ROE states. If the expressions for the Δ values in Eq. 4.101 represent desired maneuvers, Eq. 4.101 represents a system of highly non-linear equations that can be numerically solved to determine approximately the necessary velocity change needed to alter the relative trajectory.

4.3.1.2 Mathematical Concerns. It is quite significant to note that the nonlinear equation set in Eq. 4.101 suffers from constraint issues. For example, if a desired a_e is selected, there are two independent variables ($\Delta \dot{x}, \Delta \dot{y}$) to perform the maneuver. The out of plane motion is such that only a $\Delta \dot{z}$ will alter the cross-track trajectory. If Δa_e is desired, an infinite amount of solutions could exist due to the two free variables in the expression. This implies that if a Δa_e is selected, then one of either $\Delta x_d, \Delta y_d, \Delta \beta$ should be selected additionally. Selecting either Δx_d or Δy_d will yield a possible solution, as does the selection of both parameters. It is nearly mathematically impossible to select both $\Delta \psi$ and Δz_{max} unless selected at a location in which $z_{tb} = 0$. Based on these constraints, an arbitrary maneuver is not mathematically possible. There are only 3 independent variables with 6 dependent variables. One can only reach a subspace of the desired maneuver for any given

relative state at time t_b . The coupled nature of the variables is investigated in the next section.

4.3.1.3 Numerical Examples. It is instructive here to examine the effects of impulsive burns on the analytical expressions. The entire COE set of the chief is not needed as the only value needed from the derivation is the mean motion. The ROEs have been treated as parameters that can be acquired via relative navigation data, and the only needed values are those prior to the burn.

For a chief of any eccentricity representing a closed orbit with a semi-major axis of 7000 km, the following burn time ROEs are given as

$$\begin{bmatrix} a_{e-} \\ x_{d-} \\ y_{d-} \\ \beta_- \\ z_{max-} \\ \psi_- \end{bmatrix} = \begin{bmatrix} 0.01 \text{ km} \\ 0.01 \text{ km} \\ 0.02 \text{ km} \\ \pi \text{ rad} \\ 0.01 \text{ km} \\ 0.1 \text{ rad} \end{bmatrix} \quad (4.104)$$

Allowing the impulses in the radial and in-track directions to vary between -1 and 1 m/s, Fig. 4.12 provides a visualization of the coupling effect on the ROE response.

Immediately evident is the linear response in the values for x_d and y_d . Also, a linear response is noted in the response for z_{max} . The most non-linear is the response of the semi-major axis, which forms an open shape resembling a paraboloid that grows without bound. Resulting spatial responses regardless of initial conditions take the same form as a consequence of the deterministic derivation.

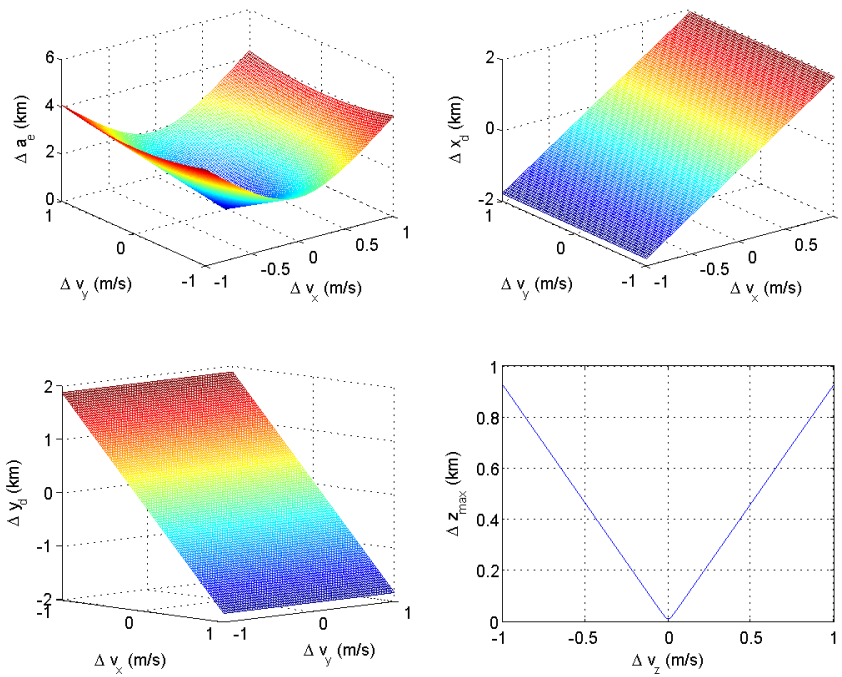


Figure 4.12: Coupling Among the Spatial ROEs with Respect to Three-Dimensional Impulsive Velocity Burns

V. Conclusions and Future Work

5.1 *A Dialogue on the Realism of Osculating Relative Orbit Elements*

Within this thesis, a method has been shown to parameterize the relative trajectory of two satellites in close proximity using geometric insight. The effects of the chief eccentricity and the J_2 perturbation on the circular chief have been investigated. For the latter, mean J_2 effects have been found to serve as a main variable of drift dependence. Perturbations in the relative orbits will only further compound in the relative dynamics. If attempting to attain geometrical insight, full inclusion of the chief eccentricity forces the model into the domain of mathematical abstraction; however, the relative orbit element (ROE) parameterization still serves as a methodology to determine the instantaneous magnitude and phasing of the oscillatory motion, in addition to a time-variant offset.

Relative motion is an abstract concept, and quite difficult to visualize without in-depth study. Oscillating relative trajectories from differential orbits and energy exchange are difficult concepts to grasp. More so, even the time-varying, rotating local-vertical, local-horizontal (LVLH) orbital frame in which the relative dynamics occur is an abstract notion. These factors compound and convolute mission critical objectives including relative navigation, guidance and control, and docking maneuvers. The idea is to obtain a geometrical parameterization that allows an operator to quickly visualize the relative motion and further the mission of close proximity operations. However, the osculating eccentric ROEs fail to meet this objective in this study; the mathematical notion of a locus of points satisfying a 2×1 ellipse does not match criteria of operational efficacy. For LEO missions, the use of a J_2 perturbed set will lead to higher accuracy in navigation; in contrast, the physical near impossibility of a true circular orbit may lead to eccentricity effects dominating the perturbations.

In this study, the mathematics have been done to fully show how the ROE parameterization grows over time with state substitution relaxing the unperturbed and the circular chief assumption. The motion was found to be fully mapped by these analytical expressions. Moreover, closed-form expressions for the relative orbit

elements to include these effects now exist. Further work is still needed to develop a fully intuitive and geometrically insightful parameterization to visualize and control the relative motion of bodies in close proximity.

5.2 Recommendations for Future Work

Throughout the course of this study, several alternate routes have been found that may be followed in the future. These may help further the use of the ROEs to finally develop a parameterization encompassing eccentricity and the J_2 perturbation.

5.2.1 Velocity Independence. The expressions for the ROEs include substitution of the relative velocity states. If one is comparing ROE states across various perturbed environments, the rotation of the LVLH frame induces different angular velocities. These angular velocities modify the velocity states significantly. The non-linear operations on the relative velocity terms compound differences. A proposed route is now to investigate the analytical HCW expressions to find ROE expressions that are simply functions of the relative position terms. This has been done using orbital element differences. The estimation of inertial positions and velocities with conversions to two sets of orbital elements is possible; however, linearizations in the model limit the range of applicability of this method. Therefore, it is highly desired to identify relative orbit elements as functions of position. Furthermore, it is recommended that a parameterization be made that is based on a model developed in inertial space.

5.2.2 Mathematical Inspection of the Yamanaka-Ankersen Topology. Similar to re-parameterizing the ROEs based on relative position terms, the Yamanaka-Ankersen model needs to be investigated and placed into a form to understand the resulting topology. The uncoupled out-of-plane and in-plane motion should be analyzed separately and later superimposed. This was somewhat attempted during this study with little gain. Placing the closed form solution into an expression that is a

function of the eccentricity of the chief in addition to initial conditions could motivate topological intuition.

5.2.3 Higher-Order Terms in the Virtual Chief Model. Propagation of the relative motion using a virtual chief approach could yield intuitive results if the accuracy of the model were increased. A linear state transition matrix was developed by Johnson [27] but was found to be error prone. The idea of retaining higher order terms in the close proximity linearization of the HCW model would undoubtedly increase the accuracy of the dual propagation.

5.2.4 Drag Effects on the Relative Orbit Elements. Inherent in the assumption in the ROE development is the idea of near identical ballistic coefficients yielding identical drag effects. An interesting route of study is to examine analytically the effects on the ROEs including the effects of atmospheric drag. As certain ROEs have been found to be functions of orbital element differences, the induced energy decay of the orbits would also effect the ROE parameters.

5.2.5 Perturbation Methods. Rather than performing full state substitution of closed-form solutions into the ROE parameterization, a worthwhile study would be to examine the effect of the ROEs using the following method. Let \mathbf{R} denote the ROE states, and \mathbf{X} denote the relative Cartesian state. The differential states can then be examined by

$$\delta\mathbf{R} = \frac{\partial\mathbf{R}}{\partial\mathbf{X}}\delta\mathbf{X} \quad (5.1)$$

Appendix A. State Transition Matrix Properties

The state transition matrix (STM) is a deterministic method of propagating a state at time t_0 to any time t . The following identities and concepts are presented as fundamental and without proof.

Typically, the propagation resembles

$$X(t) = \Phi(t, t_0)X(t_0) \quad (\text{A.1})$$

where X is the state vector and Φ is the STM. For a linear time-invariant system of the form

$$\dot{x} = Ax + Bu \quad (\text{A.2})$$

where A is the plane matrix, B is the control matrix, and u is the input vector, the solution is given, without replication of proof, as

$$X(t) = e^{A(t-t_0)}x_0 + \int_{t_0}^t e^{A(t-\tau)}Bu(\tau)d\tau \quad (\text{A.3})$$

with τ as a dummy variable of integration. The integral in Eq. A.3 is often termed the convolution integral. The matrix exponential in Eq. A.3 is often represented as

$$e^{A(t-t_0)} = \Phi(t, t_0) \quad (\text{A.4})$$

For any order of linearity, the STM must satisfy the following properties

1. $\Phi(t_2, t_0) = \Phi(t_2, t_1)\Phi(t_1, t_0)$
2. $\Phi(t_2, t_1) = \Phi^{-1}(t_1, t_2)$
3. $\Phi(t_1, t_1) = \mathbf{1}$

Also as a direct consequence of Eq. A.4, the STM must also satisfy

$$\frac{\partial \Phi(t, t_0)}{\partial t} = A\Phi(t, t_0) \quad (\text{A.5})$$

*Appendix B. Derivation of the Eccentric Osculating Relative Orbit
Elements*

The following appendix provides a more detailed derivation of the eccentric ROEs using state substitution. Defining the in-plane state vector $\begin{bmatrix} x & y & \dot{x} & \dot{y} \end{bmatrix}^T$ as \mathbf{X} , it is known from Sec. 4.1 that

$$\mathbf{X} = \mathbf{B}(t)\Lambda_{ip0} \quad (\text{B.1})$$

where $\Lambda_{ip0} = \begin{bmatrix} a_{e0} & x_{d0} & y_{d0} \end{bmatrix}^T$, and the 4×3 matrix $\mathbf{B}(t)$ is described in variables defined in Sec. 4.1 as

$$\mathbf{B}(t) = \begin{bmatrix} B_{11} & \dots & B_{13} \\ \vdots & \ddots & \vdots \\ B_{41} & \dots & B_{43} \end{bmatrix} \quad (\text{B.2})$$

Combining the above expressions, expressions for the states are found carrying out the multiplication as

$$\begin{aligned} x &= B_{11}a_{e0} + B_{12}x_{d0} + B_{13}y_{d0} \\ y &= B_{21}a_{e0} + B_{22}x_{d0} + B_{23}y_{d0} \\ \dot{x} &= B_{31}a_{e0} + B_{32}x_{d0} + B_{33}y_{d0} \\ \dot{y} &= B_{41}a_{e0} + B_{42}x_{d0} + B_{43}y_{d0} \end{aligned} \quad (\text{B.3})$$

Now, making use of our state substitution method, the ROE expressions can now be found.

B.1 Relative Semi-major Axis, a_e

From the previously described relation, a_e is found as

$$a_e = 2\sqrt{\left(\frac{\dot{x}}{n}\right)^2 + \left(3x + \frac{2\dot{y}}{n}\right)^2} \quad (\text{B.4})$$

Substituting in the expressions for x , \dot{x} , and \dot{y} , we separate the terms in parenthesis as

$$\begin{aligned} \left(\frac{\dot{x}}{n}\right) &= \frac{B_{31}a_{e0} + B_{32}x_{d0} + B_{33}y_{d0}}{n} \\ \left(3x + \frac{2\dot{y}}{n}\right) &= \left(3B_{11} + \frac{2B_{41}}{n}\right)a_{e0} + \left(3B_{12} + \frac{2B_{42}}{n}\right)x_{d0} + \left(3B_{13} + \frac{2B_{43}}{n}\right)y_{d0} \end{aligned} \quad (\text{B.5})$$

Squaring the two expressions in Eq. B.5

$$\begin{aligned} \left(\frac{\dot{x}}{n}\right)^2 &= \frac{a_{e0}^2 B_{31}^2}{n^2} + \frac{x_{d0}^2 B_{32}^2}{n^2} + \frac{y_{d0}^2 B_{33}^2}{n^2} + \dots \\ &\quad + \frac{2a_{e0}x_{d0}B_{31}B_{32}}{n^2} + \frac{2a_{e0}y_{d0}B_{31}B_{33}}{n^2} + \frac{2x_{d0}y_{d0}B_{32}B_{33}}{n^2} \\ \left(3x + \frac{2\dot{y}}{n}\right)^2 &= a_{e0}^2 \left(9B_{11}^2 + \frac{4B_{41}^2}{n^2} + \frac{12B_{11}B_{41}}{n^2}\right) + x_{d0}^2 \left(9B_{12}^2 + \frac{4B_{42}^2}{n^2} + \frac{12B_{12}B_{42}}{n^2}\right) + \dots \\ &\quad + y_{d0}^2 \left(9B_{13}^2 + \frac{4B_{43}^2}{n^2} + \frac{12B_{13}B_{43}}{n^2}\right) + \dots \\ &\quad + a_{e0}x_{d0} \left(18B_{11}B_{12} + \frac{8B_{41}B_{42}}{n^2} + \frac{12B_{12}B_{41}}{n} + \frac{12B_{11}B_{42}}{n}\right) + \dots \\ &\quad + a_{e0}y_{d0} \left(18B_{11}B_{13} + \frac{8B_{41}B_{43}}{n^2} + \frac{12B_{13}B_{41}}{n} + \frac{12B_{11}B_{43}}{n}\right) + \dots \\ &\quad + x_{d0}y_{d0} \left(18B_{12}B_{13} + \frac{8B_{42}B_{43}}{n^2} + \frac{12B_{13}B_{42}}{n} + \frac{12B_{12}B_{43}}{n}\right) \end{aligned} \quad (\text{B.6})$$

Now, collecting like terms in Eq. B.6 with respect to the initial ROEs, we can find the α coefficients described in Sec. 4.1 and detailed in Appendix C. The resulting groups need to be multiplied by a factor of 4 to compensate for the multiplication by 2 in Eq. B.4. For example,

$$\begin{aligned} \alpha_1 &= 4 \left(\frac{B_{31}^2}{n^2} + 9B_{11}^2 + 4\frac{B_{41}^2}{n^2} + 12\frac{B_{11}B_{41}}{n^2} \right) \\ &= \left(\frac{4B_{31}^2}{n^2} + 36B_{11}^2 + 16\frac{B_{41}^2}{n^2} + 48\frac{B_{11}B_{41}}{n^2} \right) \end{aligned} \quad (\text{B.7})$$

and the process would follow by inspection.

B.2 Radial Displacement, x_d

The radial displacement is expressed as

$$x_d = 4x + \frac{2\dot{y}}{n} \quad (\text{B.8})$$

This can be found through simple substitution as

$$\begin{aligned}
4x + \frac{2\dot{y}}{n} &= 4(B_{11}a_{e0} + B_{12}x_{d0} + B_{13}y_{d0}) + \frac{2(B_{41}a_{e0} + B_{42}x_{d0} + B_{43}y_{d0})}{n} \\
&= \left(4B_{11} + \frac{2B_{41}}{n}\right) a_{e0} + \left(4B_{12} + \frac{2B_{42}}{n}\right) x_{d0} + \left(4B_{13} + \frac{2B_{43}}{n}\right) y_{d0} \quad (\text{B.9}) \\
&= \sigma_1 a_{e0} + \sigma_2 x_{d0} + \sigma_3 y_{d0}
\end{aligned}$$

B.3 In-Track Displacement, y_d

Very similar to the radial displacement, the in-track displacement is expressed as

$$y_d = y - \frac{2\dot{x}}{n} \quad (\text{B.10})$$

and simple substitution yields

$$\begin{aligned}
y_d &= y - \frac{2\dot{x}}{n} \\
&= (B_{21}a_{e0} + B_{22}x_{d0} + B_{23}y_{d0}) - \frac{2(B_{31}a_{e0} + B_{32}x_{d0} + B_{33}y_{d0})}{n} \\
&= \left(B_{21} - \frac{2B_{31}}{n}\right) a_{e0} + \left(B_{22} - \frac{2B_{32}}{n}\right) x_{d0} + \left(B_{23} - \frac{2B_{33}}{n}\right) y_{d0} \quad (\text{B.11}) \\
&= \Sigma_1 a_{e0} + \Sigma_2 x_{d0} + \Sigma_3 y_{d0}
\end{aligned}$$

Interestingly, the two ROEs that are linear combinations remain in a similar form as

$$\begin{bmatrix} x_d \\ y_d \end{bmatrix} = \begin{bmatrix} \sigma_1 & \sigma_2 & \sigma_3 \\ \Sigma_1 & \Sigma_2 & \Sigma_3 \end{bmatrix} \begin{bmatrix} a_{e0} \\ x_{d0} \\ y_{d0} \end{bmatrix} \quad (\text{B.12})$$

B.4 In-Plane Phasing, β

The in-plane phasing is also found by simple state substitution. Expressing β as

$$\beta = \tan^{-1} \left(\frac{\dot{x}}{3nx + \dot{y}} \right) \quad (\text{B.13})$$

Having already found expressions similar to the numerator and denominator while finding the a_e expression, the first of Eq. B.5 is multiplied by n , and the second of Eq. B.5 is divided by n such that the resulting expression is

$$\beta = \tan^{-1} \left(\frac{B_{31}a_{e0} + B_{32}x_{d0} + B_{33}y_{d0}}{(3nB_{11} + 2B_{41})a_{e0} + (3nB_{12} + 2B_{42})x_{d0} + (3nB_{13} + 2B_{43})y_{d0}} \right) \quad (\text{B.14})$$

B.5 Out-of-Plane ROEs

The out-of-plane ROEs were derived in Sec. 4.1 and followed a rather simple development.

*Appendix C. Time-Varying Parameters of the Yamanaka-Ankersen
Derived Relative Orbit Elements*

The following describes analytically the time-varying coefficients of the relative orbit elements for an eccentric chief. The coefficients are presented assuming an initial true anomaly at perigee and epoch time of zero.

C.1 Matrices

C.1.1 Members of the A Matrix.

$$\begin{aligned}
 A_{11} &= -\frac{(-1-e)(-3c(1+e)\zeta + (-1+e^2+3(1+e))(2-3eJs)\zeta)}{1-e^2} \\
 A_{12} &= 0 \\
 A_{13} &= -\frac{(-c+2e)s\zeta^2}{(1-e^2)k^2} \\
 A_{14} &= -\frac{\zeta(c(e+2+2e)\zeta - (1+e)^2(2-3eJs)\zeta)}{(1-e^2)k^2} \\
 A_{21} &= 0 \\
 A_{22} &= (1+e)\zeta \\
 A_{23} &= -\frac{\zeta(2-e-e^2)\zeta - c(c-2e)\lambda\zeta}{(1-e^2)k^2} \\
 A_{24} &= \frac{\zeta\left(-\frac{3(1+e)^2J}{\zeta} + (e+2+2e)\lambda\zeta s\right)}{(1-e^2)k^2}
 \end{aligned} \tag{C.1}$$

$$\begin{aligned}
A_{31} &= -\frac{1}{1-e^2} (-1-e) (-3(1+e)(c\gamma + c'\Psi) + (-1+e^2+3(1+e))(\gamma(2-3eJs) - 3e\Psi(Js' + s\zeta^2))) \\
A_{32} &= 0 \\
A_{33} &= -\frac{(-c+2e)(\gamma s + \Psi s')\zeta}{(1-e^2)k^2} \\
A_{34} &= -\frac{1}{(1-e^2)k^2}\zeta \left((e+2+2e)(c\gamma + c'\Psi) - (1+e)^2(\gamma(2-3eJs) - 3e\Psi(Js' + s\zeta^2)) \right) \\
A_{41} &= \frac{1}{1-e^2} \left((-1-e) \left(-3(1+e)((2c-e)\Psi + \gamma\lambda s) + (-1+e^2+3(1+e)) \left(3\Psi(1-2eJs) + \frac{3\gamma J}{\zeta^2} \right) \right) \right) \\
A_{42} &= (1+e)\gamma \\
A_{43} &= -\zeta \frac{((2-e-e^2)\gamma + (c-2e)(-c\gamma\lambda + 2\Psi s))}{(1-e^2)k^2} \\
A_{44} &= \frac{\zeta}{(1-e^2)k^2} \left((e+2+2e)((2c-e)\Psi + \gamma\lambda s) - (1+e)^2 \left(3\Psi(1-2eJs) + \frac{3\gamma J}{\zeta^2} \right) \right)
\end{aligned} \tag{C.2}$$

where the variables λ , γ , ζ , and Ψ are

$$\begin{aligned}
\gamma &= k^2 es\zeta \\
\Psi &= k^2/\zeta \\
\zeta &= 1/\rho \\
\lambda &= 1 + \zeta
\end{aligned} \tag{C.3}$$

C.1.2 *Members of the B Matrix.*

$$\begin{aligned}
B_{11} &= A_{12} \sin \beta_0 - \frac{A_{11} \cos \beta_0}{2} + A_{14}n \cos \beta_0 + \frac{A_{13}n \sin \beta_0}{2} \\
B_{12} &= A_{11} - \frac{3nA_{14}}{2} \\
B_{13} &= A_{12} \\
B_{21} &= A_{22} \sin \beta_0 - \frac{A_{21} \cos \beta_0}{2} + A_{24}n \cos \beta_0 + \frac{A_{23}n \sin \beta_0}{2} \\
B_{22} &= A_{21} - \frac{3nA_{24}}{2} \\
B_{23} &= A_{22} \\
B_{31} &= A_{32} \sin \beta_0 - \frac{A_{31} \cos \beta_0}{2} + A_{34}n \cos \beta_0 + \frac{A_{33}n \sin \beta_0}{2} \\
B_{32} &= A_{31} - \frac{3nA_{34}}{2} \\
B_{33} &= A_{32} \\
B_{41} &= A_{42} \sin \beta_0 - \frac{A_{41} \cos \beta_0}{2} + A_{44}n \cos \beta_0 + \frac{A_{43}n \sin \beta_0}{2} \\
B_{42} &= A_{41} - \frac{3nA_{44}}{2} \\
B_{43} &= A_{42}
\end{aligned} \tag{C.4}$$

C.1.3 *Members of the C Matrix.*

$$\begin{aligned}
C_{11} &= \frac{1}{\rho_\theta \rho_{\Delta\theta}} (c_{\Delta\theta} \rho_0 - e s_0 s_{\Delta\theta}) \\
C_{12} &= \frac{s_{\Delta\theta}}{k^2 \rho_0 \rho_\theta \rho_{\Delta\theta}} \\
C_{21} &= \rho_0 k^2 \left(\frac{c_{\Delta\theta} s_\theta e - \rho_\theta^2 s_{\Delta\theta}}{\rho_\theta \rho_{\Delta\theta}} \right) - e s_0 k^2 \left(\frac{c_{\Delta\theta} \rho_\theta^2 + e s_{\Delta\theta} s_\theta}{\rho_\theta \rho_{\Delta\theta}} \right) \\
C_{22} &= \frac{1}{\rho_0} \left(\frac{c_{\Delta\theta} \rho_\theta^2 + e s_{\Delta\theta} s_\theta}{\rho_\theta \rho_{\Delta\theta}} \right)
\end{aligned} \tag{C.5}$$

C.1.4 *Members of the D Matrix.*

$$\begin{aligned}
D_{11} &= C_{11} \sin \psi_0 + C_{12}n \cos \psi_0 \\
D_{21} &= C_{21} \sin \psi_0 + C_{22}n \cos \psi_0
\end{aligned} \tag{C.6}$$

C.2 Time Varying Coefficients

C.2.1 α Coefficients.

$$\begin{aligned}
\alpha_1 &= 36B_{11}^2 + \frac{4B_{31}^2}{n^2} + \frac{16B_{41}^2}{n^2} + \frac{48B_{11}B_{41}}{n} \\
\alpha_2 &= 36B_{12}^2 + \frac{4B_{32}^2}{n^2} + \frac{16B_{42}^2}{n^2} + \frac{48B_{12}B_{42}}{n} \\
\alpha_3 &= 36B_{13}^2 + \frac{4B_{33}^2}{n^2} + \frac{16B_{43}^2}{n^2} + \frac{48B_{13}B_{43}}{n} \\
\alpha_4 &= 72B_{12}B_{13} + \frac{8B_{32}B_{33}}{n^2} + \frac{32B_{42}B_{43}}{n^2} + \frac{48B_{13}B_{42}}{n} + \frac{48B_{12}B_{43}}{n} \\
\alpha_5 &= 72B_{11}B_{12} + \frac{8B_{31}B_{32}}{n^2} + \frac{32B_{41}B_{42}}{n^2} + \frac{48B_{12}B_{41}}{n} + \frac{48B_{11}B_{42}}{n} \\
\alpha_6 &= 72B_{11}B_{13} + \frac{8B_{31}B_{33}}{n^2} + \frac{32B_{41}B_{43}}{n^2} + \frac{48B_{13}B_{41}}{n} + \frac{48B_{11}B_{43}}{n}
\end{aligned} \tag{C.7}$$

C.2.2 σ Coefficients.

$$\begin{aligned}
\sigma_1 &= 4B_{11} + \frac{2B_{41}}{n} \\
\sigma_2 &= 4B_{12} + \frac{2B_{42}}{n} \\
\sigma_3 &= 4B_{13} + \frac{2B_{43}}{n}
\end{aligned} \tag{C.8}$$

C.2.3 Σ Coefficients.

$$\begin{aligned}
\Sigma_1 &= B_{21} - \frac{2B_{31}}{n} \\
\Sigma_2 &= B_{22} - \frac{2B_{32}}{n} \\
\Sigma_3 &= B_{23} - \frac{2B_{33}}{n}
\end{aligned} \tag{C.9}$$

Appendix D. Translational Osculation for the J_2 Perturbed Circular Chief

This appendix derives the trajectory of the translational osculation described in Sec. 4.2.2. Beginning with the expressions for x_d and y_d as

$$\begin{aligned} x_d &= 4x + \frac{2\dot{y}}{n} \\ y_d &= y - \frac{2\dot{x}}{n} \end{aligned} \tag{D.1}$$

Using the closed-form non-hyperbolic expressions given in [37], the in-plane relative positions and velocities are given as

$$\begin{bmatrix} x \\ y \\ \dot{x} \\ \dot{y} \end{bmatrix} = \begin{bmatrix} \cos \theta & \frac{g}{2c} \sin \theta \\ \frac{2c}{g} \sin \theta & \cos \theta \\ -\dot{\theta} \sin \theta & \frac{\dot{\theta}g}{2c} \cos \theta \\ -\frac{2c\dot{\theta}}{g} \cos \theta & -\dot{\theta} \sin \theta \end{bmatrix} \begin{bmatrix} x_0 \\ y_0 \end{bmatrix} \tag{D.2}$$

where $\theta = gnt$ and $\dot{\theta} = gn$, with g defined previously in Sec. 4.2.2. Evaluating x_d and y_d at an epoch time, and inserting the SS relative velocities, we can express the x_{d0} and y_{d0} directly proportional to x_0 and y_0 . This is seen via Eq. D.3

$$\begin{aligned} x_{d0} &= 4x_0 + 2\frac{\dot{y}_0}{n} \\ &= 4x_0 + 2\left(\frac{-2cnx_0}{n}\right) \\ &= 4(1-c)x_0 \\ y_{d0} &= y_0 - 2\left(\frac{2\dot{x}_0}{n}\right) \\ &= y_0 - 2\left(\frac{ng^2y_0}{2c}\right) \\ &= \left(1 - \frac{g^2}{c}\right)y_0 \end{aligned} \tag{D.3}$$

After some simplification, substitution of the initial conditions of Eq. D.3 into Eq. D.2, and the resulting substitution into Eq. D.1 yields the following closed form expressions for x_d and y_d

$$\begin{bmatrix} x_d \\ y_d \end{bmatrix} = \begin{bmatrix} \cos \theta & \kappa \sin \theta \\ -\kappa^{-1} \sin \theta & \cos \theta \end{bmatrix} \begin{bmatrix} x_{d0} \\ y_{d0} \end{bmatrix} \quad (\text{D.4})$$

where $\kappa = \frac{2(c-1)g}{g^2-c}$. This looks very familiar when compared to a parameterized ellipse. We can now attempt to quantify the geometry of this ellipse. For now, assume a dummy magnitude C such that Eq. D.4 is written as

$$\begin{aligned} x_d &= C \left(\frac{x_{d0} \cos \theta}{C} + \frac{\kappa y_{d0} \sin \theta}{C} \right) \\ y_d &= C \left(-\frac{x_{d0} \sin \theta}{\kappa C} + \frac{y_{d0} \cos \theta}{C} \right) \end{aligned} \quad (\text{D.5})$$

Now, define the following dummy phase angles as

$$\begin{aligned} \sin \delta &= \frac{x_{d0}}{C} \\ \cos \delta &= \frac{\kappa y_{d0}}{C} \end{aligned} \quad (\text{D.6})$$

Substituting Eq. D.6 in Eq. D.5 now gives

$$\begin{aligned} x_d &= C (\sin \delta \cos \theta + \cos \delta \sin \theta) \\ y_d &= -Cm (\sin \delta \sin \theta - \cos \delta \cos \theta) \end{aligned} \quad (\text{D.7})$$

where $m = \kappa^{-1}$. Applying angle addition trig identities

$$\begin{aligned} \sin(\alpha + \beta) &= \sin \alpha \cos \beta + \cos \alpha \sin \beta \\ \cos(\alpha + \beta) &= \cos \alpha \cos \beta - \sin \alpha \sin \beta \end{aligned} \quad (\text{D.8})$$

we can collapse the x_d and y_d expressions to

$$x_d = C \sin(\delta + \theta) \quad y_d = Cm \cos(\delta + \theta) \quad (\text{D.9})$$

We now need to find the magnitude C by examining the x_d expression. Looking at the x_d component of Eq. D.9 and comparing with the x_d component of Eq. D.5, we observe the equality

$$C \sin(\delta + \theta) = x_{d0} \cos \theta + \kappa y_{d0} \sin \theta \quad (\text{D.10})$$

Using the expression for the linear combination of trigonometric functions

$$a \sin x + b \cos x = r \sin(x + \alpha) \quad (\text{D.11})$$

where $\alpha = \sin^{-1}(b/r)$ and $r = \sqrt{a^2 + b^2}$. Defining the oscillation C as Υ , we find the expression for the oscillation as

$$\Upsilon = \sqrt{x_{d0}^2 + \kappa^2 y_{d0}^2} \quad (\text{D.12})$$

Such that the final expression for the x_d and y_d trajectory is

$$\begin{aligned} x_d &= \Upsilon \sin(\theta + \delta_0) \\ y_d &= \Upsilon m \cos(\theta + \delta_0) \end{aligned} \quad (\text{D.13})$$

where

$$\begin{aligned} \Upsilon &= \sqrt{x_{d0}^2 + \kappa^2 y_{d0}^2} \\ \theta &= gnt \\ \delta_0 &= \sin^{-1}\left(\frac{x_{d0}}{\Upsilon}\right) \\ \kappa &= \frac{2(c-1)g}{g^2 - c} \end{aligned} \quad (\text{D.14})$$

This is the equation for an ellipse centered at the origin with a semi-major axis of Υ/κ and a semi-minor axis of Υ . The value for κ is a fixed constant. The inverse of this value is approximately 1.5 (1.499574...). This implies that for a circular chief perturbed by J_2 , the motion of the center of the 2×1 osculating ellipse follows an approximately 1.5×1 ellipse with magnitude solely determined by the initial radial and in-track displacements.

Appendix E. Circularizing the Virtual Chief Parameters

The following is a description of the mathematics to enforce the circular chief assumption into the six geometric parameters defining the initial conditions of the Virtual Chief model. This is not a primary objective of this study and is an exercise desired by the research sponsor . The process begins with a description of the parameters, simplifications with the circular assumption, and follows with the algebraic manipulation and observations to correlate the parameters with the relative orbit elements. The six Virtual Chief parameters are

- A_1 : An indication of the scale of the periodicity of the deputy motion
- ϕ_1 : Initial phase angle in-plane; also controls deputy's epoch location along with the skewness and orientation of the trajectory
- A_2 : A scaling of the drift rate; approximate in-plane bounded center is also located at $(0, A_2, 0)$
- ϕ_2 : Directly controls the drift rate
- z_{max} : Maximum amplitude of the deputy's out of plane motion
- Ψ_0 : Initial phase angle of the deputy's out of plane motion

Defining the Virtual Chief parameters as the set Ξ such that

$$\Xi = [A_1\phi_1 A_2\phi_2 z_{max}\Psi_0] \tag{E.1}$$

The set can then be defined by the following six relations

$$\begin{aligned}
A_1 &= \frac{3}{2}\sqrt{D^2 + (3A + 2C)^2} \\
\phi_1 &= n_c t_0 + \text{atan2}(3A + 2C, D) \\
A_2 &= \sqrt{(B - 2D)^2 + (4A + 2C)^2} \\
\phi_2 &= \text{atan2}(4A + 2C, B - 2D) \\
z_{max} &= \sqrt{z_0^2 + \left(\frac{\dot{z}_0}{n_c}\right)^2} \\
\Psi_0 &= \text{atan2}\left(z_0, \frac{\dot{z}_0}{n_c}\right)
\end{aligned} \tag{E.2}$$

Where n_c is the mean motion of the chief, and the variables A , B , C , and D in Equation E.2 are intermediate parameters defined as

$$\begin{aligned}
A &= \cos(\nu_{c_0} - M_{c_0})x_0 - \sin(\nu_{c_0} - M_{c_0})y_0 \\
B &= \sin(\nu_{c_0} - M_{c_0})x_0 + \cos(\nu_{c_0} - M_{c_0})y_0 \\
C &= \frac{1}{n_c}\sin(\nu_{c_0} - M_{c_0})(\dot{x}_0 - (\dot{\nu}_{c_0} - n_c)y_0) + \cos(\nu_{c_0} - M_{c_0})(\dot{y}_0 - (\dot{\nu}_{c_0} - n_c)x_0) \\
D &= \frac{1}{n_c}\cos(\nu_{c_0} - M_{c_0})(\dot{x}_0 - (\dot{\nu}_{c_0} - n_c)y_0) + \sin(\nu_{c_0} - M_{c_0})(\dot{y}_0 - (\dot{\nu}_{c_0} - n_c)x_0)
\end{aligned} \tag{E.3}$$

The variables ν and M in Equation E.3 refer to the true and mean anomalies of the chief, respectively. Immediately, the set A , B , C , and D can be reduced enforcing the circular assumption by noting that for a body in a circular orbit, the true and mean anomalies will be equivalent; this immediately will force the cosine terms to unity and null the sine terms in the parameters. The next simplification comes from noting that the time derivative of the true anomaly is equivalent to the mean motion of the circular chief. Substitution of these observations allow Equation E.3 to become

$$\begin{aligned}
A &= x_0 \\
B &= y_0 \\
C &= \frac{\dot{y}_0}{n_c} \\
D &= \frac{\dot{x}_0}{n_c}
\end{aligned} \tag{E.4}$$

Having the circular intermediate parameters (Eq E.4), we can now reduce the components of Ξ individually.

E.1 Simplifying A_1

Enforcing the circular assumption into A_1 , the parameter becomes

$$\begin{aligned}
A_1 &= \frac{3}{2} \sqrt{D^2 + (3A + 2C)^2} \\
&= \frac{3}{2} \sqrt{\left(\frac{\dot{x}_0}{n_c}\right)^2 + \left(3x_0 + \frac{2\dot{y}_0}{n_c}\right)^2}
\end{aligned} \tag{E.5}$$

An immediate observation is the similarity to the semi-major axis of the relative orbit in the Clohessy-Wiltshire equations from the ROE set, a_e

$$a_e = 2 \sqrt{\left(\frac{\dot{x}}{n_c}\right)^2 + \left(3x + \frac{2\dot{y}}{n_c}\right)^2} \tag{E.6}$$

By obvious inspection, the first parameter is a linear mapping to the relative orbit element a_e by a simple scaling factor. Evaluating Equation E.6 at epoch, it is apparent that

$$A_1 = \frac{3}{4} a_e \tag{E.7}$$

E.2 Simplifying ϕ_1

Earlier it was noted that

$$\phi_1 = n_c t_0 + \text{atan2}(3A + 2C, D) \tag{E.8}$$

Using the relation for ϕ_1 , and substituting in the circular constraints, and assuming that t_0 is equivalently 0, ϕ_1 becomes

$$\begin{aligned}
\phi_1 &= n_c t_0 + \text{atan2}(3A + 2C, D) \\
&= \text{atan2}(3A + 2C, D) \\
&= \text{atan2}\left(3x + \frac{2\dot{y}}{n_c}, \frac{\dot{x}}{n_c}\right)
\end{aligned} \tag{E.9}$$

The ROE parameter β is defined as

$$\beta = \text{atan2}(\dot{x}, 3n_c x + 2\dot{y}) \tag{E.10}$$

The two expressions in Equations E.9 and E.10 are very similar. In fact, the argument in the atan2 functions are simply inverted, and the following identity can be utilized

$$\arctan(x^{-1}) = \frac{\pi}{2} - \arctan(x) \tag{E.11}$$

This is a well known trigonometric identity and is used without proof, but observing a simple right triangle will yield this same result. Using this expression and observing the epoch conditions on β

$$\begin{aligned}
\phi_1 &= \text{atan2}\left(3x + \frac{2\dot{y}}{n_c}, \frac{\dot{x}}{n_c}\right) \\
\beta &= \text{atan2}\left(\frac{\dot{x}}{n_c}, 3x + \frac{2\dot{y}}{n_c}\right)
\end{aligned} \tag{E.12}$$

The claim is made that the parameter ϕ_1 condenses to the following for a circular chief

$$\phi_1 = \frac{\pi}{2} - \beta \tag{E.13}$$

E.3 Simplifying A_2

The parameter A_2 is defined in E.2 and upon the circular substitution, the following is found

$$\begin{aligned} A_2 &= \sqrt{(B - 2D)^2 + (4A + 2C)^2} \\ &= \sqrt{\left(y - \frac{2\dot{x}}{n_c}\right)^2 + \left(4x + 2\frac{\dot{y}}{n_c}\right)^2} \end{aligned} \quad (\text{E.14})$$

Two components of the ROE set describe the instantaneous center (x_d, y_d) of the relative ellipse by the following relation

$$\begin{aligned} x_d &= 4x + \frac{2\dot{y}}{n_c} \\ y_d &= y - \frac{2\dot{x}}{n_c} \end{aligned} \quad (\text{E.15})$$

Evaluating Equation E.15 at epoch, it is immediately observed that x_d and y_d are the parenthetical expressions in Equation E.14, and A_2 conveniently collapses to

$$A_2 = \sqrt{x_d^2 + y_d^2} \quad (\text{E.16})$$

This implies that for the circular chief, the Virtual Chief parameter A_2 is a direct measurement of the 2-norm of the in-plane position vector from the chief to the center of the relative ellipse.

E.4 Simplifying ϕ_2

The expression for ϕ_2 uses the same analytical functions as the expression for A_2 . From Equation E.2,

$$\phi_2 = \text{atan2}(4A + 2C, B - 2D) \quad (\text{E.17})$$

Having already found that the expressions for $4A+2C$ and $B-2D$ are equivalent to x_d and y_d , the direct substitution is made such that

$$\phi_2 = \text{atan2}(x_d, y_d) \quad (\text{E.18})$$

This angle can be interpreted as the angle from the center of the relative ellipse to the chief at epoch. The relation can be observed in Figure E.1

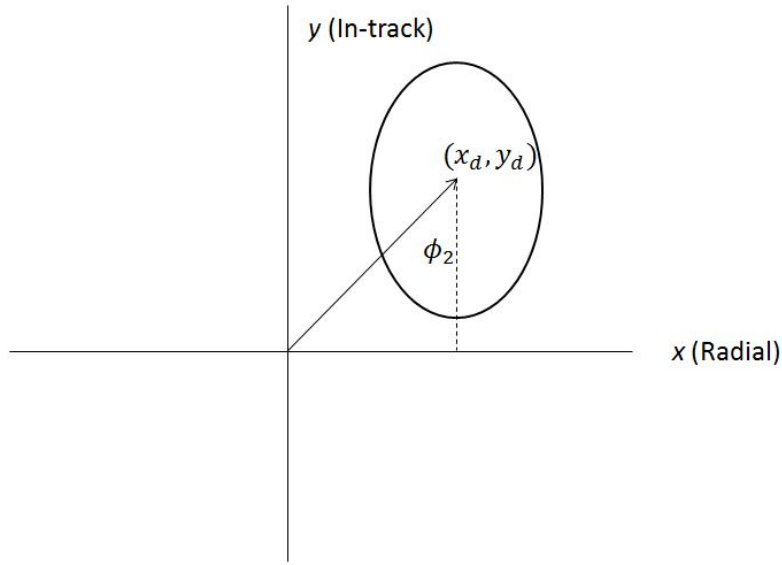


Figure E.1: ϕ_2 Visualization

E.5 Simplifying z_{max}

A direct observation between the ROE parameter z_{max} and the Virtual Chief yields duality. That is

$$z_{max} = z_{max} \quad (\text{E.19})$$

E.6 Simplifying Ψ

The final Virtual Chief parameter to map and simplify is Ψ , the expression of which is given by

$$\Psi = \text{atan2}\left(z, \frac{\dot{z}}{n_c}\right) \quad (\text{E.20})$$

Multiplying the arguments Equation E.20 by unity in the form of (n_c/n_c) , the expression is equivalent to

$$\Psi = \text{atan2}(zn_c, \dot{z}) \quad (\text{E.21})$$

The expression in Equation E.21 is, by observation, equivalent to the out of plane ROE parameter, also termed ψ .

E.7 Boundedness

For a bounded relative orbit, the Virtual Chief condition is

$$\begin{aligned} 0 &= 2A + C \\ 0 &= A_2 \sin(\phi_2) \end{aligned} \quad (\text{E.22})$$

This will hold valid for two constraints in ROE space

$$\begin{aligned} A_2 &= 0 \forall \phi_2 \in \mathfrak{R} \\ \phi_2 &= \pm k\pi (k = 0, 1, 2, \dots) \forall A_2 \in \mathfrak{R} \end{aligned} \quad (\text{E.23})$$

A value for ϕ_2 that equates to an integer value of π must imply that (from Equation E.18) x_d is a zero value, while y_d can take on any nonzero value (avoiding the discontinuity). A zero value for A_2 implies that $x_d^2 = -y_d^2$, which will not hold in

real space unless both values are equivalently zero. The implication in ROE space then follows as

$$\begin{aligned}\phi_2 = \pm k\pi (k = 0, 1, 2, \dots) &\rightarrow (x_d, y_d) = (0, y_d) \\ A_2 = 0 &\rightarrow (x_d, y_d) = (0, 0) \forall \phi_2 \neq 0 \in \mathfrak{R}\end{aligned}\tag{E.24}$$

E.8 Summary

To summarize, allowing the ROE set composed of

$$\left[a_e \quad x_d \quad y_d \quad \beta \quad \psi \quad z_{max} \right]\tag{E.25}$$

to be denoted as Λ , then the mapping from Λ to Ξ for a circular chief is the following

$$\begin{aligned}A_1 &= \frac{3}{4}a_e \\ A_2 &= \sqrt{x_d^2 + y_d^2} \\ \phi_1 &= \frac{\pi}{2} - \beta \\ \phi_2 &= \text{atan2}(x_d, y_d) \\ \Psi &= \Psi \\ z_{max} &= z_{max}\end{aligned}\tag{E.26}$$

while the inverse transformation is given by

$$\begin{aligned}
 a_e &= \frac{4}{3}A_1 \\
 \beta &= \frac{\pi}{2} - \phi_1 \\
 z_{max} &= z_{max} \\
 \Psi &= \Psi \\
 x_d &= \frac{A_2 \tan(\phi_2)}{\sqrt{1 + \tan^2(\phi_2)}} = A_2 \sin(\phi_2) \\
 y_d &= \frac{A_2}{\sqrt{1 + \tan^2(\phi_2)}} = A_2 \cos(\phi_2)
 \end{aligned} \tag{E.27}$$

Worth noting is that the (x_d, y_d) transformation is a polar representation of the in-plane motion as evident by Fig. E.1. The transformation exists in both the forward and inverse directions without encountering singularities.

Appendix F. Stationary Orbit Initialization

A popular idea in the field of relative satellite formation is that of formation maintenance. In this respect, the term stationary orbit applies to a relative orbit whose trajectory repeats itself periodically. Derived equations of motion can be investigated with respect to projected secular growth and constraints on initial conditions can be made to hinder this. For example, in the HCW derivation the condition $\dot{y}_0 = -2nx_0$ is found by analyzing the y equation to remove secular terms. For unperturbed dynamics, this repeated orbit results from an equal periodicity condition, which in turn results in equal semi-major axes between the chief and deputy. Maintaining equal orbital periods between the chief and deputy in the perturbed case is a more difficult task in that the apses rotation modifies the nominal periods of the orbits. This section presents cases to bound the orbit using relative orbit elements for the unperturbed elliptical chief, and the J_2 perturbed circular chief.

F.0.0.1 Bounding the Unperturbed Elliptical Chief. The equal periodicity constraint yields an equal semi-major axis constraint on the motion for a bounded orbit ($\delta a = 0$). Using the linearized mapping from the Hill frame to orbital element differences provided in [30] and [8], the expression for δa is given as

$$\delta a = 2\alpha(2 + 3\kappa_1 + 2\kappa_2)x + 2\alpha v(1 - 2\kappa_1 + \kappa_2)y + \frac{2\alpha^2 vp}{V_t}\dot{x} + \frac{2a}{V_t}(1 + 2\kappa_1 + \kappa_2)\dot{y} \quad (\text{F.1})$$

The coefficients α , κ_1 , κ_2 , and v can be found in [30]. However, making the assumption that the epoch condition is perigee, the coefficients and other parameters simplify to

$$\begin{aligned}
V_r &= 0 \\
\kappa_1 &= \frac{a}{r} \left(\frac{p}{r} - 1 \right) \\
\kappa_2 &= 0 \\
V_t &= r_p n \sqrt{\frac{(1+e)}{(1-e)^3}} \\
\alpha &= \frac{a}{r_p} \\
r_p &= a(1-e)
\end{aligned} \tag{F.2}$$

which reduces the δa expression to

$$\begin{aligned}
\delta a &= 0 \\
&= 2 \frac{a}{r_p} \left(2 + 3 \frac{a}{r_p} \left(\frac{p}{r_p} - 1 \right) \right) x_0 + \frac{2a}{V_t} \left(1 + 2 \frac{a}{r_p} \left(\frac{p}{r_p} - 1 \right) \right) \dot{y}_0
\end{aligned} \tag{F.3}$$

Further simplification results in

$$0 = 2 \frac{1}{1-e} \left(2 - \frac{3e}{1-e} \right) x_0 + \frac{2a}{V_t} \left(1 + \frac{2a}{a(1-e)} \left(\frac{p}{a(1-e)} - 1 \right) \right) \tag{F.4}$$

And this result further simplifies to

$$(2+e)x_0 + \frac{\dot{y}_0}{n} \sqrt{\frac{(1-e)^3}{(1+e)}} \tag{F.5}$$

Finally, Eq. F.5 can be written in general as

$$\frac{\dot{y}_0}{x_0} = - \frac{n(2+e)}{\sqrt{(1+e)(1-e)^3}} \tag{F.6}$$

which is near exact to the constraint given in [22]. To convert this expression to ROE space, we employ the Cartesian to ROE relation as

$$\begin{aligned} x_0 &= -\frac{a_{e0}}{2} \cos \beta_0 + x_{d0} \\ \dot{y}_0 &= a_{e0}n \cos \beta_0 - \frac{3nx_{d0}}{2} \end{aligned} \quad (\text{F.7})$$

Substituting the ROE expressions in Eq. F.6 and allowing $\zeta = -\frac{(2+e)}{\sqrt{(1+e)(1-e)^3}}$

$$\frac{a_{e0} \cos \beta_0 - \frac{3x_{d0}}{2}}{-\frac{a_{e0}}{2} \cos \beta_0 + x_{d0}} = \zeta \quad (\text{F.8})$$

The following derives the relationship between a_{e0} , x_{d0} , and β_0

$$\begin{aligned} a_{e0}n \cos \beta_0 - \frac{3nx_{d0}}{2}a &= \zeta \left(-\frac{a_{e0}}{2} \cos \beta_0 + x_{d0} \right) \\ a_{e0}n \cos \beta_0 + \frac{\zeta a_{e0}}{2} &= \zeta x_{d0} + \frac{3nx_{d0}}{2} \\ a_{e0} \left(n \cos \beta_0 + \frac{\zeta \cos \beta_0}{2} \right) &= x_{d0} \left(\zeta + \frac{3n}{2} \right) \end{aligned} \quad (\text{F.9})$$

At perigee ($\beta_0 = 0$) this becomes The final constraint for bounded motion becomes

$$\frac{a_{e0}}{x_{d0}} = \left(\frac{\zeta + 2n}{2\zeta + 3n} \right) \quad (\text{F.10})$$

Note that for $e = 0$, this expression reduces to $x_{d0} = 0$ which is known from [39] to produce a bounded orbit.

Figure F.1 shows the behavior of this boundedness requirement (here termed the radial ratio) and ζ . In this example a chief of semi-major axis 8000 km is used to evaluate the value of n . Instantly, it is observed that the radial ratio remains near the same constant value, and that as the eccentricity approaches unity, the value for the radial ratio approaches 0.5. This is easily observed by examining that as eccentricity approaches unity, the ζ parameter approaches infinity, and the radial ratio from Eq. F.10 approaches 0.5.

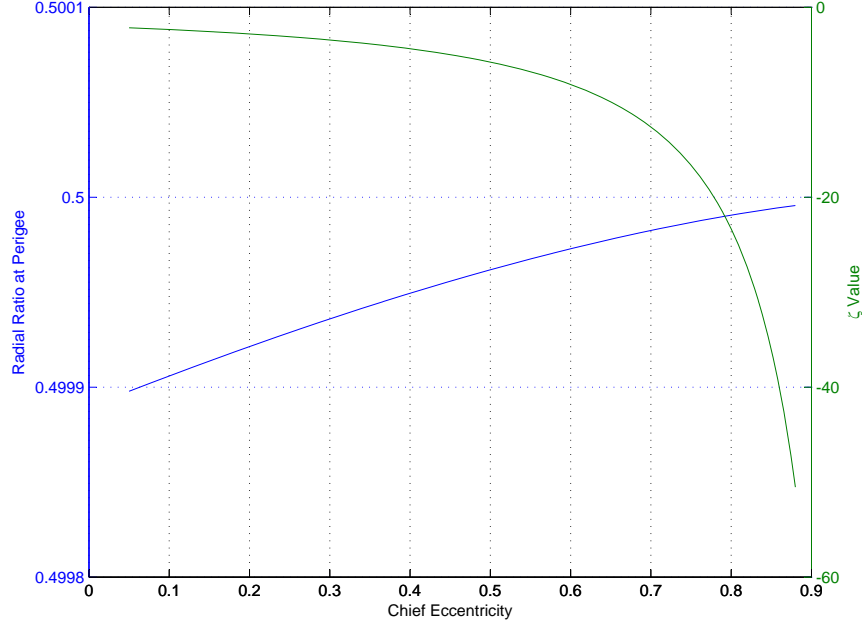


Figure F.1: Boundedness Parameters as Functions of Chief Eccentricity with a Chief Semi-major Axis of 8000 km

Also, Fig. F.2 provides a display of the radial ratio as the chief semi-major axis is varied. The general trend is followed for each different value of the semi-major axis, but the initial conditions require an increase in radial displacement.

F.0.0.2 Bounding the J_2 Perturbed Circular Chief. In bounding the relative trajectory of the circular chief perturbed by the J_2 effect there are two possible routes. In the Schweighart-Sedwick model [7], initial conditions are derived to avoid secular drift in a purely linear sense. Another approach is applying Schaub's method for initializing J_2 invariant orbits [30]. This study will determine expressions using the Schweighart initial conditions.

The initial conditions given in Schweighart [37] to remove drift are

$$\begin{aligned} \dot{x}_0 &= \frac{ng^2}{2c}y_0 \\ \dot{y}_0 &= -2cnx_0 \end{aligned} \tag{F.11}$$

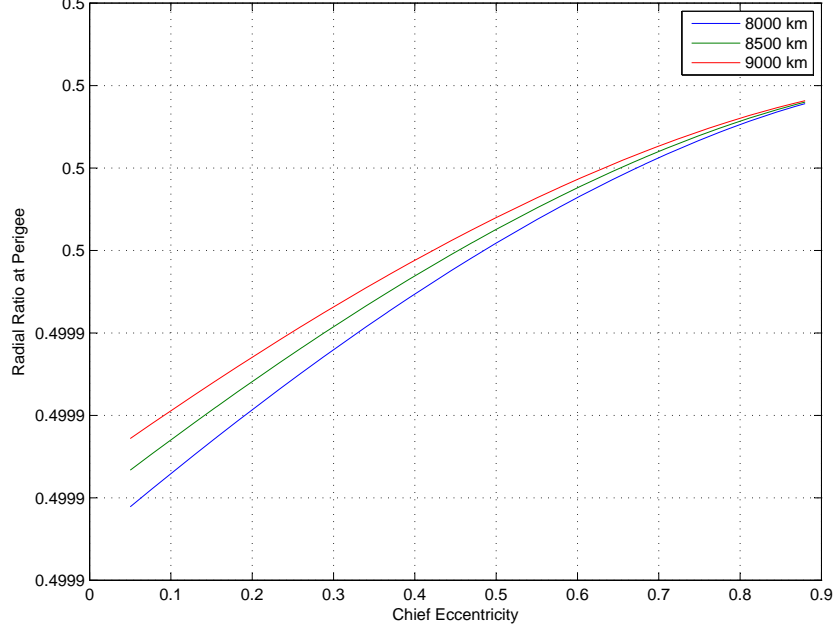


Figure F.2: Radial Ratio at Perigee as a Function of Chief Eccentricity with Varying Semi-major Axis

where the coefficients have been previously defined. The substitution for the ROEs can be made into Eq. F.11. Focusing on the \dot{x}_0 expression

$$\frac{a_{e0}}{2}n \sin \beta_0 = \frac{ng^2}{2c} (a_{e0} \sin \beta_0 + y_{d0}) \quad (\text{F.12})$$

Dividing Eq. F.12 by n , multiplying by $2c$, and collecting $a_{e0} \sin \beta_0$ terms, the condition becomes

$$a_{e0} \sin \beta_0 = \frac{g^2}{c + g^2} y_{d0} \quad (\text{F.13})$$

Now, focusing on the \dot{y}_0 expression

$$a_{e0}n \cos \beta_0 - \frac{3nx_{d0}}{2} = -2cn \left(-\frac{a_{e0}}{2} \cos \beta_0 + x_{d0} \right) \quad (\text{F.14})$$

Multiplying the right hand side of Eq. F.14 through, and collecting like terms, the condition simplifies to

$$a_{e0} \cos \beta_0 = \left(\frac{3 - 4c}{2 - 2c} \right) x_{d0} \quad (\text{F.15})$$

Squaring and summing the results of Eq. F.13 and Eq. F.15

$$(a_{e0} \cos \beta_0)^2 + (a_{e0} \sin \beta_0)^2 = \left(\frac{3-4c}{2-2c}\right)^2 x_{d0}^2 + \left(\frac{g^2}{c+g^2}\right)^2 y_{d0}^2 \quad (\text{F.16})$$

Taking the square root of Eq. F.16,

$$\sqrt{(a_{e0} \cos \beta_0)^2 + (a_{e0} \sin \beta_0)^2} = \sqrt{\left(\frac{3-4c}{2-2c}\right)^2 x_{d0}^2 + \left(\frac{g^2}{c+g^2}\right)^2 y_{d0}^2} \quad (\text{F.17})$$

which directly implies the necessary condition to bound the relative trajectory

$$a_{e0} = \sqrt{C_1 x_{d0}^2 + C_2 y_{d0}^2} \quad (\text{F.18})$$

where

$$\begin{aligned} C_1 &= \left(\frac{3-4c}{2-2c}\right)^2 \\ C_2 &= \left(\frac{g^2}{c+g^2}\right)^2 \end{aligned} \quad (\text{F.19})$$

The relation given in the bounded expression shows a parabolic surface dependent on the values for x_{d0} and y_{d0} . A very interesting note is when these initial conditions are used, the osculational translation of the relative trajectory follows a near 1.5×1 ellipse with oscillations on very low order magnitude. The derivation of this is provided in Appendix D.

Bibliography

1. Hablani, H. B., Tapper, M. L., and Dana-Bashian, D. J., "Guidance and Relative Navigation for Autonomous Rendezvous in a Circular Orbit," *Journal of Guidance, Control, and Dynamics*, Vol. 25, No. 3, 2002, pp. 553–562.
2. Silva, E. D., "A Formulation of the Clohessy-Wiltshire Equations to Include Dynamic Atmospheric Drag," Honolulu, Hawaii, August 2008.
3. Sabol, C., Burns, R., and McLaughlin, C. A., "Satellite Formation Flying Design and Evolution," *Journal of Spacecraft and Rockets*, Vol. 38, No. 2, 2001, pp. 270–278.
4. Clohessy, W. and Wiltshire, R., "Terminal Guidance System for Satellite Rendezvous," *Journal of the Aeronautical Sciences*, Vol. 27, No. 9, 1960, pp. 653–678.
5. Wiesel, W. E., "Relative Satellite Motion About an Oblate Planet," *Journal of Guidance, Control, and Dynamics*, Vol. 25, No. 4, 2002, pp. 776–785.
6. Yamanaka, K. and Ankersen, F., "New State Transition Matrix for Relative Motion on an Arbitrary Elliptical Orbit," *Journal of Guidance, Control, and Dynamics*, Vol. 25, No. 1, 2002, pp. 60–66.
7. Schweighart, S. A. and Sedwick, R. J., "High-Fidelity Linearized J_2 Model for Satellite Formation Flight," *Journal of Guidance, Control, and Dynamics*, Vol. 25, No. 6, 2002, pp. 1073–1080.
8. Gim, D.-W. and Alfriend, K. T., "State Transition Matrix of Relative Motion for the Perturbed Noncircular Reference Orbit," *Journal of Guidance, Control, and Dynamics*, Vol. 26, No. 6, 2003, pp. 956–971.
9. Goodman, J. L., "History of Space Shuttle Rendezvous and Proximity Operations," *Journal of Spacecraft and Rockets*, Vol. 43, No. 5, 2006, pp. 944–958.
10. Hill, G., "Researches in the Lunar Theory," *American Journal of Mathematics*, Vol. 1, No. 1, 1878, pp. 5–26.
11. Vadali, S. R., Sengupta, P., Yan, H., and Alfriend, K. T., "Fundamental Frequencies of Satellite Relative Motion and Control of Formations," *Journal of Guidance, Control, and Dynamics*, Vol. 31, No. 5, 2008, pp. 1239–1248.
12. Carter, T. E., "State Transition Matrices for Terminal Rendezvous Studies: Brief Survey and New Example," *Journal of Guidance, Control, and Dynamics*, Vol. 21, No. 1, 1998, pp. 148–155.
13. Karlgaard, C. D. and Lutze, F. H., "Second Order Relative Motion Equations," *Journal of Guidance, Control, and Dynamics*, Vol. 26, No. 1, 2003, pp. 41–49.
14. Lawden, D. F., *Optimal Trajectories for Space Navigation*, Butterworth, 1963.

15. Tschauner, J. F. A. and Hempel, P. R., "Rendezvous zu einem Elliptischer Bahn umlaufenden Ziel," *Astronautica Acta*, Vol. 11, No. 2, 1965, pp. 104–109.
16. Carter, T. E., "New Form for the Optimal Rendezvous Equations Near Keplerian Orbit," *Journal of Guidance, Control, and Dynamics*, Vol. 13, No. 1, 1990, pp. 183–186.
17. Alfriend, K. T. and Yan, H., "Evaluation and Comparison of Relative Motion Theories," *Journal of Guidance, Control, and Dynamics*, Vol. 28, No. 2, 2005, pp. 254–261.
18. Humi, M. and Carter, T., "Rendezvous equations in a central-force field with linear drag," *Journal of Guidance, Control, and Dynamics*, Vol. 25, No. 1, 2002, pp. 74–79.
19. Carter, T. and Humi, M., "Clohessy-wiltshire equations modified to include quadratic drag," *Journal of Guidance, Control, and Dynamics*, Vol. 25, No. 6, 2002, pp. 1058–1063.
20. Chen, W.-Y. and Jing, W.-x., "Differential Equations of Relative Motion under the Influence of J_2 Perturbation and Air Drag," Anaheim, California, September 2010.
21. Alfriend, K. T., Yan, H., and Vadali, S. R., "Nonlinear Considerations in Satellite Formation Flying," Monterey, California, August 2002.
22. Schaub, H., "Relative Orbit Geometry Through Classic Orbit Element Differences," *Journal of Guidance, Control, and Dynamics*, Vol. 27, No. 5, 2004, pp. 839–848.
23. Hamel, J.-F. and de Lafontaine, J., "Linearized Dynamics of Formation Flying Spacecraft on a J_2 -Perturbed Elliptical Orbit," *Journal of Guidance, Control, and Dynamics*, Vol. 30, No. 6, 2007, pp. 1649–1658.
24. Kolemen, E. and Kasin, N. J., "Relative Spacecraft Motion: A Hamiltonian Approach to Eccentricity Perturbations," *AAS/AIAA Spacecraft Mechanics Meeting*, Vol. 119, 2004, pp. 3075–3086.
25. Vadali, S. R., "An Analytical Solution for Relative Motion of Satellites," Cranfield, England, July 2002.
26. Sengupta, P., Vadali, S. R., and Alfriend, K. T., "Modelling and Control of Satellite Formations in High Eccentricity Orbits," *Advances in the Astronautical Sciences*, Vol. 115, 2003, pp. 325–350.
27. Johnson, K. W., *Relative Orbit Elements for Satellites in Elliptical Orbits*, Master's thesis, Graduate School of Engineering and Management, Air Force Institute of Technology (AU), Wright-Patterson AFB OH, 2010.
28. Inalhan, G., Tillerson, M., and How, J. P., "Relative Dynamics and Control of Spacecraft Formations in Eccentric Orbits," *Journal of Guidance, Control, and Dynamics*, Vol. 25, No. 1, 2002, pp. 48–59.

29. Gurfil, P., "Relative Motion Between Elliptic Orbits: Generalized Boundedness Condition and Optimal Formationkeeping," *Journal of Guidance, Control, and Dynamics*, Vol. 28, No. 4, 2005, pp. 761–767.
30. Schaub, H. and Junkins, J. L., *Analytical Mechanics of Space Systems*.
31. Vallado, D. A., *Fundamentals of Astrodynamics and Applications*, Microcosm Press, 2007.
32. Wiesel, W. E., *Spaceflight Dynamics*, Aphelion Press, 2009.
33. Lovell, T. and Tragesser, S., "A Practical Guidance Methodology for Relative Motion of LEO Spacecraft Based on the Clohessy-Wiltshire Equations," Wailea, Maui, HI, Feb 2004.
34. Jiang, e. a., "Study on Relative Orbit Geometry of Spacecraft Formations in Elliptical Reference Orbits," *Journal of Guidance, Control, and Dynamics*, Vol. 31, No. 1, 2008, pp. 123–134.
35. Sengupta, P., *Dynamics and Control of Satellite Relative Motion in a Central Gravitational Field*, Ph.D. thesis, Texas A and M University, 2006.
36. Schweighart, S. A., *Development and Analysis of a High Fidelity Linearized J_2 Model for Satellite Formation Flying*, Master's thesis, University of Illinois at Urbana-Champaign, 1999.
37. Schweighart, S. A. and Sedwick, R. J., "Cross-Track Motion of Satellite Formations in the Presence of J_2 Disturbances," *Journal of Guidance, Control, and Dynamics*, Vol. 28, No. 4, 2005, pp. 824–826.
38. Sengupta, P., Sharma, R., and Vadali, S. R., "Periodic Relative Motion Near a Keplerian Elliptic Orbit with Nonlinear Differential Gravity," *Journal of Guidance, Control, and Dynamics*, Vol. 29, No. 5, 2006, pp. 1110–1121.
39. Lovell, T. A. and Tragesser, S. G., "Guidance for Relative Motion of Low Earth Orbit Spacecraft Based on Relative Orbit Elements," *Journal of Guidance, Control, and Dynamics*, Vol. 27, No. 5, 2004, pp. 839–848.

REPORT DOCUMENTATION PAGE			<i>Form Approved</i> <i>OMB No. 0704-0188</i>		
The public reporting burden for this collection of information is estimated to average 1 hour per response, including the time for reviewing instructions, searching existing data sources, gathering and maintaining the data needed, and completing and reviewing the collection of information. Send comments regarding this burden estimate or any other aspect of this collection of information, including suggestions for reducing this burden to Department of Defense, Washington Headquarters Services, Directorate for Information Operations and Reports (0704-0188), 1215 Jefferson Davis Highway, Suite 1204, Arlington, VA 22202-4302. Respondents should be aware that notwithstanding any other provision of law, no person shall be subject to any penalty for failing to comply with a collection of information if it does not display a currently valid OMB control number. PLEASE DO NOT RETURN YOUR FORM TO THE ABOVE ADDRESS.					
1. REPORT DATE (DD-MM-YYYY) 24-03-2011		2. REPORT TYPE Master's Thesis	3. DATES COVERED (From — To) Aug 2009 – Mar 2011		
4. TITLE AND SUBTITLE Osculating Relative Orbit Elements Resulting from Chief Eccentricity and J_2 Perturbing Forces			5a. CONTRACT NUMBER		
			5b. GRANT NUMBER		
			5c. PROGRAM ELEMENT NUMBER		
6. AUTHOR(S) Hess, Joshuah A., 2d Lt, USAF			5d. PROJECT NUMBER		
			5e. TASK NUMBER		
			5f. WORK UNIT NUMBER		
7. PERFORMING ORGANIZATION NAME(S) AND ADDRESS(ES) Air Force Institute of Technology Graduate School of Engineering and Management (AFIT/ENY) 2950 Hobson Way WPAFB OH 45433-7765			8. PERFORMING ORGANIZATION REPORT NUMBER AFIT/GA/ENY/11-M07		
9. SPONSORING / MONITORING AGENCY NAME(S) AND ADDRESS(ES) Air Force Research Laboratory, Space Vehicles Directorate Attn: Dr. T. Alan Lovell (thomas.lovell@kirtland.af.mil) 3550 Aberdeen Ave SE Kirtland AFB, NM 87117-5776 (505) 853-4132 (DSN: 263-4132)			10. SPONSOR/MONITOR'S ACRONYM(S) AFRL/RV		
			11. SPONSOR/MONITOR'S REPORT NUMBER(S)		
12. DISTRIBUTION / AVAILABILITY STATEMENT APPROVED FOR PUBLIC RELEASE; DISTRIBUTION UNLIMITED					
13. SUPPLEMENTARY NOTES This material a declared a work of the U.S. Government and is not subject to copyright protection in the United States.					
14. ABSTRACT Relative orbit elements (ROEs) based on a circular chief satellite orbit are erroneous when applied to a perturbed, non-circular reference orbit. In those situations, the ROEs will encounter geometric instability and drift. To counter this, a set of time-variant ROEs have been derived to describe the relative orbit for both the unperturbed, elliptical chief, and the perturbed, circular chief. A highly coupled relationship is found that describes the relative trajectory to higher accuracy when compared to numerical integration. To show the applicability of the ROEs to formation design, methods to initialize a stationary relative orbit are detailed and an algorithm for ROE based guidance and navigation is proposed. The results provide a method to predict the relative motion, while examining time-varying parameters of the motion. Eccentricity effects are shown to induce severe time-variance to the system and introduce a level of mathematical abstraction with the current parameterization. Perturbing J_2 effects are shown to introduce periodic effects and compound the secular variations to the circular ROEs.					
15. SUBJECT TERMS Relative Satellite Motion, Rendezvous and Proximity Operations, Relative Orbit Elements, Elliptical Chief, J_2 Perturbations					
16. SECURITY CLASSIFICATION OF:			17. LIMITATION OF ABSTRACT	18. NUMBER OF PAGES	
a. REPORT	b. ABSTRACT	c. THIS PAGE	UU	137	19a. NAME OF RESPONSIBLE PERSON Douglas D. Decker, PhD
U	U	U			19b. TELEPHONE NUMBER (Include Area Code) (937) 522-6870 Email: Douglas.Decker.ctr@wpafb.af.mil